# PREDICTING INFRARED INTENSITIES OF TRIATOMIC HOX MOLECULES

By

ROBERTO GUEDES ALVES MAIA

A DISSERTATION PRESENTED TO THE GRADUATE COUNCIL
OF THE UNIVERSITY OF FLORIDA IN
PARTIAL FULFILLMENT OF THE REQUIREMENTS
FOR THE DEGREE OF DOCTOR OF PHILOSOPHY

UNIVERSITY OF FLORIDA
1980

I should like to dedicate this dissertation to my daughters, Roberta, Rosana and Renata; and to my wife, Rosa, whose understanding, patience, sacrifice and encouragement have made this work possible.

ACKNOWLEDGMENTS

I wish to express here my deepest gratitude to Professor Person for his encouragement and guidance during the course of this work.

I also wish to thank my colleagues Barbara Zilles and Jerry Rogers as well as the new members of Dr. Person's research group for their friendship over the past years.

I am grateful to the NERDC (Northeast Regional Data Center, University of Florida) for partial support for computer time, and to an NSF Research Grant No. CHE-78-18940 for additional research support. Financial support from CAPES (Coordination for the Upgrading of University Graduate Level Personnel-Brazilian Ministry of Education and Culture) is also gratefully acknowledged.

Finally, I wish to thank Ms. Joan Raudenbush for many dedicated hours spent in typing this dissertation and especially for so much help in meeting Graduate School deadlines.

TABLE OF CONTENTS

LIST OF TABLES

LIST OF FIGURES

Abstract of Dissertation Presented to the
Graduate Council of the University of Florida in
Partial Fulfillment of the Requirements for the
Degree of Doctor of Philosophy

PREDICTING INFRARED INTENSITIES OF TRIATOMIC HOX MOLECULES

by

Roberto Guedes Alves Maia

December, 1980

Chairman: Willis B. Person
Major Department: Chemistry

Ab initio self-consistent field (SCF) calculations of the atomic polar tensors (APTs) for all the atoms of the HOX series of triatomic molecules have been carried out with the GAUSSIAN 70 program using a 4-31G basis set of wavefunctions. Here the X has been Cℓ, O, H or F. We have compared these ab initio APTs with those obtained by transferring the APTs for these atoms from experimental values measured for other molecules.

The ab initio and transferred APTs have been used to predict the infrared intensities for all of the fundamental bands of the HOX series. The theoretical spectra, predicted using ab initio APTs and also from transferred APTs, have been compared with the experimental spectra for each of these molecules.

Our intensity calculations based on the ab initio APTs are on the same level of accuracy as those obtained using transferred APTs.

We have found that the intensities obtained either from ab initio SCF calculations of APTs or from transferred APTs are in good agreement with the experimental values for the absolute intensities, where available, or with the relative intensities provided the APTs are properly transferred from atoms in similar chemical environments.

In addition, we have calculated the charge, charge-flux and overlap contributions to the ab initio APTs for all of the atoms of the HOX molecules. A correlation has been found between the corresponding elements of the charge-flux tensors for the hydrogen atom of the HOX series and the Mulliken electronegativity of the X atom.

Absolute intensities calculated for HOCℓ both from the ab initio SCF calculation of APTs and from the transferred APTs are compared in some detail with available experimental data. For $HO_2$ and HOF the relative intensities from the calculations have been compared with the relative experimental intensities from matrix spectroscopic studies. The latter are fit by a computer-simulated spectrum obtained as a combination of Gaussian functions.

Our intensity calculations for HOCℓ and $HO_2$ are expected to be very useful for the application to spectroscopic infrared measurement of the concentration of those species in the earth's stratosphere.

# CHAPTER 1
# INTRODUCTION

Since the theory of atomic polar tensors (APTs) was introduced by Biarge, Herranz and Morcillo [1] and rediscovered and extended by Person and Newton [2], the chapter on studies of intensities in infrared spectroscopy has taken a new dimension with considerable promise for the future in this field. It is sufficient to say that those ingenious and revolutionary ideas make it now possible to predict successfully the infrared intensities of a number of molecular species, using intensity parameters which can be transferred from chemically related molecules, aided by quantum mechanical calculations.

This idea has always been much alive in the minds of those who have dreamed to analyze the infrared spectrum of a molecule utilizing a powerful framework of theory which enables one not only to predict the experimental frequencies but also to calculate the infrared intensities for each fundamental mode of the molecule.

The beauty of the theory of APTs is in the fact that only very few parameters are used in the prediction of infrared intensities [2,3]. Moreover, the APTs are transferred from one atom or group of atoms of a molecule to another, provided they occur in similar chemical environments [4]. Those intensity parameters may be used, for instance, to predict the computer-simulated spectrum of new molecules

from intensity parameters transferred from known molecules [5]. This can be advantageously used to predict the spectra of free radicals or reactive intermediate species trapped in a matrix, from the study of their infrared absorption spectra and some knowledge of their structure [5]. The predicted spectrum can then be compared with the experimental spectrum for qualitative identification of those unstable species. This can be done, for instance, in a computerized spectrometer for better convenience of simultaneous processing and comparison of data. Besides this important qualitative application of the theory, the quantitative aspect is also of tremendous importance. As Person [4] has pointed out and demonstrated [6], it is possible to use the ab initio quantum mechanically calculated or transferred APTs to predict the integrated molar absorption coefficient (intensity) of a fundamental band, not only of neutral molecular species, but also of free radicals [7] or other intermediate reactive species trapped in a matrix and then determine its concentration using this predicted parameter and the measured integrated band intensity. This potential analytical application of the theory could be used [4], for instance, for the infrared spectroscopic measurement of the concentration of free radical species which dominate the chemistry of planetary atmospheres [8].

One of the most interesting techniques used for selectively sampling trace species in the stratosphere is the matrix isolation technique [9]. In this technique an inert $CO_2$ matrix is used in balloon-born experiments to trap stratospheric free radical species,

and after sample collection, the matrix is returned to the laboratory for analysis. Although no measurements have yet been reported [9] using the infrared spectroscopic method of analysis, proposed in reference [4], it is expected that this new technique for analytical chemistry [5] will lead to better understanding of the chemistry of planetary atmospheres.

The APTs can also be used as a probe to investigate the electronic charge redistribution in molecules as a result of molecular vibrations. As shall be discussed in Chapter 3, this important piece of information should be very helpful in establishing the proper conditions for transferability of APTs.

We chose the HOX series of molecules for many reasons. Our interest in predicting the infrared spectra of matrix isolated $HO_2$ and HOF is to show the importance of this new spectroscopic technique for measurement of the concentration of unstable intermediates and free radical species in inert matrices. The intensity parameters for species such as HOF, $HO_2$ and HOCℓ are not easily obtained in the gas phase, and here we think that ab initio calculations will play an important role as an additional and complementary tool in this new developing area of research. We also wish to point out that our studies show for the first time that ab initio quantum mechanical calculations can be used to predict successfully the relative intensities of unstable molecules or of free radical species trapped in a matrix and indicate the importance of such predictions using ab initio SCF calculations.

Many studies have been made on the determination of the experimental infrared spectra of matrix-isolated species as reported in the vast literature of this subject. Here we think it would be interesting to use the experimental spectra parameters to simulate with a computer the predicted spectra of the matrix-isolated species. From comparison with the experimental relative intensities the concentration of those species in the matrix (if the matrix pathlength is measured) could be obtained as well as confirmation of the assignment of the bands using the relative predicted intensities as an additional criterion. Moreover, the presence of absorption in the spectrum from dimers, trimers, etc. would be easily identified. This suggests another important application of the theory in studies of inter- and intramolecular hydrogen bonded complexes.

From the molecules studied here (matrix-isolated HOO and HOF, and gas phase HOCℓ), two are of particular importance in the chemistry of the earth's stratosphere: HOO and HOCℓ. Those species have been the subject of several spectroscopic studies during the past two years. This renewed interest is due in part to the fact that both species are intermediate in the cycle of the chlorine catalyzed decomposition of ozone in the earth's stratosphere according to the following reactions [9,10]:

$$Cℓ + O_3 = ClO + O_2 \qquad (1a)$$

$$ClO + O = Cℓ + O_2 \qquad (1b)$$

$$O_3 + O = 2O_2 \qquad (1c)$$

$$ClO + HO_2 = HOCℓ + O_2 \qquad (2)$$

$$HOCℓ \xrightarrow{h\nu \equiv 330nm} HO + Cℓ \qquad (3)$$

Reactions (1a) and (1b) represent the cycle of chlorine catalyzed decomposition of $O_3$, while reaction (2) represents a possible synthesis for HOCℓ in the stratosphere. It has been pointed out [11] that reaction (2) is an important removal process for the ClO species.

The rate constant of reaction (2) has been measured by two independent groups [12, p. 2926], and a value of $3.8 \pm 0.5 \times 10^{-12}$ $cm^3$ $molecule^{-1}$ $s^{-1}$ was reported by Reimann and Kaufman [12]. This large rate constant implied that HOCℓ could be an important inert chlorine reservoir in the stratosphere if its photodissociation rate at wavelengths longer than 300 nm and the reactions with O and OH were slow processes [10]:

$$HOCℓ + OH = ClO + H_2O \quad (3)$$

$$HOCℓ + O = ClO + OH \quad (4)$$

$$HOCℓ + h\nu = Cℓ + OH \quad (5)$$

The only possible breakdown of the hypothesis that HOCℓ is an inert chlorine reservoir in the stratosphere occurs if this species would be rapidly photolyzed at the wavelength region near or beyond 300 nm. This region is important because at an altitude of 30-40 km, light with wavelengths shorter than 300 nm is almost totally attenuated due to the absorption by ozone. There had been until recently [13] considerable controversy about the extent of absorption and subsequent photodissociation by HOCℓ in this critical region. The theoretical and experimental studies of the UV photodissociation of HOCℓ led to different predictions, as did different

experimental studies. The theoretical SCF-CI studies of the UV photodissociation of HOCℓ was done by Jaffe and Langhoff [11]. They found that the calculated absorption spectrum of HOCℓ exhibits only a single peak at 220 nm with no significant absorption predicted beyond 330 nm. This theoretical study was consistent with experimental studies made by Hisatsune and by Timmons [14], but did not agree with experimental studies by Fergusson, Slotin and Style [15], by Jaffe and DeMoore [16], by Molina and Molina [10] and by Knauth, Alberti and Clausen [17]. In Table I-1 we present several values for the extinction coefficient ($\varepsilon$) in ℓ $mole^{-1}$ $cm^{-1}$ for the $(1)^1A' \rightarrow (1)^1A''$ transition at 320 nm. (Some of the measurements were made at slightly different wavelengths.)

The discrepancies among the different experimental values reported by Fergusson and DeMore seem to indicate that other species besides HOCℓ, $H_2O$ and $Cℓ_2O$ were present to different extents in their reaction systems. The discrepancies particularly at 320 nm may be explained if one assumes thermal and/or photochemical decomposition of $Cℓ_2O$ to different extents in those experimental works, combined with the absorption of $Cℓ_2O$ at 294 nm which probably have not always been taken into account to the same extent in the earlier experiments [11]. It is well known that $Cℓ_2$ also absorbs at 330 nm [18] and with a line shape similar to the 320 nm band observed in the HOCℓ experiments. Therefore, it seems that the experimental work of Fergusson is definitely wrong and that the results of DeMoore at 330 nm are probably overestimated by factor of two.

TABLE 1-1
EXTINCTION COEFFICIENTS FOR THE $(1)^1A' \rightarrow (1)^1A''$ TRANSITION OF HOCℓ (VAPOR) NEAR 310 nm

| λ nm | ε (ℓ $mole^{-1}cm^{-1}$) | Study |
|---|---|---|
| 320 | 282 | Fergusson, Slotin and Style, ref. [15] (experimental) |
| 320 | 36 | Jaffe and DeMoore, ref. [16] (experimental) |
| 310 | 25.4 | Molina and Molina, ref. [10] (experimental) |
| 310 | 15.7 | Molina, Ishiwata and Molina, ref. [13] (experimental) |
| 310 | 16.3 | Knauth, Alberti and Clausen, ref. [17] (experimental) |
| 310 | 1.0 | Timmons, ref. [14] (experimental) |
| 310 | - | Hisatsune, ref. [14] (experimental) |
| 310 | - | Jaffe and Langhoff, ref. [11] (theoretical) |

All of this controversy about the photochemical decomposition of HOCℓ has apparently finally been settled by the very recent study of Molina, Ishiwata and Molina [13]. They have used a tunable dye laser at 310 nm to produce photodecomposition of HOCℓ measured by laser-induced fluorescence. It is clear from this study that HOCℓ does undergo photodissociation by light at 310 nm, and so it cannot be a sink for Cℓ atoms in the stratosphere.

Nevertheless, there have still not been any measurements of the concentration of HOCℓ in the stratosphere, and we expect that our work will provide an alternate analytical tool for future infrared spectroscopic measurements of concentrations of those species in the earth's stratosphere.

CHAPTER 2
DESCRIPTION OF INTENSITY CALCULATIONS

## Normal Coordinate Analysis

The calculation of infrared intensities using the atomic polar tensor (APT) formalism originally introduced by Biarge, Herranz and Morcillo [1] requires an a priori solution of the vibrational eigenvalue problem represented by

$$\underline{G}\,\underline{F}\,\underline{L} = \underline{L}\,\underline{\Lambda} \qquad (1)$$

and therefore a complete normal coordinate analysis.

The mathematical approach used here to solve the vibrational eigenvalue problem is the well-known FG matrix method of Wilson [19,20]. This method is well-documented [21-24], and therefore, we shall outline only the most prominent equations which are related to this method.

The formalism which we shall discuss is applicable to a general nonlinear polyatomic molecule containing N atoms. For a nonlinear polyatomic molecule there are 3N-6 normal modes of vibration (3N-5 if the molecule is linear).

The first step toward solving the vibrational eigenvalue problem within the Born-Oppenheimer and harmonic approximation consists of starting with a convenient set of coordinates and then searching for a coordinate transformation which allows the molecular vibrations to be expressed in terms of 3N-6 (or 3N-5) independent normal harmonic motions.

We shall first form a 3Nx1 column vector which represents the displacements in position of the atoms in the molecule with respect to a space-fixed Cartesian coordinate system

$$\underline{X} = \begin{pmatrix} x_1 \\ y_1 \\ z_1 \\ x_2 \\ y_2 \\ z_2 \\ \cdot \\ \cdot \\ \cdot \\ z_N \end{pmatrix} \qquad (2)$$

for N atoms of the molecule.

This set of Cartesian displacement coordinates is not independent since there are six extra ("redundant") coordinates (3N instead of 3N-6) associated with the rotations and with the translations of the center of mass of the system. Therefore it is convenient to choose a coordinate system (for example, molecule-fixed internal displacement coordinates) in which these six redundant coordinates are removed.

The transformation from space-fixed Cartesian displacement coordinates, $\underline{X}$, to molecule-fixed internal coordinates, $\underline{R}$, is given by

$$\underline{R} = \underline{B}\,\underline{X} \qquad (3)$$

where $\underline{B}$ is a (3N-6) x 3N transformation matrix.

Taking advantage of any symmetry that the molecule may have, and using the sets of internal coordinates as basis functions, we apply the projection operator technique to set up the linear

combinations of the internal coordinates which form the proper symmetry adapted functions transforming according to each of the irreducible representations of the symmetry point group of the molecule. This set of symmetry coordinates is orthonormal.

In terms of these symmetry coordinates, the $\underline{G}$ and $\underline{F}$ matrices of the secular equation are block factored, where each block is associated only with the subset of symmetry coordinates which transform according to the same irreducible representation of the molecular point group.

The relation between the (3N-6) x 1 internal coordinate column vector and the (3N-6) x 1 symmetry coordinate column vector is given in matrix notation by

$$\underline{S} = \underline{U}\,\underline{R} \tag{4}$$

where $\underline{U}$ is a (3N-6) x (3N-6) orthogonal matrix, if the redundancies have been eliminated.

At this point, it is convenient to eliminate any redundant coordiante [23,25] by dropping it from the new basis set, since those redundancies will only contribute to zero eigenvalues.

The $\underline{G}$ matrix and the symmetrized $\underline{\mathcal{G}}$ are given by

$$\underline{G} = \underline{B}\,\underline{M}^{-1}\,\underline{B}^{\dagger} \tag{5a}$$

$$\underline{\mathcal{G}} = \underline{U}\,\underline{G}\,\underline{U}^{\dagger} \tag{5b}$$

where $\underline{M}^{-1}$ is a 3N x 3N diagonal matrix of the inverse masses,

given by

$$M^{-1} = \begin{pmatrix} 1/m_1 & & & & & & & 0 \\ & 1/m_1 & & & & & & \\ & & 1/m_1 & & & & & \\ & & & 1/m_2 & & & & \\ & & & & 1/m_2 & & & \\ & & & & & 1/m_2 & & \\ & & & & & & \ddots & \\ & 0 & & & & & & 1/m_N \end{pmatrix} \qquad (6)$$

Here $\underline{G}$ is a (3N-6)x(3N-6) symmetric matrix and is related to the vibrational kinetic energy expression, given by

$$2T = \dot{\underline{R}}^{\dagger} \underline{G}^{-1} \dot{\underline{R}} = \underline{P}^{\dagger} \underline{G} \underline{P} \qquad (7)$$

$\underline{G}$ has units of $u^{-1}$, the overhead dot indicates a time derivative, the $\dagger$ is used here to indicate the transpose of a matrix, and $\underline{P}$ is the momentum matrix conjugate to the internal coordinates, $\underline{R}$.

Expanding the vibrational potential energy function $V(R_i)$ as a power series about the equilibrium configuration and neglecting terms of order higher than $R^2$ (harmonic approximation), we can write the vibrational potential energy as

$$2V = \sum_i \sum_j F_{ij} R_i R_j = \underline{R}^{\dagger} \underline{F} \underline{R} \qquad (8a)$$

where

$$F_{ij} = \frac{\partial^2 V}{\partial R_i \partial R_j} \qquad (8b)$$

or in terms of symmetry coordinate as

$$F_{ij} = \frac{\partial^2 V}{\partial S_i \partial S_j} \qquad (8c)$$

Here $F_{ij}$ and $\mathcal{F}_{ij}$ are the force constants, or coefficients in the vibrational potential energy expression for the molecule in terms of internal or symmetry coordinates respectively.

The symmetrized $\underline{\mathcal{F}}$ matrix is then given by

$$\underline{\mathcal{F}} = \underline{U}\ \underline{F}\ \underline{U}^{\dagger} \tag{8d}$$

where $\underline{F}$ is a symmetric (3N-6)(3N-6) matrix whose elements are given by Eq. (8b). The F matrix elements have units of mdynes $\mathring{A}^{-1}$.

The units we have used for the various matrices are related to the units we have chosen for the atomic masses, the potential energy and the internal coordinates. There are two types of internal coordinates. Those involving bond stretching ($\Delta r_i$) have units of $\mathring{A}$. Those involving angle deformation (expressed as the arc, $r\,\Delta\theta$) have units of (rad x 1 $\mathring{A}$ = $\mathring{A}$). In other words, we have weighted all the angles by $r = 1\ \mathring{A}$. Therefore, the resulting force constants (see Eq.(8b)) have all units of mdynes $\mathring{A}^{-1}$, when the energy in that equation is expressed in mdynes $\mathring{A}$ (1 mdyne $\mathring{A}$ = 1 aJ = 1 attojoule). The atomic masses are given in atomic mass units (u). Table 2-1 gives a summary of matrix size, notation and units used in this work. Notice in Table 2-1 that use of weighted units has the great advantage of simplifying the matrix units.

Two important matrix relations from the normal coordinate analysis formalism are

$$\underline{L}\ \underline{L}^{\dagger} = \underline{G} \quad \text{or} \quad \underline{L}^{\dagger} = \underline{L}^{-1}\ \underline{G} \tag{9a}$$

and

$$\underline{L}^{\dagger}\ \underline{\mathcal{F}}\ \underline{L} = \underline{\Lambda} \tag{9b}$$

TABLE 2-1
SUMMARY OF MATRIX SIZE, NOTATION AND UNITS USED IN THE NORMAL COORDINATE ANALYSIS

| Matrix | Size | Matrix element | Units (unweighted) | Units[a] (weighted) |
|---|---|---|---|---|
| $\underline{X}$ | 3N x 1 | $x_i, y_i, z_i$ | Å | Å |
| $\underline{R}$ | (3N-6)x 1 | $R_i(\Delta r)$[b] | Å | Å |
| | | $R_j(\Delta\theta)$[c] | rad | Å |
| $\underline{S}$ | (3N-6)x 1 | $S_i(\Delta r)$ | Å | Å |
| | | $S_j(\Delta\theta)$ | rad | Å |
| $\underline{B}$ | (3N-6)x 3N | $B_{ij}(\Delta r)$ | - | - |
| | | $B_{kl}(\Delta\theta)$ | $Å^{-1}$rad | - |
| $\underline{U}$ | (3N-6)x(3N-6) | $U_{ij}$ | - | - |
| $\underline{F}$ | (3N-6)x(3N-6) | $F_{ii}(\Delta r,\Delta r)$ | mdynes $Å^{-1}$ | mdynes $Å^{-1}$[d] |
| | | $F_{ij}(\Delta r,\Delta\theta)$ | mdynes $rad^{-1}$ | mdynes $Å^{-1}$ |
| | | $F_{jj}(\Delta\theta,\Delta\theta)$ | mdynes Å $rad^{-2}$ | mdynes $Å^{-1}$ |
| $\underline{M}^{-1}$ | 3N x 3N | $M_{ii}^{-1}$ | $u^{-1}$ | $u^{-1}$ |
| $\underline{G}$ | (3N-6)x(3N-6) | $G_{ii}(\Delta r,\Delta r)$ | $u^{-1}$ | $u^{-1}$ |
| | | $G_{ij}(\Delta r,\Delta\theta)$ | $u^{-1}$ $Å^{-1}$ rad | $u^{-1}$ |
| | | $G_{jj}(\Delta\theta,\Delta\theta)$ | $u^{-1}$ $Å^{-2}$ $rad^2$ | $u^{-1}$ |
| $\underline{L}$ | (3N-6)x(3N-6) | $L_{ij}(\Delta r)$ | $u^{-1/2}$ | $u^{-1/2}$ |
| | | $L_{kl}(\Delta\theta)$ | $u^{-1/2}$ $Å^{-1}$rad | $u^{-1/2}$ |
| $\underline{G}\,\underline{F}$ | (3N-6)x(3N-6) | $(G\,F)_{ij}$ | $u^{-1}$mdynes $Å^{-1}$ | $u^{-1}$ mdynes $Å^{-1}$ |
| $\underline{\Lambda}$ | (3N-6)x(3N-6) | $\lambda_k$ | $u^{-1}$mdynes $Å^{-1}$ | $u^{-1}$ mdynes $Å^{-1}$ |
| $\underline{Q}$ | (3N-6)x 1 | $Q_k$ | $u^{1/2}$ Å | $u^{1/2}$ Å |

[a] Units used in this work
[b] $\Delta r$ indicates here a bond stretching displacement
[c] $\Delta\theta$ indicates here an angle bending deformation
[d] 1 mdyne $Å^{-1}$ = $10^5$dynes $cm^{-1}$ = 100Nm$^{-1}$ = 100Jm$^{-2}$ = $10^{-18}$J $Å^{-2}$ = 1 aJ $Å^{-2}$

Upon substitution of Eq. (8a) into Eq. (8b) we can easily obtain Eq. (1)

$$\underline{G}\,\underline{F}\,\underline{L} = \underline{L}\,\underline{\Lambda}$$

Therefore, we can write

$$(\underline{G}\,\underline{F} - \lambda_k \underline{I}_{3N-6})\,\underline{L} = 0 \tag{10}$$

where $\underline{I}_{3N-6}$ is the identity matrix, $\underline{\Lambda}$ is the diagonal matrix of eigenvalues, and $\underline{L}$ is a square matrix of the eigenvectors of $(\underline{G}\,\underline{F})$. The matrices $(\underline{G}\,\underline{F})$, $\underline{L}$, $\underline{I}$ and $\underline{\Lambda}$ are (3N-6) x (3N-6) matrices.

Equation (10) is equivalent to the linear equations

$$\sum_{j=1}^{3N-6} [(G\,F)_{ij} - \delta_{ij}\,\lambda_k] L_{jk} = 0 \tag{11}$$

where i = 1, ..., 3N-6 and $\delta_{ij}$ is the Kronecker delta.

Equation (11) is a set of linear homogeneous simultaneous equations which have a nontrivial solution if and only if

$$\left| (G\,F)_{ij} - \delta_{ij}\,\lambda_k \right| = 0 \tag{12}$$

The 3N-6 roots ($\lambda_k$) of this secular equation (Eq. (12)) are the eigenvalues of $(\underline{G}\,\underline{F})$ which upon substitution into Eq. (11) gives the column vectors of $\underline{L}$, which are the eigenvectors of the $(\underline{G}\,\underline{F})$ product matrix.

Here $\lambda_k$ has units of $u^{-1}$ mdyne $\mathring{A}^{-1}$ and is related to the harmonic frequencies $\omega_k$ (in $cm^{-1}$) by

$$\lambda_k = 10^{-5} N_A\, 4\pi^2 c^2 \omega_k^2 = (1302.776)^{-2} \omega_k^2 \tag{13}$$

where $N_A$ is Avogadro's number and c is the velocity of light in cm $s^{-1}$.

Using Eq. (5b), Eq. (8d) and $\underline{L}$, we can show that

$$\underline{G}\,\underline{F}\,\underline{L} = \underline{L}\,\underline{\Lambda} \tag{14}$$

where the symmetrized $\underline{L}$ matrix is given by

$$\underline{L} = \underline{U}\,\underline{L} \tag{15}$$

We now proceed to obtain the normal coordinates, $\underline{Q}$, which are related to the symmetry coordinates, $\underline{S}$, by the linear transformation

$$\underline{Q} = \underline{L}^{-1}\,\underline{S} \tag{16}$$

Since $\underline{L}^{-1}$ is in block diagonal form, we can also write for each symmetry block

$$\underline{Q}^{(s)} = \underline{L}^{-1\,(s)}\,\underline{S}^{(s)} \tag{17}$$

where $\underline{S}^{(s)}$ is a n-dimensional column vector of symmetry coordinates, which transform according to the same irreducible representation s, and span the n-dimensional space represented by the column vector of normal coordinates, $\underline{Q}^{(s)}$.

The inverse of the symmetrized matrix $\underline{L}$ can be obtained from Eq. (9b) and Eq. (15) and is given by

$$\underline{L}^{-1} = \underline{\Lambda}^{-1}\,\underline{L}^{+}\,\underline{F} \tag{18}$$

The transformation from a column vector of normal coordinates $\underline{Q}$ to the column vector of space-fixed Cartesian coordinates $\underline{X}$, is given by

$$\underline{X} = \underline{A}\,\underline{R} = \underline{A}\,\underline{U}\,\underline{L}\,\underline{Q} = \underline{A}\,\underline{L}\,\underline{Q} \tag{19}$$

where $\underline{A}$ is the normal coordinate transformation matrix from $\underline{R}$ to $\underline{X}$ and is given by

$$\underline{A} = \underline{M}^{-1}\,\underline{B}^{+}\,\underline{G}^{-1} \tag{20}$$

and $\underline{A}$ is the symmetrized $\underline{A}$ matrix.

Using the $\underline{A}$ matrix, as given by Eq. (20), and also Eq. (1) to form the $(\underline{G}^{-1}\,\underline{L})$ product matrix

$$\underline{G}^{-1}\,\underline{L} = \underline{F}\,\underline{L}\,\underline{\Lambda}^{-1} = (\underline{L}^{-1})^{+} \tag{21}$$

we can then form the $\underline{A}\ \underline{L}$ transformation matrix

$$\underline{A}\ \underline{L} = \underline{M}^{-1}\ \underline{B}^{\dagger}\ \underline{G}^{-1}\ \underline{L} = \underline{M}^{-1}\ \underline{B}^{\dagger}\ \underline{F}\ \underline{L}\ \underline{\Lambda}^{-1} \tag{22}$$

Finally, the symmetrized $(\underline{A}\ \underline{L})$ product matrix is obtained from Eq. (15), Eq. (21) and the symmetrized $\underline{B}$ and $\underline{A}$ matrices, and is given by

$$\underline{A}\ \underline{L} = \underline{M}^{-1}\ \underline{B}^{\dagger}\ \underline{F}\ \underline{L}\ \underline{\Lambda}^{-1} \tag{23}$$

where

$$\underline{B} = \underline{U}\ \underline{B} \tag{24}$$

and

$$\underline{A} = \underline{A}\ \underline{U}^{\dagger} \tag{25}$$

The $(\underline{A}\ \underline{L})$ product matrix has units of $u^{-1/2}$. This transformation is particularly useful, as will be seen in the next section, when we shall consider the atomic polar tensor formalism in different molecular frames.

Table 2-2 gives a summary of useful matrix equations involved in the normal coordinate analysis formalism.

The algebraic equations given by Eq. (11) and Eq. (12) are not suitable for computer solution of the vibrational eigenvalue problem of large molecules with low symmetry. Noticing that $\underline{L}$ is nonsingular, we can also formulate the vibrational eigenvalue problem according to

$$\underline{L}^{-1}\ (\underline{G}\ \underline{F})\ \underline{L} = \underline{\Lambda} \tag{26}$$

that is, since $(\underline{G}\ \underline{F})$ is known and $\underline{L}$ is nonsingular, it is then possible to find the matrix $\underline{L}$ which diagonalizes $(\underline{G}\ \underline{F})$. However, since $(\underline{G}\ \underline{F})$ is not symmetric and since in general, the most efficient methods for computer solution of eigenvalue problem, such as Eq. (26)

TABLE 2-2
SUMMARY OF USEFUL MATRIX EQUATIONS INVOLVED IN THE NORMAL COORDINATE ANALYSIS FORMALISM

| Using internal coordinates | Using symmetry coordinates |
|---|---|
| $\underline{R} = \underline{B}\,\underline{X}$ | $\underline{S} = \underline{U}\,\underline{R}$ |
| $\underline{G} = \underline{B}\,\underline{M}^{-1}\,\underline{B}^{+}$ | $\underline{\mathcal{G}} = \underline{U}\,\underline{G}\,\underline{U}^{+}$ |
| $F_{ij} = \dfrac{\partial^2 V}{\partial R_i \partial R_j}$ | $\mathcal{F}_{ij} = \dfrac{\partial^2 V}{\partial S_i \partial S_j}$ <br> $\underline{\mathcal{F}} = \underline{U}\,\underline{F}\,\underline{U}^{+}$ |
| $\underline{L}\,\underline{L}^{+} = \underline{G}$ <br> $\underline{L}^{+}\,\underline{F}\,\underline{L} = \underline{\Lambda}$ <br> $\underline{G}\,\underline{F}\,\underline{L} = \underline{L}\,\underline{\Lambda}$ | $\underline{\mathcal{L}}\,\underline{\mathcal{L}}^{+} = \underline{\mathcal{G}}$ <br> $\underline{\mathcal{L}}^{+}\,\underline{\mathcal{F}}\,\underline{\mathcal{L}} = \underline{\Lambda}$ <br> $\underline{\mathcal{G}}\,\underline{\mathcal{F}}\,\underline{\mathcal{L}} = \underline{\mathcal{L}}\,\underline{\Lambda}$ |
| $\sum_{j=1}^{3N-6} [(G\,F)_{ij} - \delta_{ij}\lambda_k]\,L_{jk} = 0^a \quad i=1,\ldots,3N-6$ <br> $\lvert (G\,F)_{ij} - \delta_{ij}\lambda_k \rvert = 0^a$ | $\sum_{j=1}^{3N-6} [(\mathcal{G}\,\mathcal{F})_{ij} - \delta_{ij}\lambda_k]\,\mathcal{L}_{jk} = 0^a$ <br> $\lvert (\mathcal{G}\,\mathcal{F})_{ij} - \delta_{ij}\lambda_k \rvert = 0^a$ |
| $\underline{Q} = \underline{L}^{-1}\,\underline{R}$ <br> $\underline{L}^{-1} = \underline{\Lambda}^{-1}\,\underline{L}^{+}\,\underline{F}$ | $\underline{Q} = \underline{\mathcal{L}}^{-1}\,\underline{S}$ <br> $\underline{\mathcal{L}}^{-1} = \underline{\Lambda}^{-1}\,\underline{\mathcal{L}}^{+}\,\underline{\mathcal{F}}$ |
| $\underline{X} = \underline{A}\,\underline{L}\,\underline{Q}$ <br> $\underline{A} = \underline{M}^{-1}\,\underline{B}^{+}\,\underline{G}^{-1}$ | $\underline{X} = \underline{\mathcal{A}}\,\underline{\mathcal{L}}\,\underline{Q}$ <br> $\underline{\mathcal{A}} = \underline{A}\,\underline{U}^{+}$ |

TABLE 2-2--continued

| | |
|---|---|
| $\underline{G}^{-1} = \underline{F}\,\underline{L}\,\underline{\Lambda}^{-1}\,\underline{L}^{-1} = (\underline{L}^{-1})^{\dagger}\,\underline{L}^{-1}$ | $\underline{G}^{-1} = \underline{F}\,\underline{L}\,\underline{\Lambda}^{-1}\,\underline{L}^{-1} = (\underline{L}^{-1})^{\dagger}\,\underline{L}^{-1}$ |
| $\underline{A}\,\underline{L} = \underline{M}^{-1}\,\underline{B}^{\dagger}\,\underline{F}\,\underline{L}\,\underline{\Lambda}^{-1}$ | $\underline{A}\,\underline{L} = \underline{M}^{-1}\,\underline{B}^{\dagger}\,\underline{F}\,\underline{L}\,\underline{\Lambda}^{-1}$ |
| $= \underline{M}^{-1}\,\underline{B}^{\dagger}\,(\underline{L}^{-1})^{\dagger}$ | $= \underline{M}^{-1}\,\underline{B}^{\dagger}\,(\underline{L}^{-1})^{\dagger}$ |
| $\underline{L} = \underline{U}^{\dagger}\,\underline{L}$ | $\underline{L} = \underline{U}\,\underline{L}$ |
| $\underline{B} = \underline{U}^{\dagger}\,\underline{B}$ | $\underline{B} = \underline{U}\,\underline{B}$ |

[a] See also alternative techniques suitable for computer solution of the vibrational eigenvalue problem given by Schachtschneider in ref. [26] and by Overend in ref. [27].

involve diagonalization of symmetric matrices, alternative methods have been mostly used [26,27]. Among other methods, for instance, one which is used in this work involves two successive Jacobi diagonalizations of $\underline{G}$ and $\underline{F}$. We shall now briefly outline this method [26].

The first step is a simple Jacobi diagonalization of $\underline{G}$ (step I)

$$\underline{D}^{+}\ \underline{G}\ \underline{D} = \underline{\Gamma} \tag{27}$$

where $\underline{D}$ is orthogonal.

Next, we compute $\underline{D}\ \underline{\Gamma}^{1/2}$ and form the symmetrized $\underline{H}$ matrix (step II)

$$\underline{W} = \underline{D}\ \underline{\Gamma}^{1/2} \tag{28}$$

or

$$\underline{W}^{+}\ \underline{F}\ \underline{W} = \underline{H} \tag{29}$$

Equation (29) can also be written as

$$\underline{\Gamma}^{1/2}\ \underline{D}^{+}\ \underline{F}\ \underline{D}\ \underline{\Gamma}^{1/2} = \underline{H} \tag{30}$$

since

$$\underline{W}^{+} = \underline{\Gamma}^{1/2}\ \underline{D}^{+}$$

It can be easily shown that Eq. (27) is equivalent to

$$\underline{\Gamma}^{-1/2}\ \underline{D}^{+}\ \underline{G}\ \underline{D}\ \underline{\Gamma}^{-1/2} = \underline{I}_{3N-6} \tag{31}$$

where $\underline{I}_{3N-6}$ is the identity matrix. After postmultiplying both sides of Eq. (31) by $\underline{H}$, we obtain

$$\underline{\Gamma}^{-1/2}\ \underline{D}^{+}\ \underline{G}\ \underline{D}\ \underline{\Gamma}^{-1/2}\ \underline{H} = \underline{H} \tag{32}$$

Now we substitute $\underline{H}$, as given by Eq. (30), into Eq. (32)

$$\underline{\Gamma}^{-1/2}\ \underline{D}^{+}\ \underline{G}\ \underline{D}\ \underline{\Gamma}^{-1/2}\ \underline{\Gamma}^{1/2}\ \underline{D}^{+}\ \underline{F}\ \underline{D}\ \underline{\Gamma}^{1/2} = \underline{H} \tag{33}$$

Since $\underline{D}$ is orthogonal, Eq. (33) becomes

$$\underline{\Gamma}^{-1/2}\ \underline{D}^{+}\ \underline{G}\ \underline{F}\ \underline{D}\ \underline{\Gamma}^{1/2} = \underline{H} \tag{34}$$

Since $\underline{H}$ is symmetric, it can be diagonalized by the Jacobi method (step III)

$$\underline{C}^{+}\ \underline{H}\ \underline{C} = \underline{\Lambda} \tag{35}$$

Notice that after finding the matrix $\underline{C}$ which diagonalizes $\underline{H}$ we can obtain the eigenvectors of $(\underline{G}\ \underline{F})$ by simply observing that

$$\underline{C}^{+}\ \underline{\Gamma}^{-1/2}\underline{D}^{+}\ \underline{G}\ \underline{F}\ \underline{D}\ \underline{\Gamma}^{1/2}\ \underline{C} = \underline{\Lambda} \tag{36}$$

Therefore, the eigenvectors of $(\underline{G}\ \underline{F})$ will be (step IV)

$$\underline{D}\ \underline{\Gamma}^{1/2}\ \underline{C} = \underline{L} \quad \text{or} \tag{37}$$

$$\underline{W}\ \underline{C} = \underline{L} \tag{38}$$

Up to this point, we have considered only the calculation of vibrational frequencies and normal modes from an assumed force field $\underline{F}$, the atomic masses and the equilibrium molecular geometry. We shall briefly consider now the reverse process, that is, the calculation of the force field and normal modes from the observed vibrational frequencies, the atomic masses and the equilibrium molecular geometry [28]. The solution of this problem is not a straightforward procedure [25]. In a nonlinear N-atomic molecule there are 3N-6 normal modes of vibration, but (3N-6)(3N-5)/2 independent force constants in the general harmonic force field. Obviously this number is much larger than the number of observed frequencies for a single molecule. For very simple molecules, the general harmonic force field can be obtained by using experimental frequencies from isotopic derivatives or other additional experimental data (such as Coriolis and centrifugal distortion

constants). For most molecules, however, the number of experimental data available is usually smaller than the number of force constants to be calculated and in order to make the problem solvable, one usually must assume that certain force constants can be neglected. As usual one starts with a simple model force field (valence force field or Urey-Bradley type) obtained by transfer of force constants from related molecules and makes use of the overlay least squares procedure to fit the observed frequencies. Since detailed presentations of this method have been given elsewhere [22,24-26], we shall only summarize the sequential steps used in this iterative process.

We shall first start with an initial force field $\underline{F}^{o}$, which can be obtained, for instance, by transfer of some of the force constants from related molecules.

We next solve the vibrational eigenvalue problem for the eigenvalues $\lambda_k$'s and eigenvectors $\underline{L}$ using the initial force field, $\underline{F}^{o}$ [28]. From $\underline{L}$ we can compute the Jacobian matrix, $\underline{J}$, the elements of which are the partial derivatives of $\lambda_k$'s with respect to the force constants

$$J_{k,ij} = \frac{\partial \lambda_k}{\partial F_{ij}} \tag{39}$$

It can be shown [28], that the difference between the observed and calculated eigenvalues, $\underline{\delta\lambda}$, is related to the first order correction to $\underline{F}$, according to

$$\underline{\delta\lambda} = \underline{J}\ \underline{\delta F} \tag{40}$$

The weighted least squares solution of Eq. (40) is then obtained

$$\underline{\delta F} = (\underline{J}^{\dagger}\ \underline{W}\ \underline{J})^{-1}\ \underline{J}^{\dagger}\ \underline{W}\ \ \underline{\delta\lambda} \tag{41}$$

where $\underline{W}$ is a diagonal matrix of weighting factors. This first order correction, $\delta\underline{F}$, is applied to the previous force constants to give a new matrix $\underline{F}$

$$\underline{F} = \underline{F}^{o} + \delta\underline{F} \tag{42}$$

Since Eq. (40) is an approximation derived from the assumption that $\delta\underline{\lambda}$ is a linear function of $\delta\underline{F}$, the cycle must be restarted, using now the new matrix $\underline{F}$ obtained in the previous stage. $\underline{J}$ and $\delta\underline{F}$ are recalculated and the process is repeated for each cycle until the calculation converges to an optimum set of force constants giving the best fit to the observed frequencies.

The elements of the $\underline{F}$ matrix can be expressed in terms of a chosen set of force constants $\phi$ by the relation [26]

$$F_{jk} = \sum_{\ell} Z_{jk\ell}\,\phi_{\ell} \tag{43}$$

Equation (43) can be represented in matrix notation as

$$\underline{F} = \underline{Z}\,\underline{\phi} \tag{44}$$

where $\underline{Z}$ is a retangular matrix of dimension nxm where n is the number of force constants in the $\underline{F}$ matrix and m in the number of parameters in $\phi$. Upon differentiation of Eq.(44),we obtain

$$\delta\underline{F} = \underline{Z}\,\delta\underline{\phi} \tag{45}$$

Substitution of Eq. (45) into Eq. (40) gives

$$\delta\underline{\lambda} = \underline{J}\,\underline{Z}\,\delta\underline{\phi} \tag{46}$$

hence, the weighted least squares solution of Eq. (46) give the normal equations

$$\underline{Z}^{\dagger}\,\underline{J}^{\dagger}\,\underline{W}\,\delta\underline{\lambda} = (\underline{Z}^{\dagger}\,\underline{J}^{\dagger}\,\underline{W}\,\underline{J}\,\underline{Z})\delta\underline{\phi} \tag{47}$$

Finally, the solution of Eq. (47), $\delta\underline{\phi}$, is obtained provided

that $(\underline{Z}^{+}\ \underline{J}^{+}\ \underline{W}\ \underline{J}\ \underline{Z})$ is nonsingular

$$\delta\phi = (\underline{Z}^{+}\ \underline{J}^{+}\ \underline{W}\ \underline{J}\ \underline{Z})^{-1}(\underline{Z}^{+}\ \underline{J}^{+}\ \underline{W}\ \delta\lambda) \qquad (48)$$

Failures to converge are in general due to a poor model force field, $\underline{F}^{o}$, or to singularity or near-singularity in the normal equations [26].

It is important to point out that the number of force constants to be refined should be much less than the number of observed frequencies, if meaningful results are to be achieved. Zerbi [25] has suggested that in order to assure convergence toward a statistically well defined set of parameters, one should do the calculations only when the ratio of number of experimental data to the number of parameters approximates 4 or 3.

## Intensity Relations

The theory of atomic polar tensors (APTs) was originally introduced by Biarge, Herranz and Morcillo [1]. Since, then, it has been reformulated [2] and used extensively by Person and coworkers for the analysis of infrared intensities of fluorine containing molecules, such as, $CF_x H_{4-x}$ [29], $SF_6$ and $UF_6$ [30], $XF_5$ [31,32] and the first organic molecules of the family of alkanes [33], alkyl halides [34] and ketones, alcohols, aldehydes and ethers [35].

In this theory, a tensor, $\underline{P}_r^{(\alpha)}$, associated with atom $\alpha$, gives the contribution to the change in the total molecular dipole moment, $\Delta\vec{p}$, due to a small displacement, $\vec{r}_\alpha$, of the nucleus $\alpha$ [1]. It is assumed that a linear dependence between $\Delta\vec{p}$ and $\vec{r}_\alpha$ exists for small nuclear displacements and that the simultaneous displacements of the nuclei have an additive effect on the total molecular dipole moment

change, $\Delta\vec{p}$. Therefore, we can write

$$\Delta\vec{p} = \sum_{\alpha=1}^{N} \underline{P}_x^{(\alpha)} \vec{r}_\alpha \tag{49}$$

for N atomic nuclei of the molecule.

In the space-fixed Cartesian coordinate system, the atomic polar tensor for the $\alpha$th atom of the molecule is given by

$$\underline{P}_x^{(\alpha)} = \begin{pmatrix} \partial p_x/\partial x_\alpha & \partial p_x/\partial y_\alpha & \partial p_x/\partial z_\alpha \\ \partial p_y/\partial x_\alpha & \partial p_y/\partial y_\alpha & \partial p_y/\partial z_\alpha \\ \partial p_z/\partial x_\alpha & \partial p_z/\partial y_\alpha & \partial p_z/\partial z_\alpha \end{pmatrix} \tag{50}$$

here $p_x$, $p_y$, and $p_z$ are the components of the total molecular dipole moment, p, on the space-fixed Cartesian coordinate system.

The total molecular polar tensor is formed by juxtaposition of the individual atomic polar tensors, $\underline{P}_x^{(\alpha)}$, according to

$$\underline{P}_x = \{\underline{P}_x^{(1)} \mid \underline{P}_x^{(2)} \mid \ldots \mid \underline{P}_x^{(\alpha)} \mid \ldots \mid \underline{P}_x^{(N)}\} \tag{51}$$

To transform the total molecular polar tensor $\underline{P}_x$ in space-fixed Cartesian coordinate to normal coordinate space [2], we shall use the ($\underline{A}$ $\underline{L}$) transformation matrix, obtained from the normal coordinate analysis, as given previously in Eq. (23)

$$\underline{P}_Q = \underline{P}_x \underline{A} \underline{L} \tag{52}$$

$$= \underline{P}_x \underline{M}^{-1} \underline{B}^{\dagger} \underline{F} \underline{L} \underline{\Lambda}^{-1} \tag{53}$$

here $\underline{P}_x$ has units of e, $\underline{A}$ is unitless and $\underline{L}$ has units of $u^{-1/2}$ (see also Table 2-1).

The integrated molar absorption coefficien, $A_k$, associated with the kth normal mode is related to the square of the absolute value of the total dipole moment derivative with respect to the kth

normal coordinate by [36]

$$A_k = (N\pi d_k/3c^2)\left|\partial\vec{p}/\partial Q_k\right|^2 \tag{54}$$

here N is Avogadro's number, $d_k$ is the degeneracy of the kth fundamental mode and c is the velocity of light. When $A_k$ is expressed in km/mole [2], Eq. (54) becomes

$$A_k = 976.6\left|\partial\vec{p}/\partial Q_k\right|^2 \tag{55}$$

$$= 976.6\left[\left(\frac{\partial p_x}{\partial Q_k}\right)^2 + \left(\frac{\partial p_y}{\partial Q_k}\right)^2 + \left(\frac{\partial p_z}{\partial Q_k}\right)^2\right] \tag{56}$$

where $\frac{\partial p_x}{\partial Q_k}$, $\frac{\partial p_y}{\partial Q_k}$ and $\frac{\partial p_z}{\partial Q_k}$ are the components of the dipole moment vector $(\partial\vec{p}/\partial Q_k)$ along each of the space-fixed Cartesian axes, and each has units of $e\,u^{-1/2}$.

The 3 x (3N-6) $\underline{P}_Q$ matrix of the dipole moment derivatives with respect to the normal coordinates are formed by juxtaposition of each individual column vector, $\underline{P}_{Q_k}$ [2]

$$\underline{P}_Q = \{\underline{P}_{Q_1} \mid \underline{P}_{Q_2} \mid \cdots \mid \underline{P}_{Q_k} \mid \cdots \underline{P}_{Q_{3N-6}}\} \tag{57}$$

$$= \begin{pmatrix} \partial p_x/\partial Q_1 & \cdots & \partial p_x/\partial Q_{3N-6} \\ \partial p_y/\partial Q_1 & \cdots & \partial p_y/\partial Q_{3N-6} \\ \partial p_z/\partial Q_1 & \cdots & \partial p_z/\partial Q_{3N-6} \end{pmatrix} \tag{58}$$

These dipole moment derivatives with respect to the normal or Cartesian coordinates may be obtained by two methods. The first method involves the measurement of the band intensities for each fundamental mode of the molecule and requires an a priori knowledge of the direction and sign of the dipole derivatives, as is seen by inspection of Eq. (54). The experimental $\underline{P}_Q$ matrix is then formed

according to Eq. (57) and transformed to a space-fixed Cartesian coordinate to give the experimental polar tensor matrix $\underline{P}_x$. This transformation is given by [2]

$$\underline{P}_x = \underline{P}_Q \underline{L}^{-1} \underline{B} + \underline{P}_\rho \underline{\beta} \tag{59}$$

Here the $\underline{P}_\rho \underline{\beta}$ product matrix is the rotation correction term necessary to transform from the molecule-fixed normal coordinate space to the space-fixed of Cartesian coordinates [2].

In the second method, which is the main subject of the present work, the dipole moment derivatives with respect to a space-fixed Cartesian coordinate system are obtained by quantum mechanical calculations. Once the theoretical APTs have been calculated, we then form the theoretical $\underline{P}_x$ matrix according to Eq. (51). This matrix is then transformed from a space-fixed Cartesian coordinate to a normal coordinate space according to Eq. (52), and the theoretical intensities are therefore obtained by using Eq. (55).

## Description of Quantum Mechanical Calculations

We have seen in the previous section that the problem of calculating theoretical intensities reduces to the calculation of the dipole moment derivatives with respect to space-fixed Cartesian coordinates. We have used the ab initio quantum mechanical SCF method using a 4-31G basis set to obtain the APTs and infrared intensities for a series of triatomic molecules (HOF, HOO and HOCl). Our calculations were performed using the program GAUSSIAN 70 [37] developed by Pople and coworkers [38-43]. The 4-31G basis set, which has been extensively used by Pople and coworkers [40-42],

is an extended basis of atomic orbitals expressed as fixed linear combinations of Gaussian functions. In this basis, each inner atomic orbital is represented as a linear combination of four Gaussian functions and each valence orbital is split into an inner part represented by three Gaussian functions and an outer part described by one Gaussian function. The contraction coefficients and exponents of the Gaussian functions used in the program GAUSSIAN 70, and therefore in this work, were obtained by minimizing the energy calculated for the atomic ground state of the first and second row atoms as reported in references [40-42]. The SCF calculations are based on the restricted Hartree-Fock formalism for closed-shell molecules and spin-unrestricted Hartree-Fock formalism for open-shell species [37].

To allow more flexibility of the Gaussian atomic orbitals in representing changes in orbital size in different molecular environments these atomic orbitals are replaced by rescaled forms [40], and the $\zeta$-scale factors are varied to minimize the total molecular energy. Only the inner and outer parts of the valence shell were optimized [40-42]. We have used the standard valence-shell scale factors taken as the average value of the optimum scale factors obtained from the series of molecules studied [40,41]. An optional subroutine has been also provided in program GAUSSIAN 70 to optimize these scale factors for any molecular calculation, in general, involving first and second row atoms. However, the study of Pople and coworkers [40-42] based on a series of nine molecules also indicates that the range of optimum valence-shell scale factors is quite small which justifies the use of standard scale factors. Also no polarization functions have been introduced in our calculations.

A minimum basis set, such as STO nG(n = 1, ..., 6) is also available in program GAUSSIAN 70. However, it has been shown [44] that the STO nG sets are very poor in predicting vibrational properties, and therefore no attempts have been made here to use the STO nG sets for calculation of dipole moment derivatives. It has also been shown [44] that only calculations with extended basis sets predict intensities within the experimental uncertainties.

We have used in our ab initio calculations the experimental equilibrium geometry instead of the theoretical calculated geometry. Pulay [45] has pointed out that this should be the recommended procedure. He has shown that calculation of force constants at the experimental geometry not only yields better results, but also requires less computational work. Notice also that we are interested in differences between the dipole moment calculated at a certain nuclear displacement and at the equilibrium configuration, and therefore, the use of experimental geometries is not expected to produce any substantial effect in the calculated dipole moment derivatives. Schwendeman [46] has also pointed out that the experimental equilibrium geometry should be used for quantum mechanical calculation of spectroscopic parameters, since use of the theoretical calculated equilibrium geometry may lead to errors in the calculated spectroscopic parameters.

Let us now consider how we calculated the ab initio APT elements of the $\underset{\sim}{P}_x^{(\alpha)}$ matrix given by Eq. (50) for the $\alpha$th atom. The APT elements of the $\underset{\sim}{P}_x^{(\alpha)}$ matrix were obtained in separate calculations by displacing the $\alpha$th atom from its equilibrium configuration by

by +0.02 Å and -0.02 Å along the x, y and z coordinate axes, and taking the average value of the dipole moment derivatives calculated at plus and minus displacements for each element of the tensor. Let us consider, for instance, the calculation of the dipole moment derivatives for the elements of the first column of the $\underset{\sim}{P}_x^{(\alpha)}$ matrix. We have approximated the dipole derivatives as

$$\frac{\partial \vec{p}_i}{\partial x_\alpha} \simeq \frac{\Delta \vec{p}_i}{\Delta x_\alpha} = \frac{\langle \Psi_{el} | \hat{p} | \Psi_{el} \rangle_i - \langle \Psi_{el} | \hat{p} | \Psi_{el} \rangle_{i_o}}{\Delta x_\alpha} \tag{60a}$$

Here $\langle \Psi_{el} | \hat{p} | \Psi_{el} \rangle_i$ represent the ith component (i = x, y, or z) of the total electric dipole moment of the molecule when the $\alpha$th atom is displaced from its equilibrium configuration by +0.02 Å or -0.02 Å, $\langle \Psi_{el} | \hat{p} | \Psi_{el} \rangle_{i_o}$ represent the $i_o$ ($i_o = x_o, y_o$, or $z_o$) component of the total electric dipole moment of the molecule, calculated at equilibrium molecular configuration, $\Psi_{el}$ is the electronic wave function for the molecular ground state, p is the electric dipole moment operator and $\Delta x_\alpha = x_i - x_o = \pm 0.02$ Å.

Similarly, the second and third columns of $\underset{\sim}{P}_x^{(\alpha)}$ were obtained

$$\frac{\partial \vec{p}_i}{\partial y_\alpha} \simeq \frac{\Delta \vec{p}_i}{\partial y_\alpha} = \frac{\langle \Psi_{el} | \hat{p} | \Psi_{el} \rangle_i - \langle \Psi_{el} | \hat{p} | \Psi_{el} \rangle_{i_o}}{\Delta y_\alpha} \tag{60b}$$

and

$$\frac{\partial \vec{p}_i}{\partial z_\alpha} \simeq \frac{\Delta \vec{p}_i}{\Delta z_\alpha} = \frac{\langle \Psi_{el} | \hat{p} | \Psi_{el} \rangle_i - \langle \Psi_{el} | \hat{p} | \Psi_{el} \rangle_{i_o}}{\Delta z_\alpha} \tag{60c}$$

where $\Delta y_\alpha = y_i - y_o = \pm 0.02$ Å and $\Delta z_\alpha = z_i - z_o = \pm 0.02$ Å.

We may therefore represent the dipole moment derivatives as

$$\frac{\partial \vec{p}_i}{\partial j_\alpha} \simeq \frac{\Delta \vec{p}_i}{\Delta j_\alpha} = \frac{\langle \Psi_{el} | \hat{p} | \Psi_{el} \rangle_i - \langle \Psi_{el} | \hat{p} | \Psi_{el} \rangle_i}{\Delta j_\alpha} \quad (61)$$

where j = (x, y,or z).

## Transferred APTs

We shall consider now the transferability of experimental APTs and how we also predicted the infrared intensities for some of the molecules studied here.

We have pointed out previously that the APTs in normal coordinate space for each atom of a molecule can be determined experimentally. We have also indicated how the experimental $\underline{P}_Q$ matrix is transformed to the $\underline{P}_x$ matrix. This transformation yields the intensity parameters (the experimental APTs in space-fixed Cartesian coordinate) which can be transferred from one molecule to another, provided they are transferred from chemically similar environments. We have properly transferred some of the experimental polar tensors from atoms of simple model molecules, such as, $CH_3\underline{Cl}$, $\underline{Cl}CN$, $\underline{H}_2O$, $CH_3\underline{OH}$, etc., to the terminal atoms of the molecules studied here (HOF, $HO_2$, and HOCl) and calculated the polar tensor of the central atom using the null matrix relation [2]

$$\sum_{\alpha=1}^{N} \underline{P}_x^{(\alpha)} = \underline{0} \quad (62)$$

for N atoms of the molecule. (Here N is equal to 3). The polar tensor for the central atom is not expected to be transferable due to the uniqueness of the chemical environment of the central atom of a molecule.

The experimental APT of a particular atom of a molecule (which was called here the model molecule) was transferred in a bond coordinate system for both atoms involved (the atom of the model molecule and the atom to which the APT was transferred). The bond coordinate system containing that particular atom was then rotated to the space-fixed Cartesian coordinate system of the particular molecule studied [29]. The APT for both terminal atoms were then transferred in the bond coordinate system and the polar tensor of the central atom was obtained using Eq. (62). The $\underline{P}_x$ matrix was then formed according to Eq. (51) and transformed to $\underline{P}_Q$ using Eq. (52) as indicated previously. Equation (55) was then used to calculate the intensities for each fundamental band of the molecules studied.

The infrared intensities as calculated from ab initio APTs shall be compared with the intensities predicted via transferred APTs as discussed in this section and shall be the subject of the next chapter.

CHAPTER 3
TRIATOMIC HOX MOLECULES

## Hydrogen Hypofluorite

We may now apply the equations presented in Chapter 2 to calculate the theoretical intensities for HOF. By inspection of Eq. (53) given in Chapter 2, we see that the matrices $\underline{P}_x$, $\underline{M}^{-1}$, $\underline{B}^{+}$, $\underline{F}$, $\underline{L}$ and $\underline{\Lambda}^{-1}$ have first to be evaluated in order to obtain the $\underline{P}_Q$ matrix. Once the $\underline{P}_Q$ matrix has been evaluated, the theoretical intensity for each fundamental band of HOF is then calculated using Eq. (56).

The normal coordinate analysis was carried out using the programs WMAT and CHARLY [27] from the Molecular Spectroscopy Laboratory at the University of Minnesota. The programs were originally written for the CDC 6400 computer and were revised by Sanchez [47] for use on the IBM 370/165 computer at the University of Florida.

The 4-31G calculations of dipole moment derivatives were carried out using the QCPE program GAUSSIAN 70 [37]. The intensity calculations were performed using program PVDTEN, developed by Newton [48].

### Normal Coordinate Analysis

To calculate $\underline{M}^{-1}$, $\underline{B}^{+}$, $\underline{F}$, $\underline{L}$ and $\underline{\Lambda}^{-1}$, a normal coordinate analysis was performed using the equilibrium molecular geometry from Kim,

Pearson and Appelman [49]. Figure 3-1 defines the coordinates for HOF. The structural parameters obtained by those authors were r(OH) = 0.964 Å, r(OF) = 1.442 Å and θ(HOF) = 97.2° [49]. These parameters were obtained from the analysis of the microwave spectrum of HOF. Using these geometrical parameters we calculate the equilibrium position vector for the HOF molecule, given in Table 3-1. These equilibrium position vectors for all of the atoms of HOF, were used to form the column vector, $\underline{X}$, given by Eq. (2). This column vector, the masses of the atoms (H = 1.007825, O = 15.994910, F = 18.998405 in amu), the description of the internal coordinates and the $\underline{U}$ matrix were used as input to the computer program WMAT [27] to obtain the $\underline{B}$ and $\underline{G}$ matrices (for a triatomic molecule, belonging to the $C_s$ symmetry point group, such as HOF, the $\underline{U}$ matrix is the identity matrix, $\underline{I}_3$, and the internal coordinates are therefore the symmetry coordinates of the molecule). In Table 3-2, we present the $\underline{B}$ matrix for HOF. Program WMAT also diagonalizes the $\underline{G}$ matrix and forms the $\underline{W}$ matrix according to Eq. (28). The $\underline{F}$ matrix was taken from Ogilvie [50]. It was obtained by fitting the observed infrared frequencies for HOF and DOF, using a multiple regression technique [50]. The $\underline{F}$ matrix is given in Table 3-3. The $\underline{W}$ matrix obtained from program WMAT and the $\underline{F}$ matrix were then used as input to program CHARLY [27] to obtain the eigenvectors, $\underline{L}$, and eigenvalues, $\underline{\Lambda}$, of the $\underline{G}\,\underline{F}$ product matrix. The $\underline{L}$ matrix and the calculated vibration wavenumbers of HOF are shown in Tables 3-4 and 3-5, respectively. Table 3-5 also includes the experimental values for

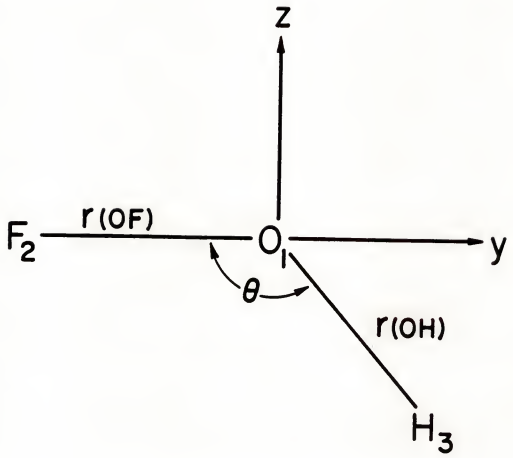


Fig. 3-1. Coordinate system and atom numbering for HOF.

TABLE 3-1
EQUILIBRIUM POSITION VECTORS FOR HOF (UNITS ARE Å)

| Atom No.[a] | x | y | z |
|---|---|---|---|
| 1 | 0.0 | 0.0 | 0.0 |
| 2 | 0.0 | -1.442000 | 0.0 |
| 3 | 0.0 | 0.120821 | -0.956399 |

[a]The atom numbering and coordinate system are given in Fig. 3-1.

TABLE 3-2
THE $\underline{B}$ MATRIX FOR HOF

| | | | | | | | | |
|---|---|---|---|---|---|---|---|---|
| 0.0 | 1.0 | 0.0 | 0.0 | -1.0 | 0.0 | 0.0 | 0.0 | 0.0 |
| 0.0 | -1.029163 | -0.823495 | 0.0 | 0.0 | 0.693482 | 0.0 | 1.029163 | 0.130013 |
| 0.0 | -0.125333 | 0.992115 | 0.0 | 0.0 | 0.0 | 0.0 | 0.125333 | -0.992115 |

Note: All elements of $\underline{B}$ are unitless since we have used a weighted unit system (see also Table 2-1). Notice also that $\underline{B} = \underline{B}$, since the $\underline{U}$ matrix is the identity matrix in this case.

TABLE 3-3
THE EXPERIMENTAL $\underline{F}$ MATRIX FOR HOF (UNITS ARE MDYNE $\text{Å}^{-1}$)

| | | |
|---|---|---|
| 4.3276 | 0.4999 | 0.0 |
| 0.4999 | 0.9330 | 0.1000 |
| 0.0 | 0.1000 | 7.2055 |

Note: $F_{11} = F_{r(OF)}$; $F_{12} = F_{r(OF),\theta}$; $F_{22} = F_{\theta}$; $F_{23} = F_{r(OH),\theta}$ and $F_{33} = F_{r(OH)}$. This $\underline{F}$ matrix was taken from Ogilvie [50]. Notice that the following force constants given by Ogilvie are scaled by the OF and OH bond lengths of HOF, according to: $F'_{\theta} = F_{\theta}/r_1\, r_2$, $F'_{r_1\theta} = F_{r_1\theta}/r_1$ and $F'_{r_2\theta} = F_{r_2\theta}/r_2$, where $r_1$ and $r_2$ are the OH and OF bond lengths respectively and the prime indicates here the scaled force constants given by Ogilvie. In addition, the force constants reported by Ogilvie are in N $m^{-1}$ and we have transformed those force constants to our units, using the relation: $F_{ij}(\text{N m}^{-1}) \times 10^{-2} = F_{ij}(\text{mdyne Å}^{-1})$. Finally, notice also that $\underline{F} = \underline{F}$ in this case, since the $\underline{U}$ matrix is the identity matrix.

TABLE 3-4
THE $\underline{L}$ MATRIX FOR HOF (UNITS ARE $u^{-1/2}$)

| | | |
|---|---|---|
| -0.009048 | 0.004638 | 0.339193 |
| -0.030387 | -1.081596 | -0.175716 |
| 1.026951 | 0.010244 | 0.004151 |

Note: Here $\underline{L} = \underline{L}$, since the $\underline{U}$ matrix is the identity matrix in this case.

TABLE 3-5
OBSERVED AND CALCULATED VIBRATIONAL WAVENUMBERS
FOR HOF(UNITS ARE $cm^{-1}$)

| Mode[a] | Observed[b] | Calculated[c] | Percent error[d] |
|---|---|---|---|
| $\nu_1$(OH) | 3578.5 | 3591.23 | 0.36 |
| $\nu_2$(Δθ) | 1354.8 | 1357.47 | 0.20 |
| $\nu_3$(OF) | 889.0 | 890.63 | 0.18 |

[a] Here $\nu_1$(OH) refers to the OH stretching mode, $\nu_2$(Δθ) to the bending mode and $\nu_3$(OF) to the OF stretching band.
[b] The experimental vibration wavenumbers of HOF in gas phase are given in ref. [51].
[c] The wavenumbers were calculated using the equilibrium molecular geometry given in ref. [49] and the force field obtained from ref. [50].
[d] [ν(calc.)-ν(obs.)] x 100/ν(obs.)

the vibrational wavenumbers of HOF in gas phase as given by Appelman and Kim [51].

Ab Initio 4-31G APTs and Calculated Intensities for HOF

We have carried out an ab initio quantum mechanical calculation, with a 4-31G basis, of the atomic polar tensors (APTs) for HOF. The APTs for the oxygen, fluorine and hydrogen atoms were calculated according to the procedure described in Chapter 2. Once the polar tensors for all of the atoms have been calculated, we constructed the $\underline{P}_x$ matrix using Eq. (51). Notice also, that the APTs for all of the atoms of HOF were calculated relative to the coordinate system shown in Fig. 3-1. In constructing the $\underline{P}_x$ matrix, the juxtaposition of each individual APT follows the same order of atom numbering shown also in Fig. 3-1. The ab initio APTs for HOF are presented in Table 3-6. The intensities for each fundamental band of HOF calculated from these ab initio 4-31G APTs are presented in Table 3-7. The comparison with experimental relative intensities for HOF and the simulated spectrum will be discussed in the next section.

We have also calculated the charge, charge-flux and overlap contributions to the total APT for HOF, according to the CCFO model developed by King [52] and extended by Zilles [53]. The charge, charge-flux and overlap (CCFO) model has been discussed in detail in reference[53]and here we need only to point out the tensor contribution terms to the ab initio APT and its physical significance. In this model the tensor contributions result from the exact quantum mechanical definition of the APT, within the LCAO-MO formalism.

TABLE 3-6

AB INITIO APTs FOR HOF (UNITS ARE e, WHERE 1e = 1.602 x $10^{-19}$ C)

$$\underset{\sim}{P}_x^O \begin{pmatrix} -0.368 & 0 & 0 \\ 0 & 0.174 & 0.228 \\ 0 & -0.020 & -0.068 \end{pmatrix}$$

$$\underset{\sim}{P}_x^F \begin{pmatrix} -0.129 & 0 & 0 \\ 0 & -0.437 & -0.157 \\ 0 & 0.046 & -0.169 \end{pmatrix}$$

$$\underset{\sim}{P}_x^H \begin{pmatrix} 0.497 & 0 & 0 \\ 0 & 0.263 & -0.071 \\ 0 & -0.026 & 0.237 \end{pmatrix}$$

Note: We have used a 4-31G basis set for the ab initio calculation of the APTs for HOF. The $\underset{\sim}{P}_x^O$ tensor was calculated using the null condition. The coordinate system is shown in Fig. 3-1.

TABLE 3-7
ABSOLUTE INTENSITIES AND EXPERIMENTAL RELATIVE INTENSITIES OF HOF(UNITS ARE km $mole^{-1}$)

| Band | $\nu(cm^{-1})$ | A(4-31G)[a] | A(Expl.)[b] |
|---|---|---|---|
| $\nu_1$(OH) | 3578.5 | 66.1 | (66.1) |
| $\nu_2(\Delta\theta)$ | 1354.8 | 53.6 | 39.6 |
| $\nu_3$(OF) | 889.0 | 11.3 | 8.7 |

[a]Calculated intensities from the ab initio 4-31G APTs given in Table 3-6.

[b]The experimental intensity for the OH stretching band was scaled to fit the intensity of $\nu_1$(OH) shown in parentheses as calculated from the ab initio 4-31G APTs. Hence, the intensities for the bending and OF stretching modes are relative band intensities (see discussion in the next section).

Accordingly, the APT of a given atom A is defined as the transpose of the gradient of the dipole moment vector with respect to the displacements of the A atom. As a result of analyzing this gradient, the total APT is broken down into three tensor contributions: the charge, charge-flux and overlap APTs.

The charge tensor contribution to the total APT on A is given according to

$$\underset{\sim}{P}_{x}^{A}\,(C) = \begin{pmatrix} Q_A & 0 & 0 \\ 0 & Q_A & 0 \\ 0 & 0 & Q_A \end{pmatrix} \qquad (63)$$

here $Q_A = Z_A - N_A$, where $Q_A$ is the gross atomic charge on atom A at equilibrium molecular configuration, $Z_A$ is the charge on nucleus A and $N_A$ is the Mulliken gross atomic population on atom A [54,55]. Therefore, the charge APT gives the contribution to the total APT from the gross atomic charge associated with A, at the equilibrium molecular configuration.

The charge-flux tensor contribution to the total APT on atom A is given by [52]

$$\underset{\sim}{P}_{x}^{A}\,(CF) = \sum_{\alpha} \vec{R}_{\alpha}\,(\nabla^{A} Q_{A})^{\dagger} \qquad \alpha = A, B, C, \ldots \qquad (64)$$

where $\vec{R}_{\alpha}$ is the position vector of nucleus $\alpha$, $(\nabla^{A} Q_{\alpha})^{\dagger}$ is the transpose of the gradient of the gross atomic charge on atom $\alpha$ and the summation is over all the atoms in the molecule. The charge-flux tensor reflects the electronic charge redistribution resulting from nuclear displacement. Expanding Eq. (64) for a triatomic

molecule, we obtain the charge-flux contribution to the total APT for atom A as the following sum of matrix products

$$\underline{P}_x^A(CF) = \begin{pmatrix} x_A \\ y_A \\ z_A \end{pmatrix} \begin{pmatrix} \frac{\partial Q_A}{\partial x_A} & \frac{\partial Q_A}{\partial y_A} & \frac{\partial Q_A}{\partial z_A} \end{pmatrix} + \begin{pmatrix} x_B \\ y_B \\ z_B \end{pmatrix} \begin{pmatrix} \frac{\partial Q_B}{\partial x_A} & \frac{\partial Q_B}{\partial y_A} & \frac{\partial Q_B}{\partial z_A} \end{pmatrix} + \begin{pmatrix} x_C \\ y_C \\ z_C \end{pmatrix} \begin{pmatrix} \frac{\partial Q_C}{\partial x_A} & \frac{\partial Q_C}{\partial y_A} & \frac{\partial Q_C}{\partial z_A} \end{pmatrix} \tag{65}$$

here the derivatives were approximated as $\frac{\partial Q_i}{\partial j_A} \simeq \frac{\Delta \bar{Q}_i}{\Delta j_A}$, where i=(A,B, or C) and j=(x,y, or z). The averaged terms $\frac{\Delta \bar{Q}_i}{\partial j_A}$ were calculated from the differences in the Mulliken gross atomic populations of each atom from the calculation at equilibrium molecular configuration, $Q_i^o$, and those from calculations made for plus and minus displacements of the atom A, by 0.02 Å along the x, y and z axes; for example

$$\frac{\Delta \bar{Q}_i}{\Delta j_A} = \frac{1}{2} \left[ \left( \frac{Q_i - Q_i^o}{\Delta j_A} \right)_+ + \left( \frac{Q_i - Q_i^o}{\Delta j_A} \right)_- \right] \tag{66}$$

here the + and - subscripts indicate that those quantities were calculated at + and - displacements respectively.

The overlap tensor $\underline{P}_x^A$ (O) is a quantum mechanical term which has no classical analogue [52,53] and represents the contribution of the hybridization effects (among others) to the changes in the

dipole moment vectors, as the molecule vibrates. Here, this tensor was calculated as the difference between the total APT and the sum of the charge and charge-flux contributions, according to Eq. (62), [53]

$$\underline{P}_x^A\ (O) = \underline{P}_x^A\ (\text{TOTAL}) - (\underline{P}_x^A\ (C) + \underline{P}_x^A\ (CF)) \qquad (67)$$

notice that similar expressions can be given for all the other atoms in the molecule.

The charge, charge-flux and overlap contributions to the ab initio 4-31G APTs for the atoms in HOF are given in Tables 3-8, 3-9 and 3-10, respectively, using the coordinate system shown in Fig. 3-1. We shall discuss these results further in Chapter 4.

Predicted and Experimental Computer-Simulated Spectra of Matrix-Isolated HOF

The band shapes [56] in the infrared spectrum of the matrix-isolated HOF were represented by the Gaussian functions

$$a(\nu) = a_{max} \exp\left[\frac{-4(\nu-\nu_o)^2 \ln 2}{\Delta\nu_{1/2}}\right] \qquad (68)$$

Here, $a(\nu)$ is the absorbance at wavenumber $\nu$, $a_{max}$ is the maximum absorbance of the band at $\nu_o$, the wavenumber at the band origin, and $\Delta\nu_{1/2}$ is the full width (in $cm^{-1}$) at half-maximum (FWHM) of the absorption band. The maximum absorbance is related to the total integrated intensity for this Gaussian line shape function by

$$\int_{\text{Band}} a(\nu)d\nu = \sqrt{\pi}(4 \ln 2)^{-1/2}\, a_{max}\, \Delta\nu_{1/2} = 1.0645\, a_{max}\, \Delta\nu_{1/2} \qquad (69)$$

TABLE 3-8
CHARGE, CHARGE-FLUX, OVERLAP AND TOTAL APT ON THE HYDROGEN ATOM OF HOF(UNITS ARE e).

$$\underline{P}_x^H\ (C) \quad \begin{pmatrix} 0.45 & 0 & 0 \\ 0 & 0.45 & 0 \\ 0 & 0 & 0.45 \end{pmatrix}$$

$$\underline{P}_x^H\ (CF) \quad \begin{pmatrix} 0 & 0 & 0 \\ 0 & -0.17 & -0.08 \\ 0 & 0.01 & 0.17 \end{pmatrix}$$

$$\underline{P}_x^H\ (O) \quad \begin{pmatrix} 0.04 & 0 & 0 \\ 0 & -0.02 & 0.01 \\ 0 & -0.03 & -0.39 \end{pmatrix}$$

$$\underline{P}_x^H\ (T) \quad \begin{pmatrix} 0.50 & 0 & 0 \\ 0 & 0.26 & -0.07 \\ 0 & -0.03 & 0.24 \end{pmatrix}$$

Note: The charge (C), charge-flux (CF) and overlap (O) contributions to the total (T) 4-31G APT on the hydrogen atom were calculated according to the CCFO model [52,52]. The coordinate system is shown in Fig. 3-1.

TABLE 3-9
CHARGE, CHARGE-FLUX, OVERLAP AND TOTAL APT ON THE FLUORINE ATOM OF HOF(UNITS ARE e).

| | | | |
|---|---|---|---|
| $\underline{P}_x^F$ (C) | -0.21 | 0 | 0 |
| | 0 | -0.21 | 0 |
| | 0 | 0 | -0.21 |
| $\underline{P}_x^F$ (CF) | 0 | 0 | 0 |
| | 0 | 0.12 | -0.12 |
| | 0 | 0.03 | 0.02 |
| $\underline{P}_x^F$ (O) | 0.08 | 0 | 0 |
| | 0 | -0.35 | -0.04 |
| | 0 | 0.01 | 0.02 |
| $\underline{P}_x^F$ (T) | -0.13 | 0 | 0 |
| | 0 | -0.44 | -0.16 |
| | 0 | 0.05 | -0.17 |

Note: The charge (C), charge-flux (CF) and overlap (O) contributions to the total (T) 4-31G APT on the fluorine atom were calculated according to the CCFO model [52,53]. The coordinate system is shown in Fig. 3-1.

TABLE 3-10
CHARGE, CHARGE-FLUX, OVERLAP AND TOTAL APT ON THE OXYGEN ATOM OF HOF(UNITS ARE e).

$\underline{P}_x^O$ (C)

$$\begin{pmatrix} -0.25 & 0 & 0 \\ 0 & -0.25 & 0 \\ 0 & 0 & -0.25 \end{pmatrix}$$

$\underline{P}_x^O$ (CF)

$$\begin{pmatrix} 0 & 0 & 0 \\ 0 & 0.06 & 0.21 \\ 0 & -0.04 & -0.19 \end{pmatrix}$$

$\underline{P}_x^O$ (O)

$$\begin{pmatrix} -0.12 & 0 & 0 \\ 0 & 0.37 & 0.03 \\ 0 & 0.02 & 0.37 \end{pmatrix}$$

$\underline{P}_x^O$ (T)

$$\begin{pmatrix} -0.36 & 0 & 0 \\ 0 & 0.19 & 0.24 \\ 0 & -0.02 & -0.06 \end{pmatrix}$$

Note: The charge (C), charge-flux (CF) and overlap (O) contributions to the total (T) 4-31G APT on the oxygen atom of HOF were calculated according to the CCFO model[52,53]. The coordinate system is shown in Fig. 3-1.

Equation (69) may also be written as

$$\int_{\text{Band}} \ln(I_o/I)d\nu = 1.0645\ a_{max}\ \Delta\nu_{1/2} \qquad (70)$$

here the absorbance $a(\nu)$ is defined as the logarithm to the base e, rather than $\log_{10}(I_o/I)$, [57]

$$a(\nu) = \ln\ (I_o/I) \qquad (71)$$

where $I_o$ and I are the intensities of the radiation before and after absorption by the sample, respectively.

The integrated molar absorption coefficient (experimental absolute intensity) of an infrared absorption band, may be defined as follows[36]

$$A_k(\text{km mole}^{-1}) = \frac{1}{100C\ell} \int_{\text{Band}} \ln(I_o/I)d\nu \qquad (72)$$

Here $A_k$ is the absolute intensity of the kth fundamental band in km $\text{mole}^{-1}$, C is the concentration of the sample in mmole $\text{cm}^{-3}$ ($\equiv$ mole $\ell^{-1}$) and $\ell$ is the cell's pathlength in cm. The factor of 100 was introduced in Eq. (72) to give $A_k$ in km $\text{mole}^{-1}$.

Equations (70) and (72) may be combined to give

$$A_k(\text{km mole}^{-1}) = 1.0645 \times 10^{-2}\ a_{max}\ \Delta\nu_{1/2}/C\ell \qquad (73)$$

where $A_k$, $a_{max}$, $\Delta\nu_{1/2}$, C, and $\ell$ have been defined previously.

Finally, we may now substitute $a_{max}$, as given by Eq. (73), into Eq. (68) to give

$$a(\nu) = \frac{93.94C\ell A_k(\text{km mole}^{-1})}{\Delta\nu_{1/2}} \exp\left[\frac{-4(\nu-\nu_o)^2 \ln 2}{\Delta\nu_{1/2}}\right] \qquad (74)$$

The predicted and experimental computer simulations of the matrix spectra of HOF were obtained according to Eq. (74), except that the absorbance values were converted to transmitances and

plotted as a function of $\nu$. The full widths at half-maximum (FWHM) for the absorption bands were estimated from values reported in reference [58] as described in Table 3-11. The absolute intensities for the three fundamental modes of HOF were calculated from the ab initio APTs of HOF. The relative intensities were obtained according to Eq. (73). The $C\ell$ parameter was adjusted until the predicted intensity of the OH stretching vibration at 3540 $cm^{-1}$ fits the observed spectrum [59], according to Eq. (73) (the reason for choosing $\nu$(OH) as the fitted band is justified at the end of this section). The value of this $C\ell$ parameter is given in Table 3-11 and was used for the computer simulation of both spectra according to Eq. (74). The relative intensities are given in Table 3-11 and the predicted and experimental spectra of the matrix-isolated HOF are shown in Fig. 3-2. We may now compare both spectra. Notice that the experimental relative intensities predicted for the bending and OF stretching modes are in remarkable agreement with the corresponding ab initio calculated intensities.

The SPECTRUM program written by Newton [60] was used to generate the spectrum shown in Fig. 3-2. This program utilizes the Gould software and plotter [61] to simulate an infrared spectrum where each band is represented by a simple Gaussian function and overlapping bands by linear combination of individual Gaussians. The input for program SPECTRUM includes the scale data information of the spectrum, the absolute intensities, the position of maximum absorption, the band limits and the full width at half-maximum intensity, for each fundamental band.

TABLE 3-11
PARAMETERS USED IN THE COMPUTER SIMULATION OF THE PREDICTED AND EXPERIMENTAL INFRARED SPECTRA OF MATRIX-ISOLATED HOF

| Predicted ($C\ell$=6.86 x $10^{-4}$ mmole $cm^{-2}$) | | | Experimental ($C\ell$=6.86 x $10^{-4}$ mmole $cm^{-2}$) | | | |
|---|---|---|---|---|---|---|
| $\nu_o$[a] ($cm^{-1}$) | $\Delta\nu_{1/2}$[b] ($cm^{-1}$) | A(abs.)[c] (km $mole^{-1}$) | $\nu_o$[a] ($cm^{-1}$) | $\Delta\nu_{1/2}$[b] ($cm^{-1}$) | A(rel.)[c] (km $mole^{-1}$) | $a_{max}$[d] |
| 3537.1 | 6.0 | 66.1 | 3537.1 | 6.0 | (66.1) | 0.71 |
| 1359.0 | 4.4 | 53.6 | 1359.0 | 4.4 | 39.6 | 0.58 |
| 886.0 | 4.0 | 11.3 | 886.0 | 4.0 | 8.7 | 0.14 |

[a] Wavenumber position of maximum absorption from the experimental matrix spectrum of HOF as reported by Goleb et al. in ref. [59].

[b] Full width at half-maximum of the band. Here we have estimated the full width at half-maximum by using the values obtained from the corresponding infrared spectrum of matrix-isolated $HO_2$ (in $A_r$ matrix) reported by Smith and Andrews in ref. [58]. The infrared spectrum of HOF in an $N_2$ matrix is reported by Goleb et al. in ref. [59]. However, the FWHM of the absorption bands of HOF are not reported in that paper.

[c] Taken from Table 3-7.

[d] The maximum absorbances, of the HOF bands as reported by Goleb et al. in ref. [59], but relative to base e. The relation between $a_{max}$ and $A_k$(rel.) is given by Eq. (73).

Fig. 3-2. Predicted and experimental computer-simulated infrared spectra of matrix-isolated HOF

(a) Computer-simulated predicted spectrum of HOF in the nitrogen matrix. The intensities were calculated from ab initio APTs. The assumed concentration of HOF is adjusted until the intensity of the OH stretching vibration at 3540 $cm^{-1}$ fits the observed spectrum.

(b) Computer simulation of the experimental HOF spectrum in the nitrogen matrix (see Fig. 3-3.

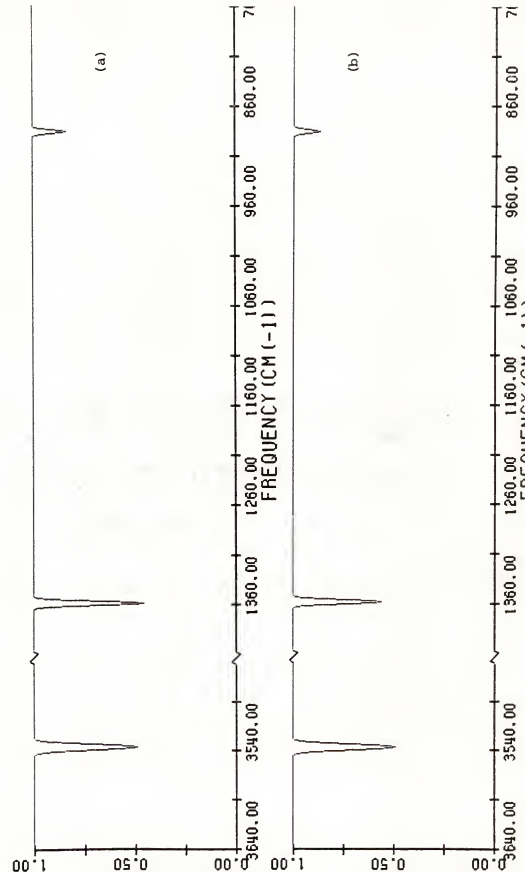
(a)
(b)
TRANSMITTANCE
1.00
0.50
0.00
3640.00
3540.00
1360.00
1260.00
1160.00
1060.00
960.00
860.00
FREQUENCY (CM(-1))

The experimental observed infrared spectrum of HOF isolated in the nitrogen matrix at 8°K [59] is shown in Fig. 3-3. The fundamental bands of HOF are seen at 3537.1 $cm^{-1}$, 1359.0 $cm^{-1}$ and 886.0 $cm^{-1}$ for the OH stretching, bending, and OF stretching modes. The bands at 3727.2 and at 1601 $cm^{-1}$ belong evidently to $H_2O$. The small band at 3880 $cm^{-1}$ is the fundamental of HF [59,62], formed from thermal decomposition of HOF before the codeposition of HOF with $N_2$ at 8°K. The small absorptions around the band at 3537 $cm^{-1}$ are believed to be due to $(H_2O)_n$ polymers and $H_2O$ hydrogen bonded to HOF or to HF [59]. The weak band at 3637 $cm^{-1}$ is the symmetric stretch ($\nu_1$) of $H_2O$. Finally, the small band at 1393 $cm^{-1}$ was assigned [59,63] to the bending mode of HOF hydrogen bonded to HF. The upper and lower spectrum shown in Fig. 3-3 were recorded at different concentrations of HOF in the $N_2$ matrix [59].

The reason for choosing the $\nu$(OH) band as the one to be fitted was based upon the reliability of the 4-31G basis set in predicting the intensity of this mode. In general, the agreement between the predicted and experimental intensities for this mode is within factor of two or better, as shown in Table 3-12 for a series of molecules studied in our laboratory.

Table 3-12 shows that the predicted intensities for $CH_3OH$ and HOCl are within a factor of 1.0 and 1.3 agreement with the corresponding experimental intensities. For the $\nu_1$ and $\nu_3$ vibrational modes of $H_2O$ the predicted intensities are within factor of 2.1 and 2.3 agreement with the corresponding experimental values. A factor of two agreement with the experimental intensities is expected

Fig. 3-3. Experimental matrix spectrum of HOF in a nitrogen matrix at 8°K. The fundamental modes of HOF are observed at 3537.1, 1359.0 and at 886.0 $cm^{-1}$ and correspond to the O-H stretching, bending and O-F stretching fundamentals respectively. The maximum absorbance of each band relative to base 10 is also shown. Taken from reference [59], with permission

(a) 3,000:1 matrix to sample.

(b) 20,000:1 matrix to sample.

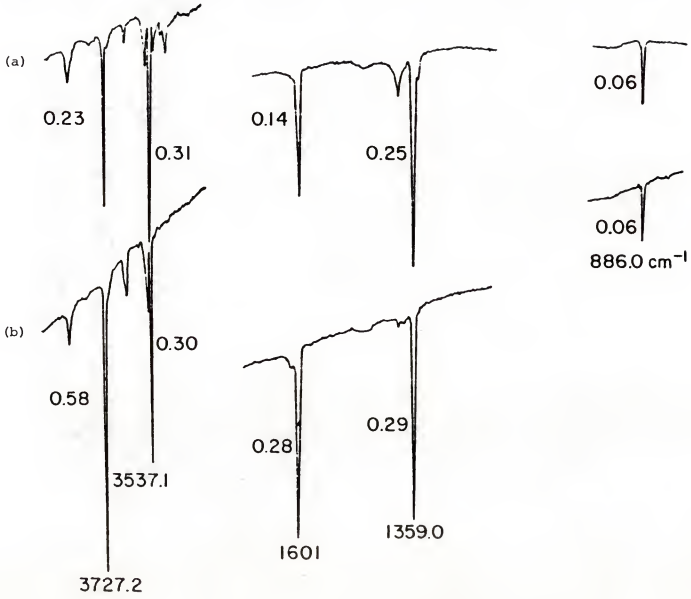
(a)
0.23
0.31
0.14
0.25
0.06
0.06
886.0 cm⁻¹
(b)
0.58
0.30
3537.1
3727.2
0.28
0.29
1601
1359.0

TABLE 3-12
EXPERIMENTAL AND QUANTUM MECHANICALLY PREDICTED INTENSITIES FOR THE ν(OH) VIBRATIONAL MODE OF $CH_3OH$, $H_2O$ AND HOCl

| Molecule (gas phase) | ν(OH) ($cm^{-1}$) | A(4-31G) (km $mole^{-1}$) | A(Expl.) (km $mole^{-1}$) |
|---|---|---|---|
| $CH_3OH$ | 3667.0 | 22.2[a] | 22.0[a] |
| $H_2O$ | 3633.2($\nu_1$) | 1.07[b] | 2.24[c] |
| | 3725.7($\nu_3$) | 19.7[b] | 44.6[c] |
| HOCl | 3626.0 | 75.3[d] | 56.6[e] |

[a] Rogers [35, p. 118]

[b] Zilles [53, p. 73]

[c] Quoted by Zilles [53, p. 73]

[d] This work, p. 114

[e] Su et al. [78]

from intensities predicted from ab initio SCF calculations using an extended basis set. This level of agreement is reasonable since it is still not surprising to find that a new measurement of a band intensity differs by a factor of two from earlier results reported in the literature.

Transferred APTs and Predicted Intensities for HOF

The intensities for HOF have been also predicted from experimental APTs transferred from other molecules. The experimental fluorine and hydrogen APTs from $CH_3F$ [29] and $H_2O$ [53] respectively were transferred in a bond coordinate system to the molecular coordinate system of HOF, shown in Fig. 3-1. The oxygen APT was calculated using the null condition given by Eq. (62). In the first column of Table 3-13, the oxygen, fluorine and hydrogen APTs, transferred from $CH_3F$ and $H_2O$ are shown, defined in the coordinate system of Fig. 3-1. We have also predicted the intensities for HOF, using the experimental APTs transferred from $CH_3F$ [29] and $CH_3OH$ [35]. This is shown in the second column of Table 3-13. For comparison, we have also included in Table 3-13, the ab initio APTs for HOF.

The intensities calculated from transferred and ab initio APTs for HOF are shown in Table 3-14. Notice that the intensities predicted either by transfer of the APTs from $CH_3F$ and $H_2O$ or $CH_3F$ and $CH_3OH$ are both in poor agreement with the intensities calculated from the ab initio APTs and also with the relative experimental intensities. The transferred APTs predict an order of increasing intensities from high wavenumbers ($\nu_1$(OH))to low ($\nu_3$(OF)), precisely

TABLE 3-13

TRANSFERRED AND AB INITIO 4-31G APTs FOR HOF (THE COORDINATE SYSTEM IS SHOWN IN FIG. 3-1 AND UNITS ARE e)

| $\underline{P}^{\alpha}_{x}$ | APTs transferred from $CH_3F$ and $H_2O$[a] | APTs transferred from $CH_3F$ and $CH_3OH$[b] | Ab initio 4-31G APTs[c] |
|---|---|---|---|
| $\underline{P}^{O}_{x}$ | $\begin{pmatrix} -0.075 & 0 & 0 \\ 0 & 0.675 & 0.033 \\ 0 & 0.048 & 0.135 \end{pmatrix}$ | $\begin{pmatrix} -0.005 & 0 & 0 \\ 0 & 0.767 & -0.021 \\ 0 & 0.067 & 0.120 \end{pmatrix}$ | $\begin{pmatrix} -0.368 & 0 & 0 \\ 0 & 0.174 & 0.228 \\ 0 & -0.020 & -0.068 \end{pmatrix}$ |
| $\underline{P}^{F}_{x}$ | $\begin{pmatrix} -0.255 & 0 & 0 \\ 0 & -0.934 & 0 \\ 0 & 0 & -0.255 \end{pmatrix}$ | $\begin{pmatrix} -0.255 & 0 & 0 \\ 0 & -0.934 & 0 \\ 0 & 0 & -0.255 \end{pmatrix}$ | $\begin{pmatrix} -0.129 & 0 & 0 \\ 0 & -0.437 & -0.157 \\ 0 & 0.046 & -0.169 \end{pmatrix}$ |
| $\underline{P}^{H}_{x}$ | $\begin{pmatrix} 0.330 & 0 & 0 \\ 0 & 0.259 & -0.033 \\ 0 & -0.048 & 0.120 \end{pmatrix}$ | $\begin{pmatrix} 0.260 & 0 & 0 \\ 0 & 0.167 & 0.021 \\ 0 & -0.067 & 0.135 \end{pmatrix}$ | $\begin{pmatrix} 0.497 & 0 & 0 \\ 0 & 0.263 & -0.071 \\ 0 & -0.026 & 0.237 \end{pmatrix}$ |

[a] $\underline{P}^{F}_{x}$ transferred from $CH_3F$ [29], $\underline{P}^{H}_{x}$ transferred from $H_2O$ [53], and $\underline{P}^{O}_{x}$ calculated from the null condition given by Eq. (62).

[b] $\underline{P}^{F}_{x}$ transferred from $CH_3F$ [29], $\underline{P}^{H}_{x}$ transferred from $CH_3OH$ [35], and $\underline{P}^{O}_{x}$ calculated from the null condition given by Eq. (62).

[c] The fluorine and hydrogen APTs were quantum mechanically calculated using a 4-31G basis set. $\underline{P}^{O}_{x}$ was calculated from the null condition given by Eq. (62).

TABLE 3-14
CALCULATED INTENSITIES FROM TRANSFERRED AND AB INITIO APTs FOR HOF (UNITS ARE km mole$^{-1}$)

| Band | $\nu_k$ (cm$^{-1}$) | $A_k$[a] | $A_k$[b] | $A_k$[c] |
|---|---|---|---|---|
| $\nu_1$(OH) | 3578.5 | 16.3 | 17.0 | 66.1 |
| $\nu_2$($\Delta\theta$) | 1354.8 | 61.3 | 30.0 | 53.6 |
| $\nu_3$(OF) | 889.0 | 73.5 | 81.2 | 11.3 |

[a] Calculated intensities, using $\underline{P}_x^F$ and $\underline{P}_x^H$ from $CH_3F$ [29] and $H_2O$ [53], respectively (see column 1 of Table 3-13)
[b] Calculated intensities, using $\underline{P}_x^F$ and $\underline{P}_x^H$ from $CH_3F$ [29] and $CH_3OH$ [35], respectively (see column 2 of Table 3-13)
[c] Calculated intensities using 4-31G APTs given in column 3 of Table 3-13.

the opposite of what is observed experimentally or predicted quantum mechanically (see Table 3-7 and Fig. 3-2). The predicted intensities for the OH and OF stretching modes of HOF, using $\underline{P}_x^F$ from $CH_3F$ and $\underline{P}_x^H$ from $H_2O$, given in column 3 of Table 3-14, are off by factors of 4 and 7 respectively, compared to the corresponding calculated intensities using ab initio APTs. Only the intensity predicted for the bending mode is in reasonable agreement with the corresponding intensity calculated from ab initio APTs. For the intensities predicted from APTs transferred from $CH_3F$ and $CH_3OH$, the results appear to be even worse (see column 4 of Table 3-14). These results are not unexpected, since the experimental APTs in fluorine and hydrogen transferred from $CH_3F$ and $CH_3OH$ or $H_2O$ are substantially different from the corresponding ab initio APTs (see Table 3-13). We may now compare the elements of the ab initio APTs for fluorine and hydrogen with the corresponding tensor elements transferred from $CH_3F$ and $H_2O$ or $CH_3OH$. Let us for instance, compare the ab initio calculated diagonal elements $\frac{\partial p_x}{\partial x}$, $\frac{\partial p_y}{\partial y}$ and $\frac{\partial p_z}{\partial z}$ of the 4-31G APTs of fluorine, given in the second row of Table 3-13, with the corresponding elements transferred from $CH_3F$ and $H_2O$ or $CH_3OH$. The $\frac{\partial p_x}{\partial x_F}$ and $\frac{\partial p_y}{\partial y_F}$ tensor elements of the ab initio APT differ by a factor of two from the corresponding values transferred from $CH_3F$. The $\frac{\partial p_z}{\partial z_F}$ is off by a factor of 1.5. It is obvious that the experimental fluorine APT of $CH_3F$ cannot be

successfully transferred to the HOF molecule. Moreover, the $\frac{\partial p_y}{\partial z_F}$ element of the ab initio APT is -0.16 e as compared to the corresponding null element of $CH_3F$.

The elements of the $\underline{P}_x^H$ tensor are also not transferable, as can be seen on the third row of Table 3-13. Here we have to consider the elements of the $\underline{P}_x^H$ tensor transferred from $CH_3OH$ and $H_2O$ separately. Let us consider first the elements of the hydrogen APT of $H_2O$. The diagonal elements $\frac{\partial p_x}{\partial x_H}$ and $\frac{\partial p_z}{\partial z_H}$ differ by a factor of 1.5 and 2.0 respectively, from the corresponding elements of the ab initio APT. Only the $\frac{\partial p_y}{\partial y_H}$ element of the transferred APT from $H_2O$ is in fairly good agreement with the corresponding ab initio APT.

For the elements of the $\underline{P}_x^H$ tensor transferred from $CH_3OH$, the diagonal elements $\frac{\partial p_x}{\partial x_H}$ and $\frac{\partial p_z}{\partial z_H}$ differ from the ab initio APT by factors of 2.0 and the $\frac{\partial p_y}{\partial y_H}$ element differs by a factor of 1.5.

An important question which may be raised at this point is the following: Why was it possible to transfer the experimental fluorine APT successfully from $CH_3F$ to predict the intensities of $CF_4$, $CF_3H$, $CH_2F_2$ [29] and $SF_6$ [64] but then fail to predict the intensity of HOF? The answer is obviously due to the different nature of the chemical bonding of the fluorine atom in

the original molecule compared to that in the molecules to which the APT is being transferred. For the molecules studied in reference [16], the electron distributions around the C-F bond in $CH_3F$, $CF_4$, $CF_3H$ and $CH_2F_2$ are similar, so that the substitution of the hydrogen atoms in $CH_3F$ by fluorine atoms does not substantially change the electron distribution in the C-F bond. For the HOF molecule, the situation is significantly different. Here, the electron distribution in the X-F bond is different in $CH_3F$ and HOF (for one reason, due to the change in symmetry) and the $P^F_x$ tensor may not be expected to be very transferable.

It is possible therefore, to generalize, concerning the transferability of APTs, by stating that the APTs are expected to be transferred from one molecule to another providing the electron distribution around the bond to which the APT is being transferred is similar to that in the original molecule. As a consequence of this rule, we may also say that within a series of chemically similar molecules the APTs are expected to be transferable, since the chemical environment near the bond to which the APT is being transferred does not change substantially from one molecule to another.

In conclusion, we should expect to be able to transfer successfully, for instance, the experimental hydrogen APT from $CH_3F$ to $CH_2F_2$ or $CHF_3$ molecules, but we should not expect to be able to transfer the experimental hydrogen APT from HOF to predict successfully the intensities of HOCℓ or HOBr molecules. Here we can expect that the change from F to Cℓ to Br will have a substantial effect in changing the electron distribution near the OH bond.

## Hydroperoxyl Radical

The hydroperoxyl radical $HO_2$ is an important intermediate species in the chemistry of the earth's stratosphere [9]. Direct observation of this species was first accomplished by Foner and Hudson in 1953 [65] using mass spectrometric technique and by Milligan and Jacox in 1963 [66] using infrared spectra matrix isolation technique. Since 1972, the number of spectroscopic studies of $HO_2$ has increased steadily [58,67-75]. The renewed interest in this species was mainly due to the fact that it takes part in several cyclic processes which remove ozone from the upper and lower stratosphere of the earth [9]. Moreover it has long been postulated as an important intermediate in numerous hydrogen-oxygen reactions (see for example, references cited in [68]).

### Normal Coordinate Analysis

The molecular geometry of $HO_2$ in its ground electronic state ($^2A''$) is well established, both by experiment [71,74] and by *ab initio* SCF calculations [75]. The structural parameters of $HO_2$ are given in Table 3-15, as reported by different research groups. The agreement between them is remarkably good. In this work we have used the geometrical parameters reported by Beers and Howard [71] as given in Table 3-15. From these geometrical parameters, we calculate the position vectors for the $HO_2$ molecule, given in Table 3-16, using the coordinate system shown in Fig. 3-4. The column vector $\underline{X}$ given by Eq. (2) was then formed using the data presented in Table 3-16. This column vector, the masses of the

TABLE 3-15
STRUCTURAL PARAMETERS OF $HO_2$ ($^2A''$)

| r(OH)[a] | r(OO)[a] | θ(HOO) | References |
|---|---|---|---|
| 0.977 | 1.335 | 104.1° | Beers and Howard, ref. [71] (microwave) |
| 0.975 | 1.329 | 104.0° | Tuckett, Freedman and Jones, ref. [74] (near infrared) |
| 0.968 | 1.384 | 106.8° | Liskow, Schaefer III and Bender, ref. [75] (*ab initio* SCF calculation) |
| 0.973 | 1.458 | 104.6° | Liskow, Schaefer III and Bender, ref. [75] (*ab initio* SCF-CI calculation) |

[a]Bond length in units of Å.

TABLE 3-16
EQUILIBRIUM POSITION VECTORS FOR $HO_2$ (UNITS ARE Å)

| Atom $N_o$[a] | x | y | z |
|---|---|---|---|
| 1(O,central) | 0.0 | 0.0 | 0.0 |
| 2(O,outer) | 0.0 | -1.335000 | 0.0 |
| 3(H) | 0.0 | 0.238012 | -0.947565 |

[a]The atom numbering and coordinate system are given in Fig. 3-4.

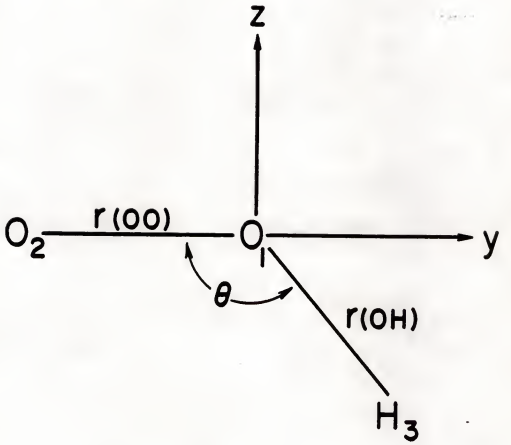


Fig. 3-4. Coordinate system and atom numbering for $HO_2$.

atoms (H = 1.007825, O = 15.994910 in amu), the description of the internal coordinates and the U matrix were used as input to program WMAT [27] to obtain the B and G matrices. The B matrix for $HO_2$ is presented in Table 3-17. The G matrix was then diagonalized by program WMAT to form the W matrix, according to Eq. (28). We used the force field reported by Ogilvie [50], which was obtained by fitting the observed infrared frequencies for eight isotopic derivatives of the $HO_2$ species, using a multiple regression technique. The F matrix is given in Table 3-18. The W matrix obtained from program WMAT and the F matrix were used as input to program CHARLY [27] to obtain the eigenvectors, L, and eigenvalues $\Lambda$, of the G F product matrix. The L matrix and the calculated vibration wavenumbers of $HO_2$ are shown in Tables 3-19 and 3-20, respectively. In Table 3-20 is also given the experimental vibration wavenumbers of $HO_2$, obtained from $HO_2$ isolated in an argon matrix, as reported by Ogilvie in reference[50].

Ab Initio 4-31G APTs and Calculated Intensities for $HO_2$

The atomic polar tensor (APTs) for $HO_2$ were quantum mechanically calculated using a 4-31G basis set. The details of this calculation have been previously discussed in Chapter 2. These APTs were calculated with respect to the coordinate system shown in Fig. 3-4. The $P_x$ matrix was then constructed according to Eq. (51), noticing that the juxtaposition of each individual APT in this equation, follows the same order of atom numbering shown in Fig. 3-4. The *ab initio* APTs for $HO_2$ are given in Table 3-21. The APT for the

TABLE 3-17
THE $\underline{B}$ MATRIX FOR $HO_2$

| | | | | | | | | |
|---|---|---|---|---|---|---|---|---|
| 0.0 | 1.0 | 0.0 | 0.0 | -1.0 | 0.0 | 0.0 | 0.0 | 0.0 |
| 0.0 | -0.992704 | -0.998415 | 0.0 | 0.0 | 0.749064 | 0.0 | 0.992704 | 0.249350 |
| 0.0 | -0.243615 | 0.969872 | 0.0 | 0.0 | 0.0 | 0.0 | 0.243615 | -0.969872 |

Note: All elements of $\underline{B}$ are unitless since we have used a weighted unit system (see also Table 2-1). Notice also that $\underline{B} = \underline{B}$, since the $\underline{U}$ matrix is the identity matrix in this case.

TABLE 3-18

THE EXPERIMENTAL FORCE CONSTANT MATRIX, $\underline{F}$, FOR $HO_2$

(UNITS ARE MDYNE $\text{Å}^{-1}$)

(1aJ $\text{Å}^{-2}$ = 1 mdyne $A^{-1}$ = 100 N $m^{-1}$)

$$\begin{pmatrix} 5.7186 & 0.3870 & 0.1000 \\ 0.3870 & 0.9870 & 0.0500 \\ 0.1000 & 0.0500 & 6.5817 \end{pmatrix}$$

Note: $F_{11} = F_{r(OO)}$; $F_{12} = F_{r(OO),\theta}$; $F_{13} = F_{r(OO),r(OH)}$; $F_{22} = F_{\theta}$; $F_{23} = F_{r(OH),\theta}$; $F_{33} = F_{r(OH)}$. Notice that the following force constants given by Ogilvie [50] are scaled by the OO and OH bond lengths of $HO_2$, according to: $F'_{\theta} = F_{\theta}/r_1 r_2$, $F'_{r_1\theta} = F_{r_1\theta}/r_1$ and $F'_{r_2\theta} = F_{r_2\theta}/r_2$, where $r_1$ and $r_2$ are the OH and OO bond lengths respectively and the prime indicates here the unscaled force constants given by Ogilvie. Notice also that the force constants reported by Ogilvie are in units of N $m^{-1}$. Here $\underline{F} = \underline{F}$, since the $\underline{U}$ matrix is the identity matrix.

TABLE 3-19
THE $\underline{L}$ MATRIX FOR $HO_2$ (UNITS ARE $u^{-1/2}$)

| | | |
|---|---|---|
| -0.014835 | 0.031959 | 0.351850 |
| -0.043829 | -1.091023 | -0.079141 |
| 1.027013 | 0.000375 | -0.000020 |

Note: Here $\underline{L} = \underline{L}$, since the $\underline{U}$ matrix is the identity matrix in this case.

TABLE 3-20
OBSERVED AND CALCULATED VIBRATIONAL WAVENUMBERS
FOR $HO_2$ (UNITS ARE $cm^{-1}$)

| Mode[a] | Observed[b] | Calculated[c] | Percent error[d] |
|---|---|---|---|
| $\nu_1$(OH) | 3410.50 | 3432.58 | 0.65 |
| $\nu_2(\Delta\theta)$ | 1389.00 | 1399.71 | 0.77 |
| $\nu_3$(OO) | 1101.00 | 1084.51 | -1.50 |

[a] Here $\nu_1$(OH), $\nu_2(\Delta\theta)$ and $\nu_3$(OO) refer to the OH stretching, the bending mode and the OO stretching band, respectively.
[b] The experimental vibration wavenumbers from $HO_2$ isolated in an argon matrix are given in refs. [50], [66] and [58]. We have used the data reported by Ogilvie in ref. [50].
[c] The wavenumbers were calculated using the equilibrium molecular geometry of $HO_2$ given in ref. [71] and the force field obtained from ref. [50].
[d] [$\nu$(calc.) - $\nu$(obs.)] x 100/$\nu$(obs.).

TABLE 3-21

AB INITIO APTs FOR $HO_2$ (UNITS ARE e, WHERE 1e = 1.602 x $10^{-19}$ C)

$$\underline{P}_x^{O(1)} = \begin{pmatrix} -0.433 & 0 & 0 \\ 0 & -0.697 & 0.183 \\ 0 & 0.0 & -0.080 \end{pmatrix}$$

$$\underline{P}_x^{O(2)} = \begin{pmatrix} -0.041 & 0 & 0 \\ 0 & 0.393 & -0.152 \\ 0 & 0.015 & -0.108 \end{pmatrix}$$

$$\underline{P}_x^{H} = \begin{pmatrix} 0.474 & 0 & 0 \\ 0 & 0.304 & -0.031 \\ 0 & -0.015 & 0.188 \end{pmatrix}$$

Note: A 4-31G basis set was used for the ab initio calculation of the APTs for $HO_2$. The $\underline{P}_x^{O(1)}$ tensor was calculated using the null condition. The coordinate system is shown in Fig. 3-4.

central atom was calculated from the null condition [Eq. (62)]. The $\underline{P}_x$ matrix was transformed from the space-fixed cartesian coordinate system to the $\underline{P}_Q$ matrix in normal coordinate space, using Eq. (53) and the intensities for each fundamental band of $HO_2$ were calculated using Eq. (56).

We have also calculated the charge, charge-flux and overlap contributions to the ab initio APTs in $HO_2$, according the the CCFO model [52,53] using Eq.s (63), (64) and (67), respectively. These APTs are given in Tables 3-22, 3-23 and 3-24. For all of these terms the coordinate system is as shown in Fig. 3-4. The charge, charge-flux and overlap contributions to the APT for $HO_2$ shall be discussed in Chapter 4, where we shall compare them for all of the molecules studied in this work.

For the intensity calculations we have used program PVDTEN developed by Newton [48]. The intensities for each fundamental band of $HO_2$ calculated from the ab initio 4-31G APTs are given in Table 3-25. Also shown in that table are the absolute intensities calculated by Komornicki and Jaffe [ 76 ] with the GRADSCF program [77] using a contracted Gaussian basis of triple-zeta accuracy plus double polarization (TZPP). We have also included in Table 3-25 the experimental intensities relative to the intensity of the OH fundamental stretching mode $\nu$(OH) of $HO_2$, obtained from the experimental spectrum of $HO_2$ in an Ar matrix, reported by Smith and Andrews in reference [25], and shown in Fig. 3-5.

It is of interest now to compare our intensities calculated with a 4-31G basis set with those predicted by Komornicki and Jaffe

TABLE 3-22
CHARGE, CHARGE-FLUX, OVERLAP AND TOTAL APTs ON THE HYDROGEN ATOM OF $HO_2$ (UNITS ARE e)

$$\underline{P}_{\underline{x}}^{H}\ (C) \quad \begin{pmatrix} 0.44 & 0 & 0 \\ 0 & 0.44 & 0 \\ 0 & 0 & 0.44 \end{pmatrix}$$

$$\underline{P}_{\underline{x}}^{H}\ (CF) \quad \begin{pmatrix} 0 & 0 & 0 \\ 0 & -0.12 & -0.06 \\ 0 & -0.02 & 0.10 \end{pmatrix}$$

$$\underline{P}_{\underline{x}}^{H}\ (O) \quad \begin{pmatrix} 0.03 & 0 & 0 \\ 0 & -0.02 & 0.03 \\ 0 & 0.004 & -0.35 \end{pmatrix}$$

$$\underline{P}_{\underline{x}}^{H}\ (T) \quad \begin{pmatrix} 0.47 & 0 & 0 \\ 0 & 0.30 & -0.03 \\ 0 & -0.02 & 0.19 \end{pmatrix}$$

Note: The charge (C), charge-flux (CF) and overlap (O) contributions to the total (T) 4-31G APT on the hydrogen atom were calculated according to the CCFO model [52,53]. The coordinate system is shown in Fig. 3-4.

TABLE 3-23
CHARGE, CHARGE-FLUX, OVERLAP AND TOTAL APTs ON THE OUTER OXYGEN (2) ATOM OF $HO_2$ (UNITS ARE e)

$$\underline{P}_x^{O(2)}(C) = \begin{pmatrix} -0.04 & 0 & 0 \\ 0 & -0.04 & 0 \\ 0 & 0 & -0.04 \end{pmatrix}$$

$$\underline{P}_x^{O(2)}(CF) = \begin{pmatrix} 0 & 0 & 0 \\ 0 & 0.39 & -0.11 \\ 0 & 0.03 & -0.003 \end{pmatrix}$$

$$\underline{P}_x^{O(2)}(O) = \begin{pmatrix} -0.002 & 0 & 0 \\ 0 & 0.05 & -0.04 \\ 0 & -0.01 & -0.07 \end{pmatrix}$$

$$\underline{P}_x^{O(2)}(T) = \begin{pmatrix} -0.04 & 0 & 0 \\ 0 & 0.39 & -0.15 \\ 0 & 0.02 & -0.11 \end{pmatrix}$$

Note: The charge (C), charge-flux (CF) and overlap (O) contributions to the total 4-31G APT on the oxygen (2) atom were calculated according to the CCFO model [52,53]. The coordinate system is shown in Fig. 3-4.

TABLE 3-24
CHARGE, CHARGE-FLUX, OVERLAP AND TOTAL APTs
ON THE CENTRAL OXYGEN (1) ATOM OF $HO_2$
(UNITS ARE e)

$$\underline{P}_x^{O(1)}(C) \begin{pmatrix} -0.40 & 0 & 0 \\ 0 & -0.40 & 0 \\ 0 & 0 & -0.40 \end{pmatrix}$$

$$\underline{P}_x^{O(1)}(CF) \begin{pmatrix} 0 & 0 & 0 \\ 0 & -0.23 & 0.15 \\ 0 & -0.003 & -0.10 \end{pmatrix}$$

$$\underline{P}_x^{O(1)}(O) \begin{pmatrix} -0.04 & 0 & 0 \\ 0 & -0.03 & 0.01 \\ 0 & 0.01 & 0.42 \end{pmatrix}$$

$$\underline{P}_x^{O(1)}(T) \begin{pmatrix} -0.45 & 0 & 0 \\ 0 & -0.66 & 0.16 \\ 0 & 0.01 & -0.08 \end{pmatrix}$$

Note: The charge (C), charge-flux (CF) and overlap (O) contributions to the total (T) 4-31G APT on the oxygen (1) atom were calculated according to the CCFO model [52,53]. The coordinate system is shown in Fig. 3-4.

TABLE 3-25
ABSOLUTE INTENSITIES AND EXPERIMENTAL RELATIVE INTENSITIES OF $HO_2$ (UNITS ARE km $mole^{-1}$)

| | | Calculated | | Relative experimental | |
|---|---|---|---|---|---|
| Band | $\nu(cm^{-1})$ | A(4-31G)[a] | A(TZPP)[b] | A[c] | A[d] |
| $\nu_1$(OH) | 3410.5 | 47.6 | 67.5 | 47.6 | 67.5 |
| $\nu_2(\Delta\theta)$ | 1389.0 | 78.5 | 53.2 | 148.3 | 210.1 |
| $\nu_3$(OO) | 1101.0 | 25.9 | 46.3 | 91.3 | 129.4 |

[a] Calculated intensities using the 4-31G APTs given in Table 3-21 (this work).

[b] Calculated by Komornicki and Jaffe and reported in ref. [76] using a triple-zeta plus double polarization (TZPP) basis set of Gaussian functions contracted to (5s3p2d/3s2p), for the calculation of the dipole moment derivatives.

[c] Experimental intensities relative to A(4-31G). Relative experimental intensities scaled to fit the intensity of the $\nu$(OH) band calculated by 4-31G APTs.

[d] Experimental intensities relative to A(TZPP). Relative experimental intensities scaled to fit the intensity of the $\nu$(OH) band calculated by TZPP basis set.

Fig. 3-5. Experimental matrix spectrum of $HO_2$ in an argon matrix. $HO_2$ bands were observed at 3414.3, 1389.7 and 1101.4 $cm^{-1}$. The bands at 1290 and 1040 $cm^{-1}$ were assigned to $H_2O_2$ and $O_3$, respectively. Taken from reference [58], with permission.

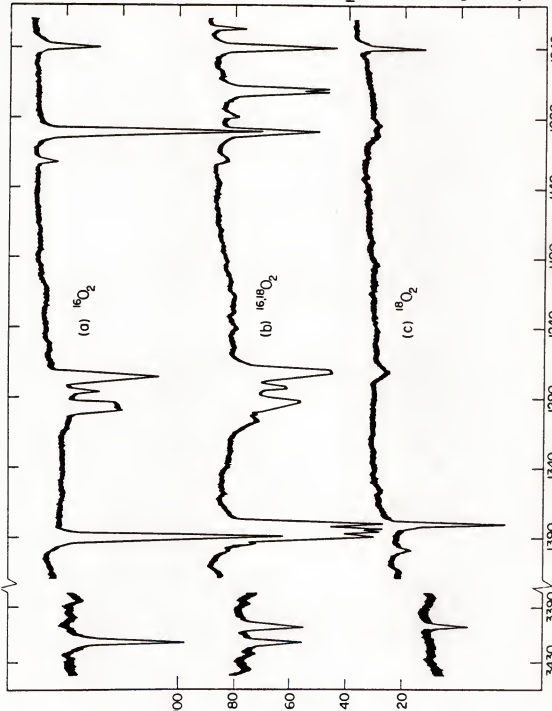
PERCENT TRANSMISSION
FREQUENCY (cm⁻¹)
(a) $^{16}O_2$
(b) $^{16,18}O_2$
(c) $^{18}O_2$
spectrum (a)
spectrum (b)
spectrum (c)
100
80
60
40
20
3430
3390
1390
1340
1290
1240
1190
1140
1090
1040

using the TZPP basis and also compare both calculated intensities with the relative experimental intensities of $HO_2$. The SCF calculations reported by Komornicki and Jaffe predict the most intense band to be associated with the OH stretching mode which is not observed experimentally [58]. Our SCF calculations predict the bending mode to be the strongest band of $HO_2$ in agreement with the experimental relative intensities. Our absolute intensities are also consistent with the experimental observations of Jacox and Milligan [67] who pointed out that the bending mode of $HO_2$ is definitely stronger than the OO stretching band. Let us now compare the absolute intensities calculated with the 4-31G and TZPP bases with the corresponding relative intensities from experiments. The intensity pattern for the HOO bending mode and OO stretching mode calculated with a 4-31G basis and using the APT formalism is good, when compared with the corresponding experimental pattern. We have apparently underestimated the relative intensity only for the OO stretching mode. However, the intensity pattern calculated with the TZPP basis does not match the experimental pattern so well (see Fig. 3-7 in the next section) since it predicted all bands to have about the same relative intensity in contrast to the variations found experimentally. Although the relative intensities from this calculation appear to agree with the experimental values within factors of 2-4, we believe that our calculated intensities are, in general, more consistent with the experimental observation than are those predicted with the TZPP basis set. It is possible that the TZPP basis set [ 76 ] is not well-balanced [55] leading to some error in predicting dipole moment derivatives, as shall be discussed in more detail later.

Predicted and Experimental Computer-Simulated Spectra of Matrix-Isolated $HO_2$

The theoretical and experimental computer-simulated spectra of $HO_2$ in an argon matrix [58] were obtained according to the procedure described previously for the computer simulation of the matrix spectrum of HOF. The computer-simulated predicted spectrum of $HO_2$ is shown in Fig. 3-6(a). Here the intensities were calculated from the ab initio 4-31G APTs given in Table 3-21, just as described previously for HOF. Using Eq. (69) we calculated the (Cℓ) product needed to scale the plot of the predicted spectrum by fitting the predicted intensity of the OH stretching mode (3410 $cm^{-1}$) to the observed values of $a_{max}$ and $\Delta\nu_{1/2}$ for that band estimated from the experimental spectrum of $HO_2$ in the argon matrix [58]. Figure 3-6(b) shows the computer simulation of the experimental spectrum of $HO_2$ in the argon matrix. The predicted band intensity for the bending anode at 1390 $cm^{-1}$ is within factor of two agreement with the corresponding band of the experimental spectrum and the underestimated band intensity for the OO stretching mode is shown at 1090 $cm^{-1}$. The general pattern for all the bands is consistent with the observed spectrum of $HO_2$. The parameters used for the computer simulation of both spectra are listed in Table 3-26.

We have also compared the theoretical spectrum predicted from intensities calculated by Komornicki and Jaffe from a TZPP quality basis set [ 76 ], with the experimental matrix spectrum of $HO_2$ in Fig. 3-7. It can be seen that even this extended basis set does not predict very well the general pattern for all the bands of $HO_2$.

Fig. 3-6. Theoretical and experimental computer-simulated infrared spectra of matrix-isolated $HO_2$. (Theoretical spectrum predicted from intensities calculated from 4-31G APTs.)

(a) Computer-simulated predicted spectrum of $HO_2$ in the argon matrix. The intensities were calculated from *ab initio* APTs as described in text. The assumed concentration of $HO_2$ is adjusted until the intensity of the OH stretching vibration at 3410.5 $cm^{-1}$ fits the observed spectrum.

(b) Computer simulation of the experimental $HO_2$ spectrum in the argon matrix (see Fig. 3-5).

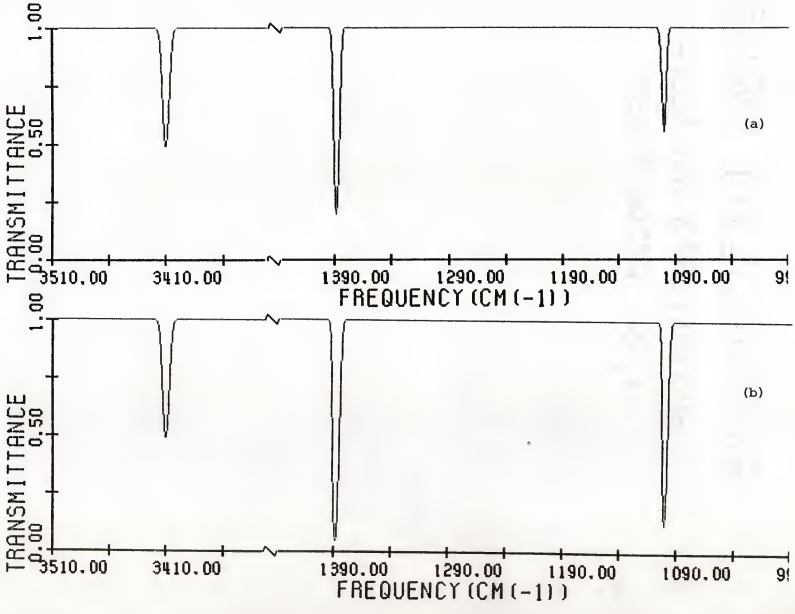
TRANSMITTANCE
1.00
0.50
0.00
(a)
3510.00
3410.00
1390.00
1290.00
1190.00
1090.00
FREQUENCY (CM(-1))
TRANSMITTANCE
1.00
0.50
0.00
(b)
3510.00
3410.00
1390.00
1290.00
1190.00
1090.00
FREQUENCY (CM(-1))

TABLE 3-26
PARAMETERS USED FOR THE COMPUTER SIMULATION OF THE THEORETICAL AND EXPERIMENTAL SPECTRA OF MATRIX-ISOLATED $HO_2$ (REFER TO FIG. 3-6)

| Theoretical ($C\ell$=9.79 x $10^{-4}$ mmole $cm^{-2}$) | | | Experimental ($C\ell$=9.79 x $10^{-4}$ mmole $cm^{-2}$) | | | |
|---|---|---|---|---|---|---|
| $\nu_o$[a] ($cm^{-1}$) | $\Delta\nu_{1/2}$[b] ($cm^{-1}$) | A(abs.)[c] (km $mole^{-1}$) | $\nu_o$[a] ($cm^{-1}$) | $\Delta\nu_{1/2}$[b] ($cm^{-1}$) | A[c] (km $mole^{-1}$) | $a_{max}$[d] |
| 3410.5 | 6.0 | 47.6 | 3410.5 | 6.0 | 47.6 | 0.73 |
| 1389.0 | 4.4 | 78.5 | 1389.0 | 4.4 | 148.3 | 3.1 |
| 1101.0 | 4.0 | 25.9 | 1101.0 | 4.0 | 91.3 | 2.1 |

[a] Wavenumber position of maximum absorption from the experimental matrix spectrum of $HO_2$ as reported by Smith and Andrews in ref. [68].
[b] Full width at half-maximum of the band estimated from the matrix-isolated spectrum [68].
[c] Taken from Table 3-25.
[d] The maximum absorbances of the $HO_2$ bands estimated from the experimental matrix spectrum of $HO_2$ in the argon matrix [68].

Fig. 3-7. Theoretical and experimental computer-simulated infrared spectra of matrix-isolated $HO_2$. (Theoretical spectrum predicted from intensities given by Komornicki and Jaffe and calculated using a TZPP quality basis set [ 76 ].)

(a) Computer-simulated predicted spectrum of $HO_2$ in the argon matrix. The intensities were calculated by the gradient method using a contracted Gaussian basis set of triple-zeta accuracy plus double polarization [ 76 ]. The assumed concentration of $HO_2$ is adjusted until the intensity of the OH stretching vibration at 3410.5 $cm^{-1}$ fits the observed spectrum.

(b) Computer simulation of the experimental $HO_2$ spectrum in the argon matrix (see Fig. 3-5).

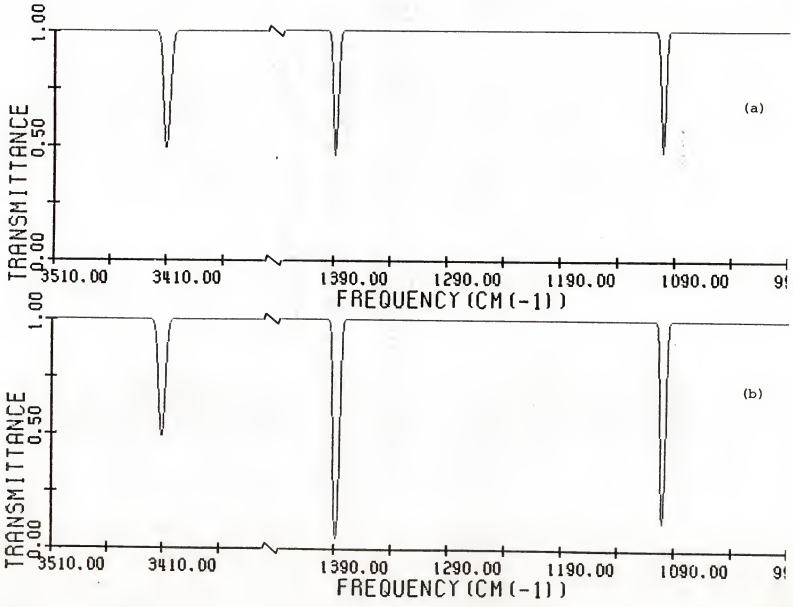
TRANSMITTANCE
1.00
0.50
0.00
3510.00
3410.00
1390.00
1290.00
1190.00
1090.00
FREQUENCY (CM(-1))
(a)
(b)

In particular, the relative band intensity of the OO stretching is also underestimated. The parameters used for the computer simulation of both spectra are shown in Table 3-27.

Computer Simulation of the Matrix Spectrum of $HO_2$ Predicted by Transfer of APTs

We have seen previously that the transferability of the APTs depends on the chemical environment of the atom in the original molecule and that in the molecule to which the APT is being transferred. For the special case of the $HO_2$ molecule, the best approach would be to transfer the APT for the oxygen atom from a system containing the OO bond, and the APT for the hydrogen atom from $H_2O$, for instance. Since an APT for a model oxygen atom in an OO bond has not yet been determined experimentally, we decided to investigate, as a first approximation, whether or not the APTs transferred from $CH_3OH$, (for the central O atom) and $H_2O$ (for the H atom) would predict successfully the intensities of $HO_2$. However, to predict the intensities for $HO_2$ by simply transferring the APT directly from $H_2O$ and $CH_3OH$ would not be realistic since the central oxygen APT is expected to be substantially different in $CH_3OH$ and $HO_2$. To prove that this is the case, we need to compare the contributions to the ab initio APT for the oxygen atom in both molecules. This comparison is shown in Table 3-28. These APTs were calculated relative to the coordinate system shown in Fig. 3-8. Notice that the main change is in the charge contribution to the ab initio APT of the oxygen atom (-0.74 as compared to -0.40 for $CH_3OH$ and $HO_2$, respectively). Notice also that the charge-flux and overlap APTs are different for the two systems, particularly the $\frac{\partial p_x}{\partial x}(CF)$, $\frac{\partial p_z}{\partial z}(CF)$ and $\frac{\partial p_x}{\partial x}(O)$ elements.

TABLE 3-27

PARAMETERS USED FOR THE COMPUTER SIMULATION OF THE THEORETICAL AND EXPERIMENTAL SPECTRA OF MATRIX-ISOLATED $HO_2$ ( REFER TO FIG. 3-7 )

| Theoretical ($C\ell$=6.91 x $10^{-4}$ mmole $cm^{-2}$) | | | Experimental ($C\ell$=6.91 x $10^{-4}$ mmole $cm^{-2}$) | | | |
|---|---|---|---|---|---|---|
| $\nu_o$[a] ($cm^{-1}$) | $\Delta\nu_{1/2}$[b] ($cm^{-1}$) | A[c] (km $mole^{-1}$) | $\nu_o$[a] ($cm^{-1}$) | $\Delta\nu_{1/2}$[b] ($cm^{-1}$) | A[c] (km $mole^{-1}$) | $a_{max}$[d] |
| 3410.5 | 6.0 | 67.5 | 3410.5 | 6.0 | 67.5 | 0.73 |
| 1389.0 | 4.4 | 53.2 | 1389.0 | 4.4 | 210.1 | 3.1 |
| 1101.0 | 4.0 | 46.3 | 1101.0 | 4.0 | 129.4 | 2.1 |

[a] Wavenumber position of maximum absorption from the experimental matrix spectrum of $HO_2$ as reported by Smith and Andrews in ref. [68].

[b] Full width at half-maximum of the band estimated from the matrix-isolated spectrum [68].

[c] Taken from Table 3-25.

[d] The maximum absorbances of the $HO_2$ bands estimated from the experimental matrix spectrum of $HO_2$ in the argon matrix [68].

TABLE 3-28
CHARGE, CHARGE-FLUX AND OVERLAP CONTRIBUTIONS TO THE AB INITIO APT ON THE CENTRAL OXYGEN ATOM OF $CH_3OH$ AND $HO_2$ (ATOM 1)
(UNITS ARE e)

| $\underline{P}_x^{(O)}$ | $CH_3OH$[a] | $HO_2$[b] |
|---|---|---|
| $\underline{P}_x^{(O)}$ (C) | $\begin{pmatrix} -0.74 & 0 & 0 \\ 0 & -0.74 & 0 \\ 0 & 0 & -0.74 \end{pmatrix}$[c] | $\begin{pmatrix} -0.40 & 0 & 0 \\ 0 & -0.40 & 0 \\ 0 & 0 & -0.40 \end{pmatrix}$ |
| $\underline{P}_x^{(O)}$ (CF) | $\begin{pmatrix} 0.07 & 0 & 0.13 \\ 0 & 0.05 & 0 \\ -0.01 & 0 & -0.04 \end{pmatrix}$[c] | $\begin{pmatrix} -0.19 & 0 & 0.17 \\ 0 & 0 & 0 \\ 0.02 & 0 & -0.14 \end{pmatrix}$ |
| $\underline{P}_x^{(O)}$ (O) | $\begin{pmatrix} -0.19 & 0 & 0.13 \\ 0 & -0.07 & 0 \\ 0.21 & 0 & 0.36 \end{pmatrix}$[c] | $\begin{pmatrix} 0.003 & 0 & 0.12 \\ 0 & -0.04 & 0 \\ 0.11 & 0 & 0.39 \end{pmatrix}$ |
| $\underline{P}_x^{(O)}$ (T) | $\begin{pmatrix} -0.86 & 0 & 0.25 \\ 0 & -0.76 & 0 \\ 0.19 & 0 & -0.42 \end{pmatrix}$ | $\begin{pmatrix} -0.59 & 0 & 0.29 \\ 0 & -0.45 & 0 \\ 0.13 & 0 & -0.15 \end{pmatrix}$ |

[a] Taken from Rogers [35] and expressed in the coordinate system shown in Fig. 3-8.
[b] This work. The coordinate system is shown in Fig. 3-8.
[c] Rogers (private communication) and expressed in the coordinate system shown in Fig. 3-8.

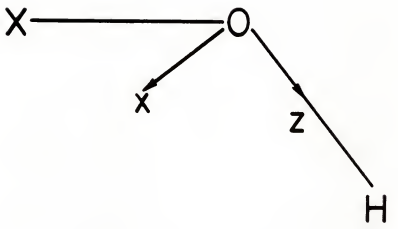


Fig. 3-8. Coordinate system for the oxygen atom of HOX, X = $CH_3$, O.

However, the most substantial difference is indeed in the charge contribution. In order to take this change into account we scaled the experimental APT for the oxygen atom of $CH_3OH$ according to

$$\underline{P}_x^{O(1)}(\text{scaled}) = \underline{P}_x^{O(1)}(CH_3OH,\text{Expl.}) - \underline{P}_x^{O(1)}(CH_3OH,(C),\text{ ab initio}) + \underline{P}_x^{O(1)}(HO_2,(C),\text{ab initio})$$

This is equivalent to adding a correction term given by

$$\underline{P}_x^{O(1)}(\text{correction}) = \underline{P}_x^{O(1)}(H_2O,(C),\text{ab initio}) - \underline{P}_x^{O(1)}(CH_3OH,(C),\text{ab initio})$$

to the experimental APT for the oxygen atom of $CH_3OH$. We have used the same procedure to transfer the hydroxylic hydrogen APT from $CH_3OH$ and the oxygen APT scaled also from $CH_3OH$. The final APTs relative to the coordinate system shown in Fig. 3-4, are given in Table 3-29. The predicted intensities for these transferred APTs are shown in Table 3-30 and the computer-simulated spectra in Figs. 3-9 and 3-10. The parameters used for the computer simulation of both spectra are shown in Table 3-31.

It is of interest now to compare the transferred and ab initio APTs for $HO_2$, which is also presented in Table 3-29. Notice that there are differences between the corresponding elements of the hydrogen APTs and oxygen APTs as compared to the corresponding elements of the ab initio APTs. The difference in the $\underline{P}_x^{O(1)}$ APT for $CH_3OH$ and the ab initio APT is due to the fact that the charge-flux and overlap contributions to the ab initio APT of $CH_3OH$ have not been corrected (see Table 3-28) in the experimental APT for the oxygen atom of $CH_3OH$. Moreover, there are differences between

TABLE 3-29

TRANSFERRED AND AB INITIO 4-31G APTs FOR $HO_2$ (THE COORDINATE SYSTEM IS SHOWN IN FIG.3-4 AND UNITS ARE e)

| $\underline{P}_x^{\alpha}$ | APTs transferred from $H_2O$ and $CH_3OH$ (scaled)[a] | APTs transferred from $CH_3OH$ and $CH_3OH$ (scaled)[b] | Ab initio 4-31G APTs[c] |
|---|---|---|---|
| $\underline{P}_x^{O(1)}$ | $\begin{pmatrix} -0.105 & 0 & 0 \\ 0 & -0.529 & 0.102 \\ 0 & 0.033 & 0.028 \end{pmatrix}$ | $\begin{pmatrix} -0.105 & 0 & 0 \\ 0 & -0.529 & 0.102 \\ 0 & 0.033 & 0.028 \end{pmatrix}$ | $\begin{pmatrix} -0.433 & 0 & 0 \\ 0 & -0.697 & 0.183 \\ 0 & 0 & -0.080 \end{pmatrix}$ |
| $\underline{P}_x^{O(2)}$ | $\begin{pmatrix} -0.225 & 0 & 0 \\ 0 & 0.262 & -0.086 \\ 0 & -0.003 & -0.140 \end{pmatrix}$ | $\begin{pmatrix} -0.155 & 0 & 0 \\ 0 & 0.357 & -0.128 \\ 0 & 0.029 & -0.158 \end{pmatrix}$ | $\begin{pmatrix} -0.041 & 0 & 0 \\ 0 & 0.393 & -0.152 \\ 0 & 0.015 & -0.108 \end{pmatrix}$ |
| $\underline{P}_x^{H(3)}$ | $\begin{pmatrix} 0.330 & 0 & 0 \\ 0 & 0.267 & -0.016 \\ 0 & -0.030 & 0.112 \end{pmatrix}$ | $\begin{pmatrix} 0.260 & 0 & 0 \\ 0 & 0.172 & 0.026 \\ 0 & -0.062 & 0.130 \end{pmatrix}$ | $\begin{pmatrix} 0.474 & 0 & 0 \\ 0 & 0.304 & -0.031 \\ 0 & -0.015 & 0.188 \end{pmatrix}$ |

a $\underline{P}_x^{H(3)}$ transferred from $H_2O$ [53], $\underline{P}_x^{O(1)}$ scaled from $CH_3OH$ (see text) and $\underline{P}_x^{O(2)}$ calculated from the null condition given by Eq. (62).

b $\underline{P}_x^{H(3)}$ transferred from $CH_3OH$ [35], $\underline{P}_x^{O(1)}$ scaled from $CH_3OH$ and $\underline{P}_x^{O(2)}$ calculated from the null condition given by Eq. (62).

c $\underline{P}_x^{H(3)}$ and $\underline{P}_x^{O(2)}$ were quantum mechanically calculated using a 4-31G basis set. $\underline{P}_x^{O(1)}$ was calculated from the null condition given by Eq. (62).

TABLE 3-30
CALCULATED INTENSITIES FROM TRANSFERRED AND AB INITIO APTs FOR $HO_2$ (UNITS ARE km $mol^{-1}$)

| Band | $\nu_k$ ($cm^{-1}$) | $A_k$ [a] | $A_k$ [b] | $A_k$ [c] |
|---|---|---|---|---|
| $\nu_1$(OH) | 3410.5 | 20.2 | 18.7 | 47.6 |
| $\nu_2$($\Delta\theta$) | 1389.0 | 63.0 | 30.3 | 78.5 |
| $\nu_3$(OO) | 1101.0 | 12.6 | 19.4 | 25.9 |

[a] Calculated intensities by transfer of the APT from $H_2O$ (for the OH hydrogen) and from $CH_3OH$ (for the OH oxygen). The APTs are presented in column 1 of Table 3-29.

[b] Calculated intensities by transfer of the APT from $CH_3OH$ (for the OH hydrogen and oxygen atoms). The APTs are given in column 2 of Table 3-29.

[c] Calculated intensities using 4-31G APTs given in column 3 of Table 3-29.

Fig. 3-9. Comparison of the computer simulation of the $HO_2$ spectrum predicted by transfer of APTs from $H_2O$ (for the OH hydrogen) and from $CH_3OH$ (for the OH oxygen) with the computer simulation of the experimental matrix spectrum of $HO_2$.

(a) Predicted by transfer of APTs from $H_2O$ and $CH_3OH$. The concentration has been adjusted in the predicted spectrum as described previously for Fig. 3-6.

(b) Computer simulation of the experimental $HO_2$ spectrum in the argon matrix (see Fig. 3-5).

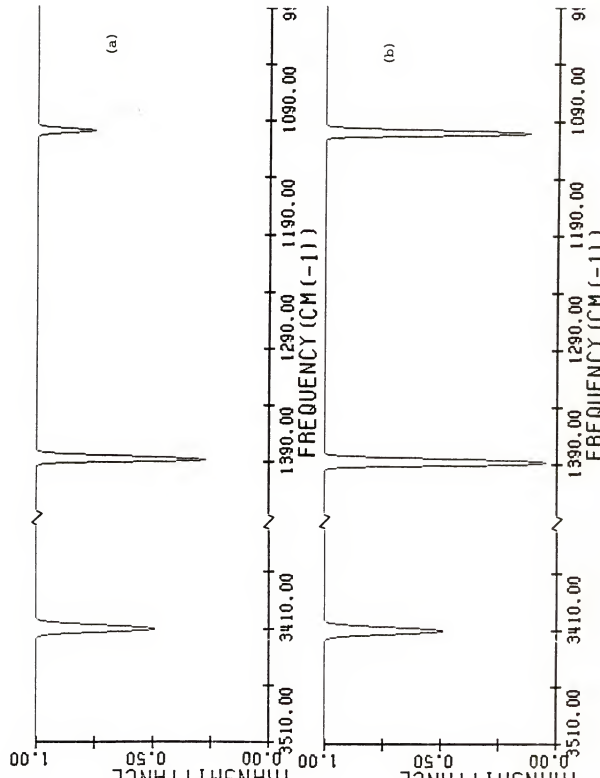
(a)
(b)
TRANSMITTANCE
1.00
0.50
0.00
3510.00
3410.00
1390.00
1290.00
1190.00
1090.00
FREQUENCY(CM(-1))

Fig. 3-10. Comparison of the computer simulation of the $HO_2$ spectrum predicted by transfer of APTs from $CH_3OH$ (for the OH hydrogen) and from $CH_3OH^2$ (for the OH oxygen) with the computer simulation of the experimental matrix spectrum of $HO_2$.

(a) Predicted by transfer of APTs from $CH_3OH$. The concentration has been adjusted in the predicted spectrum as described previously for Fig. 3-6.

(b) Computer simulation of the experimental $HO_2$ spectrum in the argon matrix (see Fig. 3-5).

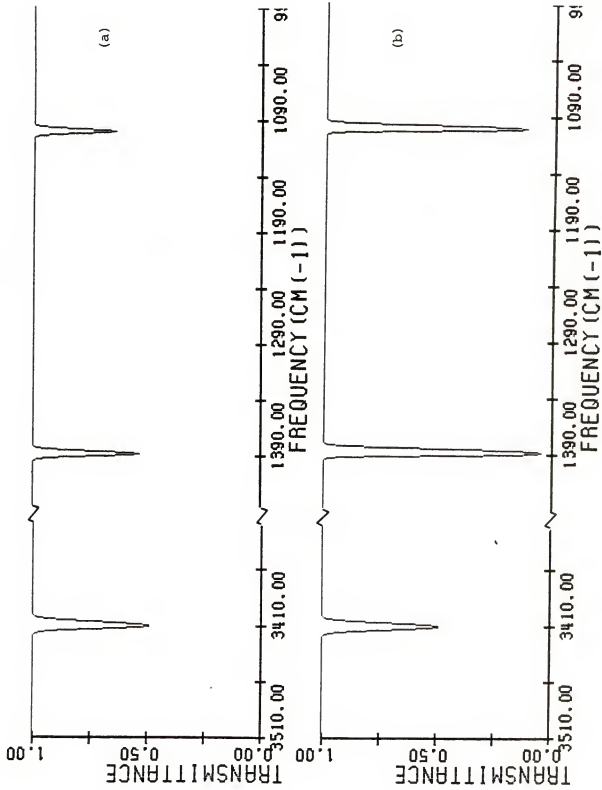
(a)
(b)
TRANSMITTANCE
1.00
0.50
0.00
3510.00
3410.00
1390.00
1290.00
1190.00
1090.00
FREQUENCY (CM(-1))

TABLE 3-31
PARAMETERS USED FOR THE COMPUTER SIMULATION OF THE MATRIX SPECTRUM OF $HO_2$ PREDICTED BY TRANSFER OF APTs

| Predicted by transfer of APTs for $H_2O$ and $CH_3OH$ ($C\ell$=9.79 x $10^{-4}$ mmole $cm^{-2}$) | | | Predicted by transfer of APTs from $CH_3OH$ ($C\ell$=9.79 x $10^{-4}$ mmole $cm^{-2}$) | | |
|---|---|---|---|---|---|
| $\nu_o$[a] ($cm^{-1}$) | $\Delta\nu_{1/2}$[b] ($cm^{-1}$) | A[c] (km $mole^{-1}$) | $\nu_o$[a] ($cm^{-1}$) | $\Delta\nu_{1/2}$[b] ($cm^{-1}$) | A[c] (km $mole^{-1}$) |
| 3410.5 | 6.0 | 47.6 | 3410.5 | 6.0 | 47.6 |
| 1389.0 | 4.4 | 63.0 | 1389.0 | 4.4 | 30.3 |
| 1101.0 | 4.0 | 12.6 | 1101.0 | 4.0 | 19.4 |

[a] Wavenumber position of maximum absorption from the experimental matrix spectrum of $HO_2$ as reported by Smith and Andrews in ref. [58].
[b] Full width at half-maximum of the band [68].
[c] Taken from Table 3-30.

the corresponding elements of the $\underline{P}_x^{(H)}$ APT transferred from $H_2O$ or $CH_3OH$ as compared with the corresponding elements of the ab initio APT of $HO_2$. Those differences reflect in the intensity calculated from these transferred APTs. For instance, Table 3-30 shows that the intensities predicted by transfer of APT from $H_2O$ and $CH_3OH$ are within factor of two or better agreement with the corresponding predicted intensity from ab initio APTs, except for the OH stretching mode. This was to be expected due to the differences between the APT for the hydrogen atom of $H_2O$ and $HO_2$ (see Table 3-29). The intensity for this mode is within factor of 2.4 agreement with the corresponding predicted intensity from ab initio APTs. Table 3-30 also shows the intensities predicted by transfer of APTs from $CH_3OH$. In this case, the intensities predicted for the $\nu_1$ and $\nu_2$ modes of $HO_2$ are within factor of 2.5 agreement with the corresponding intensities predicted from ab initio APTs. Only the intensity predicted for the OO stretching mode is in good agreement with the 4-31G intensity (within factor of 1.3).

We can observe that the general pattern of the spectrum shown in Fig. 3-9 is very similar to that predicted from ab initio APTs shown in Fig. 3-6. Finally, Fig. 3-10 shows that the hydrogen APT from $CH_3OH$ can not be transferred successfully to predict the intensities of $HO_2$. We shall discuss in Chapter 4, the reasons for nontransferability of the hydrogen APTs in terms of charge, charge-flux and overlap contributions to the ab initio APT, for the series of molecules studied in this work.

## Hydrogen Hypochlorite

As was previously discussed in the introduction of this work, the hydrogen hypochlorite molecule is one of the intermediate species in the cycle of the chlorine catalyzed decomposition of ozone in the earth's stratosphere. We have also mentioned that the controversy about the photodissociation cross section of HOCl near 320 nm has recently been settled by Molina, Ishiwata and Molina [13]. Their studies indicated that HOCl is not a long-lived species in the stratosphere and therefore it does not play an important role as a possible inert reservoir for stratospheric chlorine. Nevertheless, we think that our ab initio SCF calculation of the intensity of HOCl will be of interest for comparison with available gas phase experimental intensities [78] and with the ab initio SCF calculations as reported by Komornicki and Jaffe [76]. Their calculation [76] was carried out with the gradient SCF method using a contracted gaussian basis set of triple zeta accuracy plus double polarization. We have performed our ab initio calculations using a 4-31G basis set.

Here we want to digress for a moment to point out that we have not included polarization functions in the basis set for our calculations in HOCl since we think it is important to keep the size and quality of the basis set consistent throughout the calculations if meaningful comparisons are to be made of the predicted properties for a series of related molecules. Therefore, we want to know what changes in the contributions to the ab initio APT are

to be expected when the chemical environment changes within a series of related systems. This is a point which we want to emphasize throughout this study. Only by calculations of the APTs made with the same basis set, can changes in these properties be investigated and analyzed. For instance, it is not appropriate to calculate the intensity for one particular molecule with a minimum STO-3G basis, and then choose an extended basis for the intensity calculations of a second molecule and a double-zeta quality basis set for a third calculation and then try to investigate the variations in the predicted APTs or in their various contributions when the chemical environment is changed from one particular molecule to another. We also want to point out that the inclusion of polarization functions in one basis set may improve the predicted intensity for one specific band; for example, for the O-Cℓ stretching mode. However, this change may overestimate or underestimate the intensities for other bands of the molecule, depending on the particular case studied. We shall discuss this matter, which is of crucial importance in more detail later.

We have also predicted the intensities for the fundamental modes of HOCℓ by transfer of the APTs from other molecules. These predictions are compared with the ab initio and experimental results. These studies of HOCℓ intensities are presented in the next sections of this chapter. We have also investigated the correlation of the ab initio charge-flux contribution to the APT for the hydrogen atom of HOCℓ with the Mulliken electronegativity, as shall be discussed in Chapter 4.

Normal Coordinate Analysis

The geometrical structure of HOCℓ is well established both by microwave [79,80] and infrared spectroscopic studies [81] and by ab initio SCF calculations [11] (see Table 3-32). In our calculations we have used the structural parameters given by Lindsey, Lister and Millen [79]. The parameters $r(OC\ell)=1.69$ Å, $r(OH)=0.97$ Å and $\theta(HOC\ell)=103°$ were taken from reference[79] and used to calculate the position vector for the HOCℓ molecule as given in Table 3-33, according to the coordinate system shown in Fig. 3-11. The column vector given by Eq. (2) was formed using the data presented in Table 3-33. This column vector, the masses of the atoms (H=1.007825, O=15.994910 and Cℓ=34.968854 in amu), the description of the internal coordinates and the U matrix were used as input to program WMAT [27] to obtain the B and G matrices, In Table 3-34 the B matrix for HOCℓ is presented. The G matrix was then diagonalized by program WMAT to form the W matrix, according to Eq. (28). The force field was taken from Schwager and Arkell [82] and is presented in Table 3-35. This force field was obtained by fitting the gas-phase vibrational wavenumbers of HOCℓ and three other isotopically substituted molecules, using the least-squares procedure presented in Chapter 2. Table 3-35 also compares that force field with the one obtained by Ogilvie [50]. The main differences between those force fields is observed in the interaction force constants $F_{r_{(OH)},\theta}$ and $F_{r(OC\ell),\theta}$. We decided to apply both force fields to investigate the effect in the predicted intensities. We find no appreciable change in the

TABLE 3-32
STRUCTURAL PARAMETERS OF HOCℓ

| r(OH)[a] | r(OCℓ)[a] | θ(HOCℓ) | References |
|---|---|---|---|
| 0.975 | 1.689 | 102.5° | Mirri, Scappini and Cazzoli, ref. [80] (microwave) |
| 0.97 | 1.69 | 103° | Lindsey, Lister and Millen, ref. [79] (microwave) |
| 0.97 | 1.689 | 104.8° | Ashby , ref. [81] (infrared) |
| 0.97 | 1.69 | 105° | Jaffe and Langhoff, ref. [ 11 ] (ab initio SCF-CI calculation) |

[a]Bond length in units of Å

TABLE 3-33
EQUILIBRIUM POSITION VECTORS FOR HOCℓ (UNITS ARE Å)

| Atom No | x | y | z |
|---|---|---|---|
| O, 1 | 0.0 | 0.0 | 0.0 |
| H, 2 | 0.0 | -0.970000 | 0.0 |
| Cℓ, 3 | 0.0 | 0.380167 | -1.646685 |

[a]The atom numbering and coordinate system are given in Fig. 3-11.

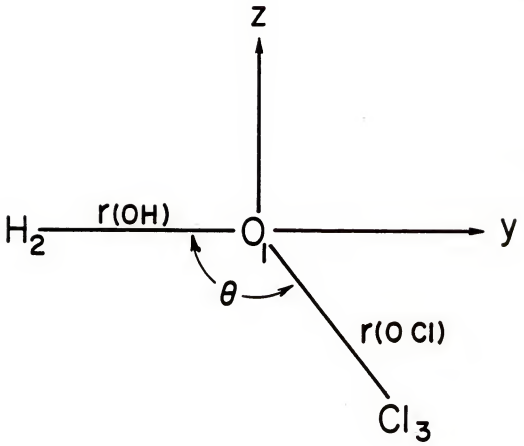


Fig. 3-11. Coordinate system and atom numbering for HOCl.

TABLE 3-34
THE $\underline{B}$ MATRIX FOR HOCℓ

| | | | | | | | | |
|---|---|---|---|---|---|---|---|---|
| 0.0 | 1.0 | 0.0 | 0.0 | -1.0 | 0.0 | 0.0 | 0.0 | 0.0 |
| 0.0 | -0.576551 | -1.164035 | 0.0 | 0.0 | 1.030928 | 0.0 | 0.576551 | 0.133107 |
| 0.0 | -0.224951 | 0.974370 | 0.0 | 0.0 | 0.0 | 0.0 | 0.224951 | -0.974370 |

Note: All elements of $\underline{B}$ are unitless since we have used a weighted unit system (see also Table 2-1). Notice also that $\underline{B} = \underline{B}$, since the $\underline{U}$ matrix is the identity matrix in this case.

TABLE 3-35
THE EXPERIMENTAL F MATRICES FOR HOCℓ
(UNITS ARE MDYNES Å$^{-1}$)
(1 aJ Å$^{-2}$ = 1 mdyne Å$^{-1}$ = 100 N m$^{-1}$)

From Schwager[a]

$$\begin{pmatrix} 7.104 & 0.0 & 0.0 \\ 0.0 & 0.775 & 0.677 \\ 0.0 & 0.677 & 3.980 \end{pmatrix}$$

From Ogilvie[b]

$$\begin{pmatrix} 7.3177 & -0.1000 & 0.0 \\ -0.1000 & 0.7860 & 0.3844 \\ 0.0 & 0.3844 & 3.6205 \end{pmatrix}$$

[a]Taken from Schwager and Arkell and reported in ref. [82] $F_{11} = F_{r(OH)}$; $F_{22} = F_{\theta}$; $F_{23} = F_{r(OC\ell),\theta}$ and $F_{33} = F_{r(OC\ell)}$.

[b]Taken from Ogilvie and reported in ref. [50]. $F_{11} = F_{r(OH)}$; $F_{12} = F_{r(OH),\theta}$; $F_{22} = F_{\theta}$; $F_{23} = F_{r(OC\ell),\theta}$ and $F_{33} = F_{r(OC\ell)}$. Notice that the following force constants given by Ogilvie are scaled by the OCℓ and OH bond lengths of HOCℓ, according to: $F'_{\theta} = F_{\theta}/r_1 r_2$, $F'_{r_1\theta} = F_{r_1\theta}/r_1$ and $F'_{r_2\theta} = F_{r_2\theta}/r_2$, where $r_1$ and $r_2$ are the OH and OCℓ bond lengths of HOCℓ respectively and the prime indicates here the scaled force constants given by Ogilvie. Notice also that the force constants reported by Ogilvie are in units of N m$^{-1}$. Here $\underline{F} = \underline{F}$, since the $\underline{U}$ matrix in the identity matrix.

predicted intensities for HOCℓ that can be attributed to the changes in the force field. The W matrix obtained from program WMAT and the F matrix were used as input to program CHARLY [27] to obtain the eigenvectors L, and eigenvalues $\Lambda$ of the G F product matrix. The L matrix generated from both force fields and the calculated vibrational wavenumbers of HOCℓ are shown in Tables 3-36 and 3-37, respectively.

Ab Initio 4-31G APTs and Calculated Intensities for HOCℓ

The APTs for HOCℓ were quantum mechanically calculated as before for HOF and $HO_2$ using a 4-31G basis set. The details of this calculation have been discussed in Chapter 2. The APTs were calculated with respect to the coordinate system shown in Fig. 3-11. The ab initio 4-31G APTs for HOCℓ are given in Table 3-38. The APT for the central O atom (1) was calculated from the null condition given by Eq. (62). The intensities for each fundamental band of HOCℓ calculated from the ab initio 4-31G APTs are given in Table 3-39. Also shown in that Table are the absolute intensities calculated by Komornicki and Jaffe [76] with the GRADSCF program [37] using a contracted gaussian basis set of triple-zeta accuracy plus double polarization (TZPP). The experimental intensities for HOCℓ gas have been measured by Su et al. [78], with a Fourier transform infrared (FTIR) spectrometer, and these values are also included in Table 3-39. This Table shows that the intensities predicted from a 4-31G basis set are within a factor of two agreement with the corresponding experimental intensities except for the OCℓ vibrational mode. The inclusion of

TABLE 3-36
THE $\underline{L}$ MATRICES FOR HOCl (UNITS ARE $u^{-1/2}$)

| | | | |
|---|---|---|---|
| $\begin{pmatrix} 1.026992 & 0.006174 & 0.001843 \\ -0.040833 & 1.040859 & -0.291563 \\ -0.014374 & 0.023306 & 0.300611 \end{pmatrix}$ | [a] |
| $\begin{pmatrix} 1.026785 & 0.021614 & 0.000500 \\ -0.057663 & 1.074216 & -0.113130 \\ -0.013263 & -0.027549 & 0.300303 \end{pmatrix}$ | [b] |

[a] $\underline{L}$ matrix generated from the force field given by Schwager and Arkell [82].
[b] $\underline{L}$ matrix generated from the force field given by Ogilvie [50].

TABLE 3-37

OBSERVED AND CALCULATED VIBRATIONAL WAVENUMBERS FOR HOCℓ (UNITS ARE $cm^{-1}$)

| Mode[a] | Observed[b] | Calculated[c] | Percent error[d] | Observed[e] | Calculated[f] | Percent error[d] |
|---|---|---|---|---|---|---|
| $\nu_1$(OH) | 3626.0 | 3567.80 | -1.61 | 3609.20 | 3623.3 | 0.39 |
| $\nu_2$(Δθ) | 1242.0 | 1218.93 | -1.86 | 1239.90 | 1226.47 | -1.08 |
| $\nu_3$(OCℓ) | 739.0 | 721.92 | -2.31 | 725.00 | 726.10 | 0.15 |

[a]Here $\nu_1$(OH), $\nu_2$(Δθ) and $\nu_3$(OCℓ) refer to the OH stretching, the bending mode and the OCℓ stretching band, respectively.

[b]K. Hedberg and R. M. Badgar, J. Chem. Phys. 19, 508 (1951).

[c]The wavenumbers were calculated using the equilibrium molecular geometry of HOCℓ given in ref. [79] and the force field obtained from ref. [82].

[d][ν(calc.) - ν(obs.)] x 100/ν(obs).

[e]Ogilvie [50].

[f]Calculated from the equilibrium molecular geometry of HOCℓ reported in ref. [ 79 ] and the force field obtained from ref. [50].

TABLE 3-38
AB INITIO APTs FOR HOCℓ(UNITS ARE e)

| | | | |
|---|---|---|---|
| $\underset{\sim}{P}^{O}_{x}$ | -0.562 | 0 | 0 |
| | 0 | -0.295 | 0.010 |
| | 0 | 0.209 | -0.018 |
| $\underset{\sim}{P}^{H}_{x}$ | 0.488 | 0 | 0 |
| | 0 | 0.244 | -0.0314 |
| | 0 | -0.105 | 0.208 |
| $\underset{\sim}{P}^{C\ell}_{x}$ | 0.0743 | 0 | 0 |
| | 0 | 0.0512 | 0.0210 |
| | 0 | -0.104 | -0.190 |

Note: A 4-31G basis set was used for the ab initio calculations of the APTs for HOCℓ. The $\underset{\sim}{P}^{O}_{\vec{x}}$ tensor was calculated using the null condition. The coordinate system is shown in Fig. 3-11.

TABLE 3-39
ABSOLUTE AND EXPERIMENTAL INTENSITIES OF HOCℓ (UNITS ARE km $mole^{-1}$)

| Band | $\nu(cm^{-1})$ | A(4-31G)[a] | A(TZPP)[b] | A(Expl.)[c] |
|---|---|---|---|---|
| $\nu$(OH) | 3609.2 | 75.3 | 122.3 | 56.6 |
| $\nu(\Delta\theta)$ | 1239.9 | 39.3 | 45.8 | 73.9 |
| $\nu$(OCℓ) | 725.0 | 0.089 | 6.2 | 10.6 |

[a] Calculated intensities using the 4-31G APTs given in Table 3-38 (this work)
[b] Calculated by Komornicki and Jaffe and reported in ref. [ 76 ] using a contracted gaussian basis set of triple-zeta accuracy plus double polarization (6s4p2d/5s3p2d/3s2p), for the calculation of the dipole moment derivatives.
[c] Experimental absolute intensities, given by Su et al. [78].

polarization function is definitely important for predicting the intensity for this mode, but then we find that the intensity for the OH stretching band is overestimated as has been previously discussed. We have not included polarization functions in our basis set for reasons also discussed in the introduction to the section.

We have also calculated the charge, charge-flux and overlap contributions to the 4-31G ab initio APTs for the atoms in HOCℓ, according to the CCFO model [52,53], using Eqs. (63), (64) and (67) respectively. These APTs are given in Tables 3-40, 3-41 and 3-42. The coordinate system is shown in Fig. 3-11. In Chapter 4, we shall compare the elements of those APTs for all of the molecules studied in this work.

Predicted and Experimental Computer-Simulated Gas-Phase Spectra of HOCℓ

The theoretical and experimental computer-simulated spectra of HOCℓ in gas phase are shown in Figs. 3-12 and 3-13. The parameters used for the computer simulation are shown in Table 3-43. Figure 3-12 shows the predicted spectrum of HOCℓ from ab initio 4-31G APTs compared to the computer fit to the experimental spectrum of HOCℓ in gas phase. Notice that the intensity predicted for the OH stretching at 3600 $cm^{-1}$ and the bending mode at 1240 $cm^{-1}$ are within factor of two or better agreement with the corresponding experimental intensities. The band at 725 $cm^{-1}$ is not shown in that spectrum since its intensity is only 0.089 km $mole^{-1}$ as predicted from the 4-31G APTs.

TABLE 3-40
CHARGE, CHARGE-FLUX, OVERLAP AND TOTAL APTs
ON THE HYDROGEN ATOM OF HOCℓ
(UNITS ARE e)

$$\underline{P}_x^H(C) = \begin{pmatrix} 0.44 & 0 & 0 \\ 0 & 0.44 & 0 \\ 0 & 0 & 0.44 \end{pmatrix}$$

$$\underline{P}_x^H(CF) = \begin{pmatrix} 0 & 0 & 0 \\ 0 & 0.12 & 0.05 \\ 0 & -0.06 & -0.24 \end{pmatrix}$$

$$\underline{P}_x^H(O) = \begin{pmatrix} 0.04 & 0 & 0 \\ 0 & -0.32 & -0.08 \\ 0 & -0.05 & 0.004 \end{pmatrix}$$

$$\underline{P}_x^H(T) = \begin{pmatrix} 0.49 & 0 & 0 \\ 0 & 0.24 & -0.03 \\ 0 & -0.10 & 0.21 \end{pmatrix}$$

Note: The charge (C), charge-flux (CF) and overlap (O) contributions to the total (T) 4-31G APT on the hydrogen atom were calculated according to the CCFO model [52,53]. The coordinate system is shown in Fig. 3-11.

TABLE 3-41
CHARGE, CHARGE-FLUX, OVERLAP AND TOTAL APTs ON THE CHLORINE ATOM OF HOCℓ(UNITS ARE e)

$$\underline{P}_{x}^{C\ell}(C) \quad \begin{pmatrix} 0.22 & 0 & 0 \\ 0 & 0.22 & 0 \\ 0 & 0 & 0.22 \end{pmatrix}$$

$$\underline{P}_{x}^{C\ell}(CF) \quad \begin{pmatrix} 0 & 0 & 0 \\ 0 & -0.02 & 0.21 \\ 0 & 0.09 & -0.99 \end{pmatrix}$$

$$\underline{P}_{x}^{C\ell}(O) \quad \begin{pmatrix} -0.15 & 0 & 0 \\ 0 & -0.15 & -0.19 \\ 0 & -0.19 & 0.57 \end{pmatrix}$$

$$\underline{P}_{x}^{C\ell}(T) \quad \begin{pmatrix} 0.07 & 0 & 0 \\ 0 & 0.05 & 0.02 \\ 0 & -0.10 & -0.19 \end{pmatrix}$$

Note: The charge (C), charge-flux (CF) and overlap (O) contributions to the total (T) APT on the chlorine atom were calculated according to the CCFO model [52,53]. The coordinate system is shown in Fig. 3-11.

TABLE 3-42
CHARGE, CHARGE-FLUX, OVERLAP AND TOTAL APTs ON THE OXYGEN ATOM OF HOCℓ (UNITS ARE e)

$\underline{P}_x^O$ (C)

$$\begin{pmatrix} -0.67 & 0 & 0 \\ 0 & -0.67 & 0 \\ 0 & 0 & -0.67 \end{pmatrix}$$

$\underline{P}_x^O$ (CF)

$$\begin{pmatrix} 0 & 0 & 0 \\ 0 & -0.10 & -0.26 \\ 0 & -0.03 & 1.23 \end{pmatrix}$$

$\underline{P}_x^O$ (O)

$$\begin{pmatrix} 0.10 & 0 & 0 \\ 0 & 0.47 & 0.27 \\ 0 & 0.24 & -0.58 \end{pmatrix}$$

$\underline{P}_x^O$ (T)

$$\begin{pmatrix} -0.56 & 0 & 0 \\ 0 & -0.30 & 0.01 \\ 0 & 0.21 & -0.02 \end{pmatrix}$$

Note: The charge (C), charge-flux (CF) and overlap (O) contributions to the total (T) 4-31G APT on the oxygen atom were calculated according to the CCFO model [52,53]. The coordinate system is shown in Fig. 3-11.

Fig. 3-12. Computer simulation of the predicted spectrum of HOCℓ from 4-31G APTs and the computer-simulated gas phase spectrum of HOCℓ.

(a) Predicted

(b) Experimental

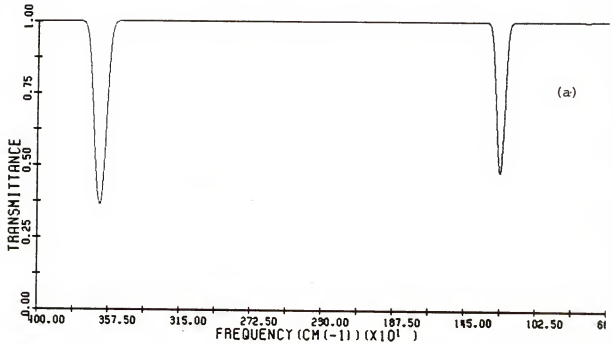
TRANSMITTANCE
1.00
0.75
0.50
0.25
0.00
400.00
357.50
315.00
272.50
230.00
187.50
145.00
102.50
FREQUENCY (CM(-1)) (X10¹ )
(a)

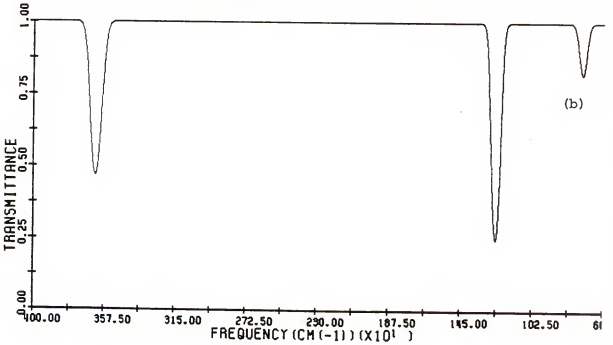
TRANSMITTANCE
1.00
0.75
0.50
0.25
0.00
400.00
357.50
315.00
272.50
230.00
187.50
145.00
102.50
FREQUENCY (CM(-1)) (X10¹ )
(b)

Fig. 3-13. Computer simulation of the predicted spectrum of HOCℓ using a contracted gaussian basis set of triple-zeta accuracy plus double polarization and the computer-simulated gas phase infrared spectrum of HOCℓ.

(a) Predicted (Komornicki and Jaffe in ref. [76]).

(b) Experimental.

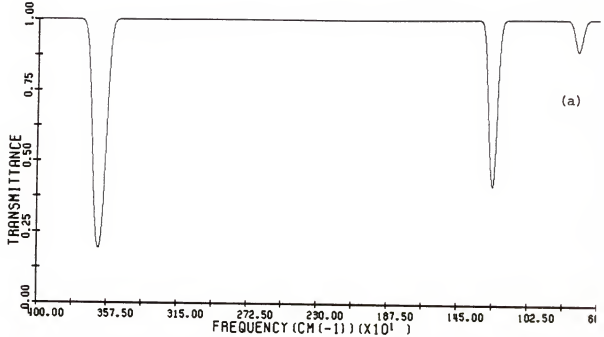
TRANSMITTANCE
1.00
0.75
0.50
0.25
0.00
(a)
400.00
357.50
315.00
272.50
230.00
187.50
145.00
102.50
FREQUENCY (CM(-1)) (X10¹ )

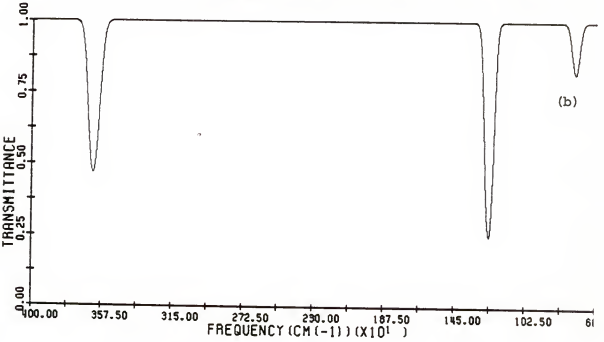
TRANSMITTANCE
1.00
0.75
0.50
0.25
0.00
(b)
400.00
357.50
315.00
272.50
230.00
187.50
145.00
102.50
FREQUENCY (CM(-1)) (X10¹ )

TABLE 3-43
PARAMETERS USED FOR THE COMPUTER SIMULATION OF THE PREDICTED AND EXPERIMENTAL GAS PHASE SPECTRA OF HOCℓ

| Predicted (4-31G APTs) ($C\ell$=1 x $10^{-3}$ mole $\ell^{-1}$cm) | | | Predicted (TZPP) ($C\ell$=1 x $10^{-3}$ mole $\ell^{-1}$cm) | | | Experimental ($C\ell$=1 x $10^{-3}$ mole $\ell^{-1}$ cm) | | |
|---|---|---|---|---|---|---|---|---|
| $\nu_o$[a] ($cm^{-1}$) | $\Delta\nu_{1/2}$[b] ($cm^{-1}$) | A[c] (km $mole^{-1}$) | $\nu_o$[a] ($cm^{-1}$) | $\Delta\nu_{1/2}$[b] ($cm^{-1}$) | A[c] (km $mole^{-1}$) | $\nu_o$[a] ($cm^{-1}$) | $\Delta\nu_{1/2}$[b] ($cm^{-1}$) | A[c] (km $mole^{-1}$) |
| 3609.2 | 70.0 | 75.3 | 3609.2 | 70.0 | 122.3 | 3609.2 | 70.0 | 56.6 |
| 1239.9 | 50.0 | 39.3 | 1239.9 | 50.0 | 45.8 | 1239.9 | 50.0 | 73.9 |
| 725.0 | 50.0 | 0.089 | 725.0 | 50.0 | 6.2 | 725.0 | 50.0 | 10.6 |

[a] Wavenumber position of maximum absorption from the exeprimental gas phase spectrum of HOCℓ [50].
[b] Full width at half-maximum of the band estimated from the gas phase spectrum of HOCℓ and reported in ref. [78]
[c] Taken from Table 3-39.

Figure 3-13 shows the computer simulation of the infrared spectrum of HOCℓ calculated from the intensities reported by Komornicki and Jaffe [76]. Notice that the OCℓ stretching mode now appears with appreciable predicted intensity at 725 $cm^{-1}$. The bands at 1240 and 725 $cm^{-1}$ are in very good agreement with the experimental intensities. However the intensity for the OH stretching mode is overestimated. Komornicki and Jaffe suggested that electron correlation effects could make a large contribution to the calculated dipole derivatives for the OH stretching mode in HOCℓ.

It is well known that calculations at the SCF-CI level with an extended basis set including polarization functions result in reduced Hartree-Fock force constants and dipole moments [83]. However, it is also true that calculations of dipole moments derivatives are very sensitive to the quality of the basis set used. Let us consider, for example, the predicted intensity for the $\nu_1$ vibrational mode of $H_2O$. This is shown in Table 3-44, where the predicted intensity for this mode are ordered according to the quality of the basis set. Notice that 1.07 km $mole^{-1}$ is the intensity predicted with a 4-31G basis set. The next three subsequent intensity values were predicted with very large basis sets of increasing quality at Hartree-Fock level and including different sets of polarization functions [84-86].

That Table also includes several experimental values reported for the intensity of this mode [87-89]. It is interesting now to notice that by increasing the quality of the basis set and

TABLE 3-44
COMPARISON OF THE SIZE AND QUALITY OF A BASIS SET WITH THE PREDICTED INTENSITY FOR THE $\nu_1$ VIBRATIONAL MODE OF $H_2O$

| $A_1(H_2O)$[a] (km mole$^{-1}$) | $E_o$ (Hartrees) | Description |
|---|---|---|
| 1.07[a] | -75.909 | SCF level(4-31G basis) |
| 8.77[b] | -76.035 | SCF-HF level |
| 13.6[c] | -76.041 | SCF-HF level |
| 15.4[d] | -76.051 | SCF-HF level |
| (2.24)[e],(2.51)[f],(2.26)[g] | -76.431 | Experimental |

[a] Quoted by Zilles [53,p.73]. The intensities for the $\nu_2$ and $\nu_3$ modes are within factor of two agreement with the corresponding experimental values.
[b] Pulay [84].
[c] Smith, Jorgensen and Ohrn [85].
[d] Krohn and Kern [86].
[e] Clough et al. [87].
[f] Toth [88].
[g] Flaud and Camy-Peyret [89].

performing the calculations at the Hartree-Fock level causes the intensities to be overestimated by factors of 4,6 and 7. However, the predicted intensity with the 4-31G basis is within factor of two agreement with the experimental results.

This does not seem to be attributable to the error in the Hartree-Fock approximation (dissociation to ions instead of neutral atoms). Instead, we believe this error is due to the criterion chosen to measure the quality of the basis set: namely, that it produces a lower energy eigenvalue. It is unrealistic to believe that basis sets including different sets of polarization functions which have been optimized only from energy eigenvalue considerations would also necessarily reflect the proper flexibility to accommodate the electronic charge-flux redistribution when an atom is displaced from its equilibrium configuration.

In fact, we suggest that the discrepancies in the predicted values for the dipole moment derivatives with different basis sets (for example those from a double or triple-zeta plus polarization basis set compared with results from a 4-31G basis for $H_2O$, HOCℓ and $HO_2$) can be understood on these terms. The inclusion of polarization functions can be very important for lowering the total molecular energy but it does not assure the use of a perfect formally balanced basis set for dipole moment derivative calculations. In other words, the orbital exponents of the polarization functions are not scaled to reflect the proper charge-flux redistribution in a molecule for a bond stretching or bending deformation. It is important to point out that energy eigenvalues (variation theorem)

should not be used, in general, as the sole criterion for quantum mechanical calculations of properties depending as sensitivily as dipole moments on the charge distribution.

Mulliken [55] was the first to recognize the difficulty of choosing a formally balanced polarization set for heteiopolar molecules and has pointed out that there is no assurance that 2p polarization function on the hydrogen of HF would provide a perfect balance for the d polarization set of the fluorine atom. Clementi [90] has also pointed out that if the dipole moment would have been included as an additional criterion for the optimization of the orbital exponents of the basis set chosen, a better agreement between experiment and theory could have been obtained for the dipole moment calculation of HF. However, it is clear that dipole moment can not be the best criterion for choosing a quality basis set, since it is not an atomic property and therefore different sets of orbital exponents would have to be used for different molecules. However, it is possible that an extended flexibility of a basis set could be achieved at the SCF-HF level if intensity parameters could be used as an additional criterion in choosing a quality basis set. Accordingly, we suggest that effective atomic charges could be used as an additional criterion for optimization of the outer-shell orbital exponents of a basis set, since this atomic property is invariant to the normal coordinate analysis and seems to be transferable among a great number of molecules [52].

In Chapter 4 we investigate further the prediction of the spectrum of HOCℓ using a 4-31G basis set, without the inclusion of

polarization functions. It is shown that if a reasonable correction is made to the charge-flux tensor of the hydrogen atom, the predicted spectrum almost superimposes on the corresponding experimental spectrum of HOCℓ.

Computer Simulation of the Gas-Phase Spectrum of HOCℓ Predicted by Transfer of APTs

In this section we shall discuss several attempts to transfer experimental APTs from related molecules to predict the spetrum of HOCℓ. This study involves APTs transferred from four sets of molecules: ($C\ell CN$ [91], $H_2O$ [53]), ($CH_3C\ell$ [34], $H_2O$ [53]), ($C\ell CN$[91], $CH_3OH$ [35]), and ($CH_3C\ell$ [34], $CH_3OH$ [35]). The APTs transferred from those molecules are shown in Tables 3-45, 3-46, 3,47 and 3-48 respectively, and the coordinate system relative to those APTs is shown in Fig. 3-11. The predicted intensities are compared in Table 3-49 and the computer simulations of the predicted and experimental spectra are shown in Figs. 3-14 to 3-17. The parameters used for the computer simulation are listed in Table 3-50.

It is interesting to compare the elements of the chlorine APTs for $C\ell CN$ and $CH_3C\ell$. Notice, for instance, that the elements of the chlorine APTs for $C\ell CN$ and $CH_3C\ell$ as given, for instance in Tables 3-45 and 3-46 are substantially different. These differences are expected, since a chlorine atom bonded to the CN group is chemically quite different from one bonded to the methyl group. The most substantial differences are observed for the $\partial p_x/\partial x$ and $\partial p_y/\partial y$ elements. Notice also, that the signs of the derivatives for those elements are also different. It is also interesting to notice that the $\partial p_z/\partial z$ elements are approximately the same for both molecules.

TABLE 3-45
TRANSFERRED EXPERIMENTAL APTs FROM C$\ell$CN AND $H_2O$
(UNITS ARE e)

$$\underline{P}_x^O = \begin{pmatrix} -0.473 & 0 & 0 \\ 0 & -0.246 & -0.063 \\ 0 & -0.078 & 0.160 \end{pmatrix}$$

$$\underline{P}_x^H = \begin{pmatrix} 0.330 & 0 & 0 \\ 0 & 0.132 & -0.064 \\ 0 & -0.049 & 0.247 \end{pmatrix}$$

$$\underline{P}_x^{C\ell} = \begin{pmatrix} 0.143 & 0 & 0 \\ 0 & 0.114 & 0.127 \\ 0 & 0.127 & -0.407 \end{pmatrix}$$

Note: $\underline{P}_x^O$ was calculated from the null condition given by Eq. (62).
$\underline{P}_x^H$ was transferred from $H_2O$ [53].
$\underline{P}_x^{C\ell}$ was transferred from C$\ell$CN [91]. The original APTs were transformed to the coordinate system shown in Fig. 3-11.

TABLE 3-46
TRANSFERRED EXPERIMENTAL APTs FROM $CH_3Cl$ AND $H_2O$
(UNITS ARE e)

| | | | |
|---|---|---|---|
| $\underline{P}_x^O$ | -0.096 | 0 | 0 |
| | 0 | 0.113 | 0.017 |
| | 0 | 0.002 | 0.188 |
| $\underline{P}_x^H$ | 0.330 | 0 | 0 |
| | 0 | 0.132 | -0.064 |
| | 0 | -0.049 | 0.247 |
| $\underline{P}_x^{Cl}$ | -0.234 | 0 | 0 |
| | 0 | -0.245 | 0.047 |
| | 0 | 0.047 | -0.435 |

Note: $\underline{P}_x^O$ was calculated from the null condition given by Eq. (62).
$\underline{P}_x^H$ was transferred from $H_2O$ [53].
$\underline{P}_x^{Cl}$ was transferred from $CH_3Cl$ [34].
The coordinate system is shown in Fig. 3-11.

TABLE 3-47
TRANSFERRED EXPERIMENTAL APTs FROM ClCN AND $CH_3OH$
(UNITS ARE e)

$$\underline{P}_x^O = \begin{pmatrix} -0.403 & 0 & 0 \\ 0 & -0.255 & -0.057 \\ 0 & -0.145 & 0.246 \end{pmatrix}$$

$$\underline{P}_x^H = \begin{pmatrix} 0.260 & 0 & 0 \\ 0 & 0.141 & -0.070 \\ 0 & 0.018 & 0.161 \end{pmatrix}$$

$$\underline{P}_x^{Cl} = \begin{pmatrix} 0.143 & 0 & 0 \\ 0 & 0.114 & 0.127 \\ 0 & 0.127 & -0.407 \end{pmatrix}$$

Note: $\underline{P}_x^O$ was calculated from the null condition given by Eq. (62).
$\underline{P}_x^H$ was transferred from $CH_3OH$ [35].
$\underline{P}_x^{Cl}$ was transferred from ClCN [91].
The coordinate system is shown in Fig. 3-11.

TABLE 3-48
TRANSFERRED EXPERIMENTAL APTs FROM $CH_3Cl$ AND $CH_3OH$
(UNITS ARE e)

$$\underline{P}_x^O = \begin{pmatrix} -0.026 & 0 & 0 \\ 0 & 0.104 & 0.023 \\ 0 & -0.065 & 0.274 \end{pmatrix}$$

$$\underline{P}_x^H = \begin{pmatrix} 0.260 & 0 & 0 \\ 0 & 0.141 & -0.070 \\ 0 & 0.018 & 0.161 \end{pmatrix}$$

$$\underline{P}_x^{Cl} = \begin{pmatrix} -0.234 & 0 & 0 \\ 0 & -0.245 & 0.047 \\ 0 & 0.047 & -0.435 \end{pmatrix}$$

Note: $\underline{P}_x^O$ was calculated from the null condition given by Eq. (62).
$\underline{P}_x^H$ was transferred from $CH_3OH$ [35].
$\underline{P}_x^{Cl}$ was transferred from $CH_3Cl$ [34].
The coordinated system is shown in Fig. 3-11.

TABLE 3-49
PREDICTED INTENSITIES FROM TRANSFERRED APTs FOR HOCℓ(UNITS ARE km mole$^{-1}$)

| Band | $\nu$ (cm$^{-1}$) | $(C\ell\overset{*}{C}N, \overset{A}{H_2}\overset{*}{O})$ | $(CH_3C\ell, \overset{A}{H_2}\overset{*}{O})$ | $(C\ell\overset{*}{C}N, \overset{A}{C}H_3O\overset{*}{H})$ | $(CH_3C\ell, \overset{*}{\overset{A}{C}}H_3O\overset{*}{H})$ | A (Expl.) |
|---|---|---|---|---|---|---|
| $\nu$(OH) | 3609.2 | 21.4 | 16.2 | 23.1 | 16.8 | 56.6 |
| $\nu(\Delta\theta)$ | 1239.9 | 65.6 | 66.2 | 31.6 | 33.3 | 73.9 |
| $\nu$(OCℓ) | 725.0 | 3.5 | 3.9 | 6.8 | 7.3 | 10.6 |

Note: The transferred APTs are given in Tables 3-45 to 3-48. The experimental intensities are given by Su et al. in ref. [ 78 ] and are expressed here in km mole$^{-1}$. The * indicates the atoms from which the APTs were transferred.

Fig. 3-14. Computer simulation of the predicted spectrum of HOCℓ from transferred APTs from CℓCN and $H_2O$ and the computer-simulated gas phase spectrum of HOCℓ.

(a) Predicted

(b) Experimental

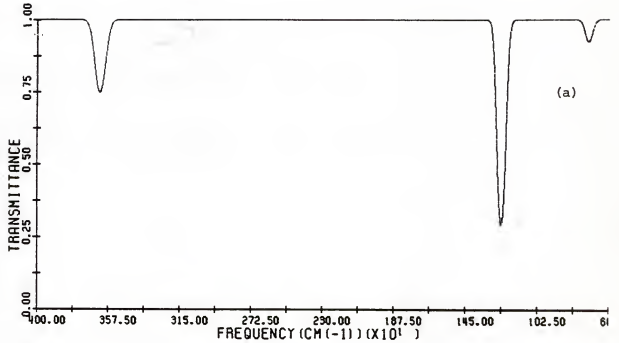
1.00
0.75
0.50
0.25
0.00
TRANSMITTANCE
(a)
400.00
357.50
315.00
272.50
230.00
187.50
145.00
102.50
FREQUENCY (CM(-1)) (X10¹ )

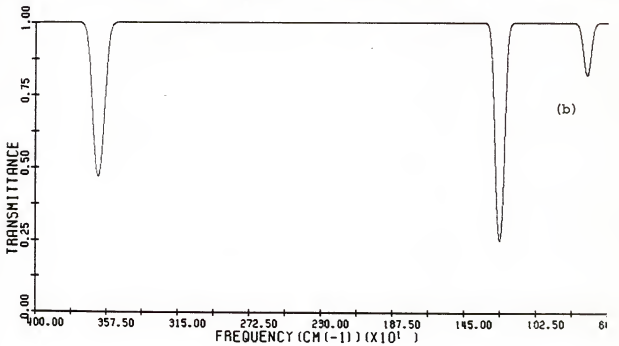
1.00
0.75
0.50
0.25
0.00
TRANSMITTANCE
(b)
400.00
357.50
315.00
272.50
230.00
187.50
145.00
102.50
FREQUENCY (CM(-1)) (X10¹ )

Fig. 3-15. Computer simulation of the predicted spectrum of HOCℓ from transferred APTs from $CH_3Cℓ$ and $H_2O$ and the computer-simulated gas phase spectrum of HOCℓ.

(a) Predicted

(b) Experimental

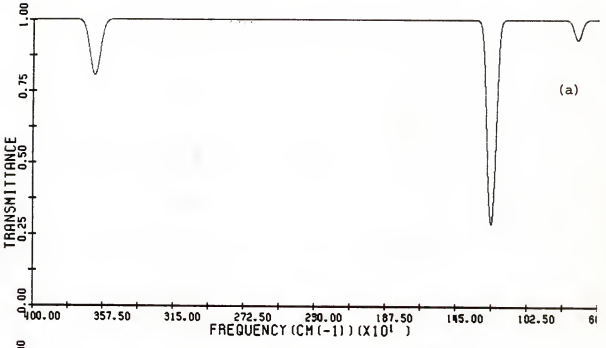
1.00
0.75
0.50
0.25
0.00
TRANSMITTANCE
(a)
400.00
357.50
315.00
272.50
230.00
187.50
145.00
102.50
FREQUENCY (CM(-1)) (X10¹ )

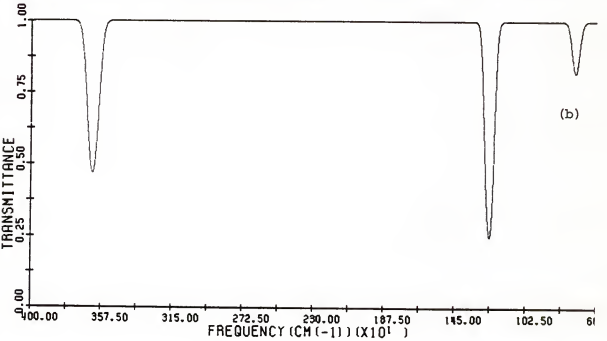
1.00
0.75
0.50
0.25
0.00
TRANSMITTANCE
(b)
400.00
357.50
315.00
272.50
230.00
187.50
145.00
102.50
FREQUENCY (CM(-1)) (X10¹ )

Fig. 3-16. Computer simulation of the predicted spectrum of HOCℓ from transferred APTs from CℓCN and $CH_3OH$ and the computer-simulated gas phase spectrum of HOCℓ.

(a) Predicted

(b) Experimental

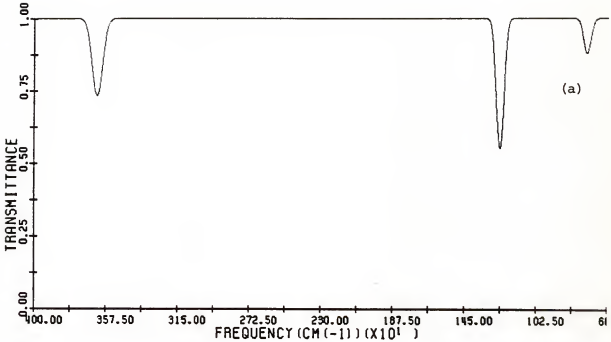
1.00
0.75
0.50
0.25
0.00
TRANSMITTANCE
(a)
400.00
357.50
315.00
272.50
230.00
187.50
145.00
102.50
FREQUENCY (CM(-1)) (X10¹ )

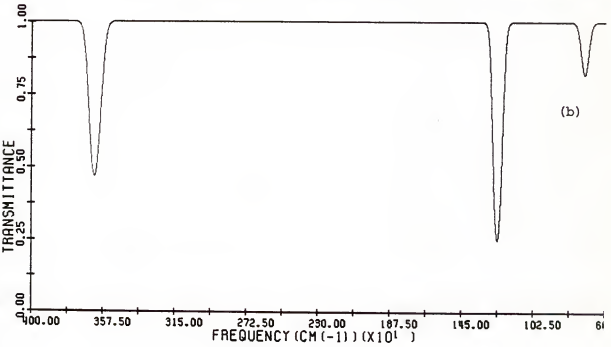
1.00
0.75
0.50
0.25
0.00
TRANSMITTANCE
(b)
400.00
357.50
315.00
272.50
230.00
187.50
145.00
102.50
FREQUENCY (CM(-1)) (X10¹ )

Fig. 3-17. Computer simulation of the predicted spectrum of HOCℓ from transferred APTs from $CH_3Cℓ$ and $CH_3OH$ and the computer-simulated gas phase spectrum of HOCℓ.

(a) Predicted

(b) Experimental

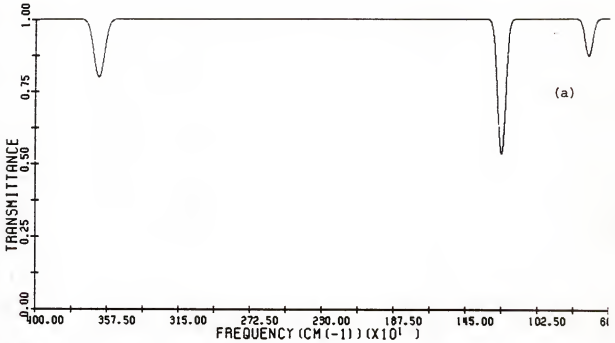
TRANSMITTANCE
1.00
0.75
0.50
0.25
0.00
(a)
400.00
357.50
315.00
272.50
230.00
187.50
145.00
102.50
FREQUENCY (CM(-1))(X10¹)

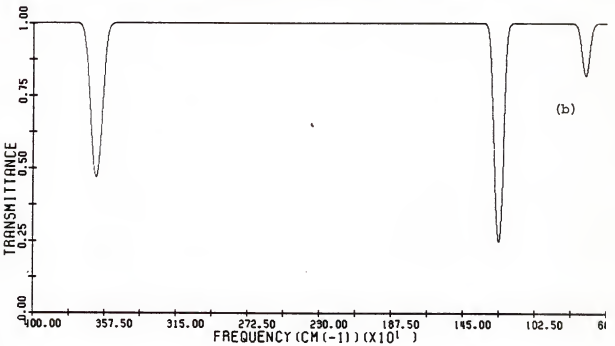
TRANSMITTANCE
1.00
0.75
0.50
0.25
0.00
(b)
400.00
357.50
315.00
272.50
230.00
187.50
145.00
102.50
FREQUENCY (CM(-1))(X10¹)

TABLE 3-50
PARAMETERS USED FOR THE COMPUTER SIMULATION OF THE GAS-PHASE SPECTRUM OF HOCℓ
PREDICTED BY TRANSFER OF APTs

| Predicted ($C\ell$=1 x $10^{-3}$mole $\ell^{-1}$cm) | | | | | | Experimental ($C\ell$=1 x $10^{-3}$mole $\ell^{-1}$cm) | | |
|---|---|---|---|---|---|---|---|---|
| $\nu_o$[a] ($cm^{-1}$) | $\Delta\nu_{1/2}$[b] ($cm^{-1}$) | A[c] ($C\ell CN, H_2O$) | A[c] ($CH_3C\ell, H_2O$) | A[c] ($C\ell CN, CH_3OH$) | A[c] ($CH_3C\ell, CH_3OH$) | $\nu_o$[a] ($cm^{-1}$) | $\Delta\nu_{1/2}$[b] ($cm^{-1}$) | A[c] |
| 3609.2 | 70.0 | 21.4 | 16.2 | 23.1 | 16.8 | 3609.2 | 70.0 | 56.6 |
| 1239.9 | 50.0 | 65.6 | 66.2 | 31.6 | 33.3 | 1239.9 | 50.0 | 73.9 |
| 725.0 | 50.0 | 3.5 | 3.9 | 6.8 | 7.3 | 725.0 | 50.0 | 10.6 |

[a] Wavenumber position of maximum absorption from the experimental gas phase spectrum of HOCℓ[50].
[b] Full width at half-maximum of the band estimated from the gas phase spectrum of HOCℓ reported in ref. [78].
[c] Units are km $mole^{-1}$ (taken from Table 3-49).

The absolute difference is only 0.03e, which is within the experimental error.

From our previous discussion about the transferability of APTs, we expect that the predicted intensities for HOCℓ from APTs transferred from the (CℓCN, $H_2O$) pair may be in better agreement with experiment than predictions from any of the other sets of transferred APTs. This comparison is shown in Table 3-49. Notice that the predicted intensities are in general within factor of two agreement with the experimental intensities for intensities predicted from CℓCN and $H_2O$ (see also Fig. 3-14). However, in spite of our arguments concerning expected transferability, the results in Table 3-49 for all four sets of parameters are close enough to the experimental values that we can not choose between them.

CHAPTER 4
AN ANALYSIS OF THE ATOMIC POLAR TENSORS

## Introduction

In the last chapter we have examined the differences between the elements of the APTs for several molecules, to find that some APTs are transferable and others are not, depending upon the chemical environment of the atom or group of atoms from which the APT is being transferred and that of the new molecule. We have been able, therefore, to predict successfully the relative or absolute intensities of molecules such as HOO and HOCℓ, by proper transfer of the APTs from $H_2O$, $CH_3OH$ and CℓCN. This last example shows that APTs are indeed transferable intensity parameters, providing that some judgement is used in the transfer.

We have also shown that our ab initio calculations using a 4-31G basis set gave predicted absolute intensities that are accurate within the experimental uncertainties, as do also the predictions made by transferring APTs. We have found that only the intensity of the OCℓ stretching mode for HOCℓ is poorly predicted with the 4-31G basis. We have also compared the predicted spectrum for HOCℓ using the 4-31G basis set with that predicted [76] with a triple-zeta accuracy basis set plus double polarization. In this chapter we are interested in investigating the changes in the fluorine APT of the $CH_3F$ and HOF molecules which explain why this

tensor is not transferable, as well as the changes in the hydrogen APTs for the HOX series of molecules which take place as a result of the perturbing X atom in terms of the CCFO quantum mechanical model for the APT discussed in the last chapter. As a result of the HOX study, we shall find a correlation between the overlap ($\underline{P}_x^H(O)$) and charge-flux ($\underline{P}_x^H(CF)$) contributions to the APT for the hydrogen atom and the Mulliken electronegativity of the X atom. Using this correlation to modify the APT calculated for the hydrogen atom in HOCℓ, it was possible to predict accurately the spectrum of HOCℓ. The overlap tensor from the 4-31G calculation of the hydrogen atom in HOCℓ already obeys this correlation. The charge tensor-contribution, $\underline{P}_x^H(C)$, to the APT for the hydrogen atom was found to be almost constant regardless of the X atom, except where X=H for the $H_2O$ molecule.

We believe that the 4-31G basis does not accurately predict the polar tensor for the atoms in HOCℓ because the basis set should include polarization functions. Hence it seems reasonable to use the correlations with electronegativity established for the more accurately calculated APTs for HOX molecules to correct the APT for the hydrogen atom. We think that it would be possible to improve the basis set and make more accurate quantum mechanical calculations by a simple modification of the basis set used. Namely, we should optimize the orbital exponents of added polarization functions with respect to some intensity parameter (here we suggest the atomic effective charges) and then use a standard molecular set of these scaled factors based on an average of the

optimum values obtained from a series of model molecules. This additional criterion could prove to be extremely important for calculations of dipole moments and derivatives, within the Hartree-Fock formalism. This new basis set will reflect criteria based both on energy eigenvalue calculations and also on dipole moment derivative calculations.

In the next section we shall compare the contributions of the CCFO terms to the ab initio 4-31G APTs for $CH_3F$ and HOF. Following that we show how we can proceed to modify the charge-flux contributions to the hydrogen atom APT for the HOX series of molecules, based on these electronegativity correlations.

### Comparison of the Ab Initio 4-31G APTs for the Fluorine Atom in $CH_3F$ with that in the HOF Molecule

We have seen in the previous chapter that the fluorine APT from $CH_3F$ can not be successfully transferred to predict the intensities for HOF (see, for example, Table 3-14). We have shown that the predicted intensities for HOF by transfer of the fluorine APT from $CH_3F$ and the hydrogen APT from $H_2O$ are in poor agreement with intensities predicted from ab initio APTs for HOF or from relative experimental intensities of this molecule. Accordingly, the intensities predicted from APTs tranferred from $CH_3F$ and $H_2O$ show an order of increasing intensities from high wavenumber $\nu_1$(OH) to low $\nu_3$(OH) precisely the opposite of what is observed experimentally or predicted quantum mechanically. The reason for the nontransferability of the fluorine APT from $CH_3F$ to HOF shows in the contributions to the ab initio APT for both molecules,

as compared in Table 4-1. This Table shows that the charge-tensor contributions are substantially different for the two F atoms. The fluorine charge tensor gives the contribution from the gross atomic charge on the fluorine atom at equilibrium molecular configuration and reflects the chemical differences between the F atoms in the $CH_3F$ and HOF molecules. Therefore, the fluorine APT of $CH_3F$ and HOF is different in each molecule and obviously not transferable. Notice that the diagonal elements $\frac{\partial p_Y}{\partial v}$ of the charge-flux and overlap tensor contributions are also substantially different. This particular example is in itself an answer for those who still believe that the fluorine atom is so electronegative that it does not matter in its electronic properites just what atom it is attached to.

## Predicted Vibrational Intensity and the APTs For Diatomic OCℓ

Before considering in some detail the electronegativity correlation with the charge-flux tensor of the hydrogen atom for the HOX series of molecules we wish to point out the logical reasoning which led us to this study.

We have previously noticed that the experimental chlorine APT for CℓCN and the ab initio predicted APT for the chlorine atom in HOCℓ are quite different. Therefore it would be of interest, for example, to compare both APTs with the ab initio APT of the chlorine atom in the diatomic OCℓ molecule. This comparison is shown in Table 4-2. The APT for the chlorine atom in diatomic OCℓ

TABLE 4-1
COMPARISON OF THE CHARGE, CHARGE-FLUX AND OVERLAP CONTRIBUTIONS TO THE AB INITIO 4-31G APT FOR $CH_3F$ AND HOF

| $P_x^F$[a] | $CH_3F$[b] | HOF[c] |
|---|---|---|
| $P_x^F(C)$ | $\begin{pmatrix} -0.46 & 0 & 0 \\ 0 & -0.46 & 0 \\ 0 & 0 & -0.46 \end{pmatrix}$ | $\begin{pmatrix} -0.21 & 0 & 0 \\ 0 & -0.21 & 0 \\ 0 & 0 & -0.21 \end{pmatrix}$ |
| $P_x^F(CF)$ | $\begin{pmatrix} 0.02 & 0 & 0 \\ 0 & -0.24 & 0 \\ 0 & 0 & 0.02 \end{pmatrix}$ | $\begin{pmatrix} 0 & 0 & 0 \\ 0 & 0.12 & -0.12 \\ 0 & 0.03 & 0.02 \end{pmatrix}$ |
| $P_x^F(O)$ | $\begin{pmatrix} 0.06 & 0 & 0 \\ 0 & -0.17 & 0 \\ 0 & 0 & 0.06 \end{pmatrix}$ | $\begin{pmatrix} 0.08 & 0 & 0 \\ 0 & -0.35 & -0.04 \\ 0 & 0.01 & 0.02 \end{pmatrix}$ |
| $P_x^F(T)$ | $\begin{pmatrix} -0.38 & 0 & 0 \\ 0 & -0.87 & 0 \\ 0 & 0 & -0.38 \end{pmatrix}$ | $\begin{pmatrix} -0.13 & 0 & 0 \\ 0 & -0.44 & -0.16 \\ 0 & 0.05 & -0.17 \end{pmatrix}$ |

[a] The charge (C), charge-flux (CF) and overlap (O), contributions to the total 4-31G APT on the fluorine atom were calculated according to the CCFO model [52,53]. The coordinate system is shown in Fig. 3-1.

[b] The fluorine APT from $CH_3F$ was from Chin (private communication of work in progress at the University of Florida).

[c] This work.

TABLE 4-2
COMPARISON OF THE CHLORINE APT FOR SEVERAL MOLECULES
(THE COORDINATE SYSTEM IS SHOWN IN FIG.3-11)

| $\underline{P}_x^{(Cl)}$ | | | |
|---|---|---|---|
| 0.164 | 0 | 0 | |
| 0 | 0.133 | 0.135 | $OCl^a$ |
| 0 | 0.135 | -0.423 | |
| 0.143 | 0 | 0 | |
| 0 | 0.114 | 0.127 | $ClCN^b$ |
| 0 | 0.127 | -0.407 | |
| 0.0743 | 0 | 0 | |
| 0 | 0.0512 | 0.021 | $HOCl^c$ |
| 0 | -0.104 | -0.190 | |
| -0.234 | 0 | 0 | |
| 0 | -0.245 | 0.047 | $CH_3Cl^d$ |
| 0 | 0.047 | -0.435 | |

[a] Ab initio 4-31G APT (this work).

[b] Experimental chlorine APT reported in ref. [91] and expressed here in the coordinate system shown in Fig. 3-11(see also Table 3-45 of this work).

[c] Ab initio 4-31G APT taken from Table 3-38 (this work)

[d] Taken from Table 3-46.

can be written [1,92]

$$\underset{\sim}{P}_x^{C\ell} = \begin{pmatrix} p^o/R_e & & 0 \\ & p^o/R_e & \\ 0 & & \partial p_z/\partial z \end{pmatrix}$$

Here $p^o$ is the magnitude of the permanent dipole moment vector at equilibrium molecular configuration, $R_e$ is the equilibrium internuclear distance in OCℓ and $\partial p_z/\partial_z$ is the magnitude of the dipole derivative with respect to the z axis. The experimental values for $p^o$ and $R_e$ were obtained from reference [93] [$p^o$=1.239 D (compared to a calculated value of $p^o$=1.112 D) and $R_e$=1.569 Å] and the $\partial p_z/\partial z$ element of this tensor was calculated as described for the molecules using a 4-31G basis set. Table 4-2 shows the comparison of this APT for Cℓ in OCℓ, CℓCN, HOCℓ and $CH_3C\ell$. The coordinate system is shown in Fig. 3-11. Notice, for instance, that the chlorine APTs from OCℓ and CℓCN are quite similar, in contrast with the predicted chlorine APT for HOCℓ. It seems clear that the chlorine APT of HOCℓ is not well-predicted using a 4-31G basis set, probably due to the lack of polarization functions on the hydrogen and chlorine atoms.

Here it is interesting to mention that the Pauling electronegativity of the O atom and the electronegativity of the CN group are practically the same (3.44 compared to 3.3 [94]) and the polarity of the C Cℓ bond in both molecules is the same ($C\ell^+O^-$, $C\ell^+CN^-$). For the $CH_3C\ell$ molecule the polarity of the C Cℓ bond ($C^+C\ell^-$) is the opposite to that of CℓO or CℓCN. However, we have not observed in Figs. 3-14 and 3-15 any substantial effect on the predicted

spectrum of HOCℓ from APTs transferred from either molecule. Nevertheless, we think the Cℓ atom in HOCℓ is expected to be more like those in CℓCN or CℓO than like that in $CH_3Cℓ$.

In the next section we shall discuss how we modified the charge-flux tensor of the hydrogen atom in HOCℓ to predict the intensities for this molecule, using also the chlorine APT as calculated in this section.

Further Discussion and Interpretation of the HOCℓ APTs

We have chosen the set of coordinates shown in Fig. 4-1 to analyze the total hydrogen atom APT in terms of the CCFO contributions for the series of triatomic molecules studied in this work. In this bond coordinate system the z axis is placed along the OH bond and the x axis is directed toward the perturbing x atom. The charge tensor is diagonal and obviously invariant to the coordinate system used. The hydrogen atom APTs in the original coordinates were given in Tables 3-8 , 3-22 and 3-40. The APTs in the bond coordinate system are presented in Tables 4-3 to 4-6 arranged to show each separate contribution to $P^H_{-x}$ for all four HOX molecules, for purposes of comparison. Table 4-3 shows that the main changes in the total hydrogen atom APTs for HOX from molecule to molecule are observed in the values for the $\partial p_x/\partial x$ and $\partial p_z/\partial z$ elements, as might be expected (see Fig. 4-1). Table 4-4 shows that there is no substantial change from one molecule to another in the charge tensors for HOX. However, Tables 4-5 and 4-6 show that there are substantial differences in the charge-flux and overlap tensors particularly in the $\partial p_x/\partial x(CF)$, $\partial p_z/\partial z(CF)$, and $\partial p_z/\partial z(O)$ elements.

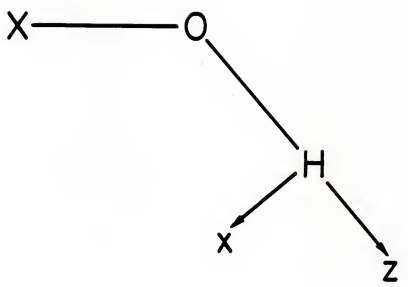


Fig. 4-1. Bond coordinate system for the hydrogen atom of the HOX series of molecules, X = H, Cℓ, O, and F.

TABLE 4-3
AB INITIO 4-31G APTs ON THE HYDROGEN ATOM FOR HOX
(UNITS ARE e)

| $\underline{P}_x^H$ (Total) | | | X |
|---|---|---|---|
| 0.34 | 0 | -0.02 | H |
| 0 | 0.47 | 0 | |
| -0.10 | 0 | 0.09 | |
| 0.21 | 0 | -0.11 | Cℓ |
| 0 | 0.49 | 0 | |
| -0.03 | 0 | 0.24 | |
| 0.29 | 0 | -0.06 | O |
| 0 | 0.47 | 0 | |
| -0.04 | 0 | 0.21 | |
| 0.25 | 0 | -0.07 | F |
| 0 | 0.50 | 0 | |
| -0.03 | 0 | 0.25 | |

Note: The coordinate system is shown in Fig. 4-1.

TABLE 4-4
THE CHARGE CONTRIBUTION, $\underline{P}^{H}_{\overrightarrow{X}}(C)$ TO THE HYDROGEN ATOM APT FOR HOX (UNITS ARE e)

| $\underline{P}^{H}_{\overrightarrow{X}}(C)$ | | | X |
|---|---|---|---|
| 0.41 | 0 | 0 | H |
| 0 | 0.41 | 0 | |
| 0 | 0 | 0.41 | |
| 0.44 | 0 | 0 | Cl |
| 0 | 0.44 | 0 | |
| 0 | 0 | 0.44 | |
| 0.44 | 0 | 0 | O |
| 0 | 0.44 | 0 | |
| 0 | 0 | 0.44 | |
| 0.45 | 0 | 0 | F |
| 0 | 0.45 | 0 | |
| 0 | 0 | 0.45 | |

TABLE 4-5
THE CHARGE-FLUX CONTRIBUTION $\underline{P}_x^H(CF)$ TO THE HYDROGEN ATOM APT FOR HOX (UNITS ARE e)

| $\underline{P}_x^H(CF)$ | | | X |
|---|---|---|---|
| -0.08 | 0 | 0.02 | H |
| 0 | 0 | 0 | |
| -0.06 | 0 | -0.04 | |
| -0.24 | 0 | -0.06 | Cℓ |
| 0 | 0 | 0 | |
| 0.05 | 0 | 0.12 | |
| -0.12 | 0 | -0.01 | O |
| 0 | 0 | 0 | |
| 0.04 | 0 | 0.10 | |
| -0.17 | 0 | -0.04 | F |
| 0 | 0 | 0 | |
| 0.05 | 0 | 0.18 | |

Note: The coordinate system is shown in Fig. 4-1.

TABLE 4-6
THE OVERLAP CONTRIBUTION $\underline{P}_{\underline{x}}^{H}(O)$ TO THE HYDROGEN ATOM APT FOR HOX
(UNITS ARE e)

| $\underline{P}_{\underline{x}}^{H}(O)$ | | | X |
|---|---|---|---|
| 0.01 | 0 | -0.04 | |
| 0 | 0.06 | 0 | H |
| -0.04 | 0 | -0.28 | |
| 0.004 | 0 | -0.05 | |
| 0 | 0.04 | 0 | Cℓ |
| -0.08 | 0 | -0.32 | |
| -0.03 | 0 | -0.05 | |
| 0 | 0.03 | 0 | O |
| -0.08 | 0 | -0.34 | |
| -0.03 | 0 | -0.03 | |
| 0 | 0.04 | 0 | F |
| -0.08 | 0 | -0.38 | |

Note: The coordinate system is shown in Fig. 4-1.

Let us first consider the overlap tensor elements of the hydrogen atom of the HOX series, shown in Table 4-6. A more careful inspection of this Table shows that the diagonal element $\partial p_z/\partial z$ appears to be correlated with the Mulliken electronegativity of the X atom. This correlation appears to be valid even for the overlap tensor element $\partial p_z/\partial z(O)$ for the hydrogen atom of HOCℓ. This correlation plot is shown in Fig. 4-2.

Consider the reasonning that has led to this plot. First we observed that, with the exception of the diagonal $\partial p_z/\partial z(O)$ elements of the hydrogen atom for this series of HOX molecules, all the other elements of the overlap tensors are quite small and approximately constant from one molecule to another. However the diagonal $\partial p_z/\partial z$ tensor elements change from -0.28e for the hydrogen atom of HOH to -0.38e for the hydrogen atom of HOF. We observed that if we plot each zz element of the overlap tensor versus the electronegativity of the x atom we obtain a beautiful straight line shown in Fig. 4-2. The corresponding overlap tensor element for the hydrogen atom of $CH_3OH$ is also included in that figure in order to show that this element from this molecule also fits the electronegativity correlation. This linear electronegativity correlation was also observed for all of the elements of the charge-flux tensors of the hydrogen atom of the HOX series of molecules (shown in Table 4-5) with the exception of the charge-flux tensor elements for the hydrogen atom of HOCℓ. These additional electronegativity correlations are shown in Fig. 4-3 to 4-6.

Fig. 4-2. A plot of the $\frac{\partial p_z}{\partial z_H}$ (O) tensor elements for HOX, versus the Mulliken electronegativity of the X atom (X = H, C, Cℓ, O, and F). The electronegativity values of the X atoms were taken from Wells [94].

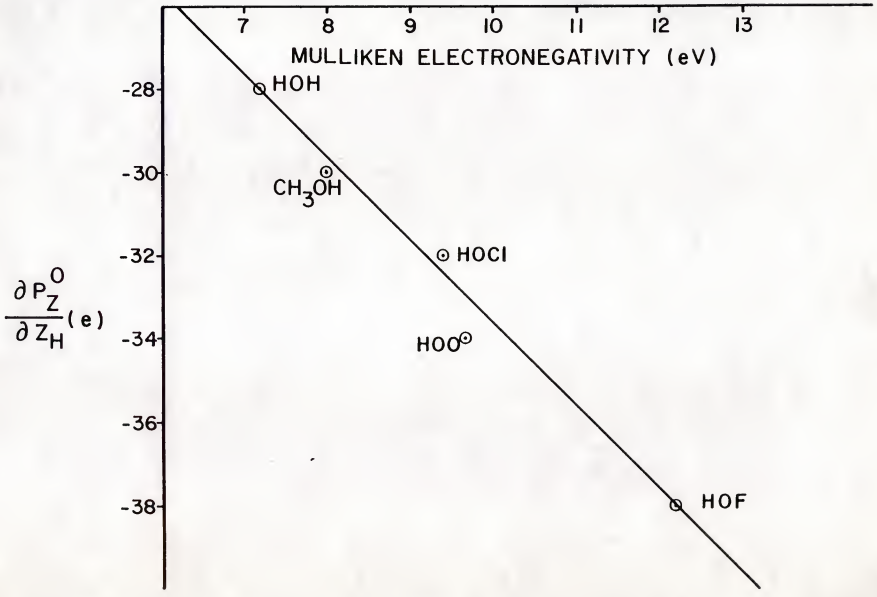
7
8
9
10
11
12
13
MULLIKEN ELECTRONEGATIVITY (eV)
-28
-30
-32
-34
-36
-38
HOH
CH3OH
HOCl
HOO
HOF
∂P_Z^O / ∂Z_H (e)

Fig. 4-3. A plot of the $\frac{\partial p_x}{\partial x_H}$ (CF) charge-flux tensor elements for HOX, versus the Mulliken electronegativity of the X atom (X = H, O, and F). The electronegativity values were taken from Wells [94].

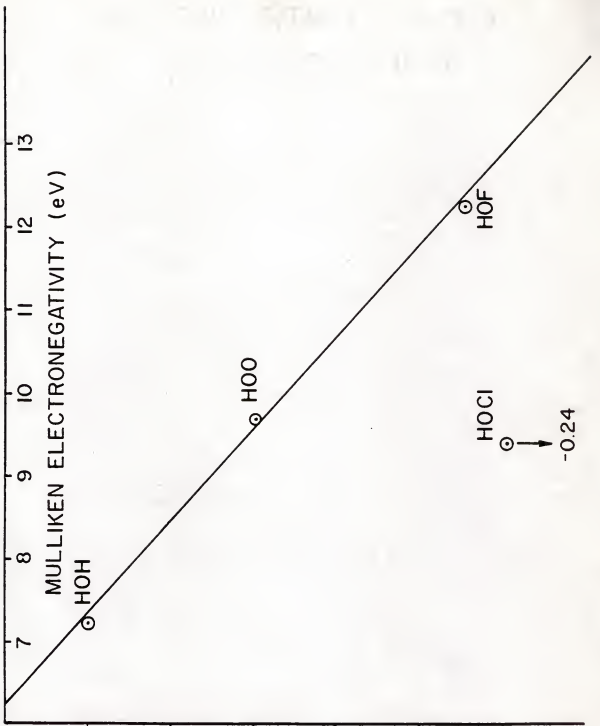
$\frac{\partial P_X^{CF}}{\partial X_H}$(e)
-0.08
-0.10
-0.12
-0.14
-0.16
-0.18
7
8
9
10
11
12
13
MULLIKEN ELECTRONEGATIVITY (eV)
HOH
HOO
HOCl
-0.24
HOF

Fig. 4-4. A plot of the $\frac{\partial p_z}{\partial x_H}$ (CF) charge-flux tensor elements for the HOX, versus the Mulliken electronegativity of the X atom (X = H, O, and F). The electronegativity values were taken from Wells [94].

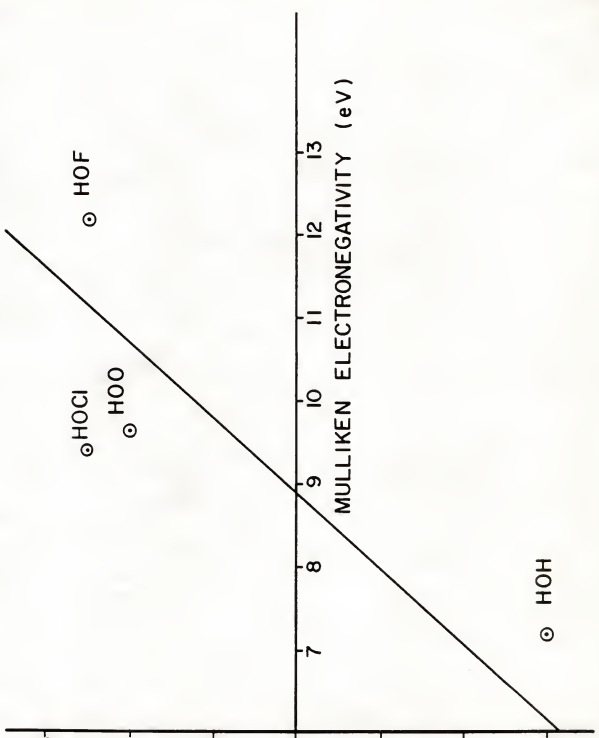
0.06
0.04
0.02
0
-0.02
-0.04
-0.06
$\frac{\partial P_Z^{CF}}{\partial X_H}$ (e)
7
8
9
10
11
12
13
MULLIKEN ELECTRONEGATIVITY (eV)
HOF
HOCl
HOO
HOH

Fig. 4-5. A plot of the $\frac{\partial p_x}{\partial z_H}$ (CF) charge-flux tensor elements for HOX, versus the Mulliken electronegativity of the X atom (X = H, O, and F). The electronegativity values were taken from Wells [94].

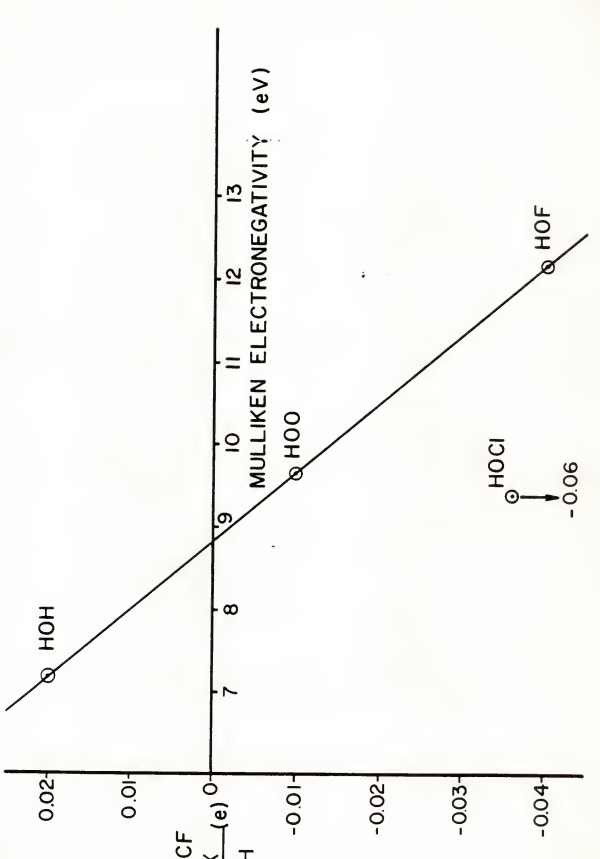
0.02
0.01
0
-0.01
-0.02
-0.03
-0.04
$\frac{\partial P_X^{CF}}{\partial Z_H}$ (e)
7
8
9
10
11
12
13
MULLIKEN ELECTRONEGATIVITY (eV)
HOH
HOO
HOCl
-0.06
HOF

Fig. 4-6. A plot of the $\frac{\partial p_z}{\partial z_H}$ (CF) charge-flux tensor elements for HOX, versus the Mülliken electronegativity of the X atom (X = H, O, and F). The electronegativities were taken from Wells [94].

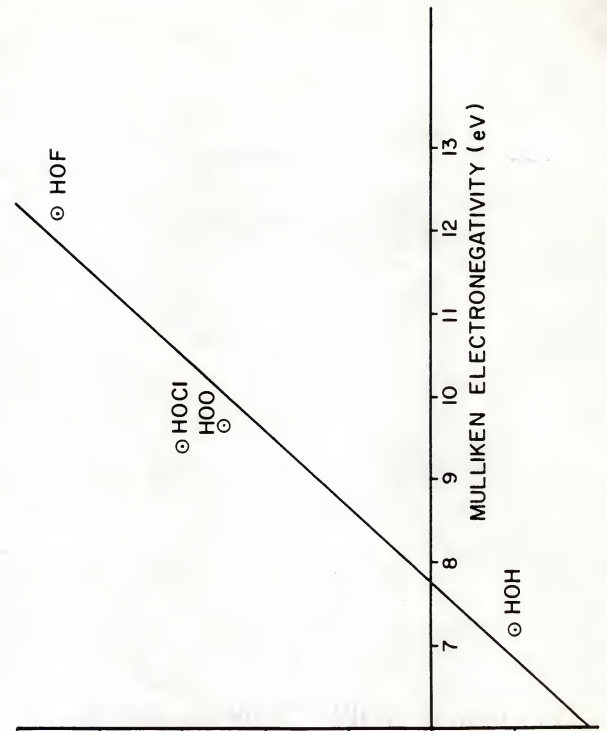
0.20
0.16
0.12
0.08
0.04
0
-0.04
$\frac{\partial P_Z^{CF}}{\partial Z_H}$ (e)
7
8
9
10
11
12
13
MULLIKEN ELECTRONEGATIVITY (eV)
HOF
HOCl
HOO
HOH

We therefore used the electronegativity correlation of the charge-flux tensor elements of the hydrogen atoms shown in Fig. 4-3 to 4-6 to obtain the "predicted" charge-flux tensor for the hydrogen atom of HOCℓ by reading the charge-flux tensor elements directly from the electronegativity of the chlorine atom. This predicted tensor was added to the charge and overlap tensors as calculated with the 4-31G basis set to obtain the total APT for the hydrogen atom of HOCℓ. The comparison between the 4-31G and this modified APT for the hydrogen atom of HOCℓ is shown in Table 4-7.

Next we rotated the coordinate system of the hydrogen atom modified tensor to the coordinate system shown in Fig. 3-11. This tensor and the chlorine APT from OCℓ given in Table 4-2 were used to obtain the oxygen atom APT for HOCℓ from the null condition given by Eq.(62). The resulting APTs for HOCℓ are shown in Table 4-8. Using these APTs we then predicted the intensities for HOCℓ as listed in Table 4-9. We have also included in this Table the predicted intensities calculated from a 4-31G basis set and from a TZPP basis [76] for purposes of comparison. This Table shows that the predicted intensities using the APTs shown in Table 4-8 are in remarkable agreement with the experimental intensities. The computer-simulated spectrum predicted from intensities calculated from the modified APTs from Table 4-8 is compared with the computer simulation of the experimental spectrum of HOCℓ in Fig. 4-7.

TABLE 4-7
COMPARISON BETWEEN THE 4-31G AND MODIFIED $\underline{P}_x^H$ FOR HOCℓ
(UNITS ARE e)

| $\underline{P}_x^H$ | 4-31G | Modified |
|---|---|---|
| $\underline{P}_x$ (C) | $\begin{pmatrix} 0.44 & 0 & 0 \\ 0 & 0.44 & 0 \\ 0 & 0 & 0.44 \end{pmatrix}$ | $\begin{pmatrix} 0.44 & 0 & 0 \\ 0 & 0.44 & 0 \\ 0 & 0 & 0.44 \end{pmatrix}$ |
| $\underline{P}_x$ (CF) | $\begin{pmatrix} -0.24 & 0 & -0.06 \\ 0 & 0 & 0 \\ 0.05 & 0 & 0.12 \end{pmatrix}$ | $\begin{pmatrix} -0.10 & 0 & 0.002 \\ 0 & 0 & 0 \\ -0.004 & 0 & 0.06 \end{pmatrix}$ |
| $\underline{P}_x$ (O) | $\begin{pmatrix} 0.004 & 0 & -0.05 \\ 0 & 0.04 & 0 \\ -0.08 & 0 & -0.32 \end{pmatrix}$ | $\begin{pmatrix} 0.004 & 0 & -0.05 \\ 0 & 0.04 & 0 \\ -0.08 & 0 & -0.32 \end{pmatrix}$ |
| $\underline{P}_x$ (T) | $\begin{pmatrix} 0.21 & 0 & -0.11 \\ 0 & 0.49 & 0 \\ -0.03 & 0 & 0.24 \end{pmatrix}$ | $\begin{pmatrix} 0.34 & 0 & -0.05 \\ 0 & 0.48 & 0 \\ -0.08 & 0 & 0.18 \end{pmatrix}$ |

Note: The coordinate system is shown in Fig. 4-1.

TABLE 4-8
MODIFIED APTs FOR HOCℓ USED TO CALCULATE PREDICTED SPECTRUM IN FIG. 4-7(UNITS ARE e)

$$\underline{P}_x^O = \begin{pmatrix} -0.64 & 0 & 0 \\ 0 & -0.32 & -0.06 \\ 0 & -0.07 & 0.10 \end{pmatrix}$$

$$\underline{P}_x^H = \begin{pmatrix} 0.48 & 0 & 0 \\ 0 & 0.19 & -0.07 \\ 0 & -0.06 & 0.32 \end{pmatrix}$$

$$\underline{P}_x^{C\ell} = \begin{pmatrix} 0.16 & 0 & 0 \\ 0 & 0.13 & 0.13 \\ 0 & 0.13 & -0.42 \end{pmatrix}$$

Note: $\underline{P}_x^O$ Obtained from the null condition, given by Eq. (62)
$\underline{P}_x^H$ (Modified), see text
$\underline{P}_x^{C\ell}$ (Ab initio 4-31G), this work.
The coordinate system and atom numbering are shown in Fig. 3-11.

TABLE 4-9
PREDICTED INTENSITIES FROM AB INITIO AND MODIFIED APTs FOR HOCℓ
(UNITS ARE km mole$^{-1}$)

| Band | $\nu$(cm$^{-1}$) | A(4-31G) | A(TZPP) | A(4-31G)* | A(Expl.) |
|---|---|---|---|---|---|
| $\nu$(OH) | 3609.2 | 75.3 | 122.3 | 41.9 | 56.6 |
| $\nu$($\Delta\theta$) | 1239.9 | 39.3 | 45.8 | 99.8 | 73.9 |
| $\nu$(OCℓ) | 725.0 | 0.089 | 6.2 | 9.5 | 10.6 |

Note: See also Table 3-39. A(4-31G)* are the modified 4-31G intensities.

Fig. 4-7. Computer simulation of the predicted spectrum of HOCℓ from modified 4-31G APTs and the computer-simulated gas phase spectrum of HOCℓ.

(a) Predicted

(b) Experimental

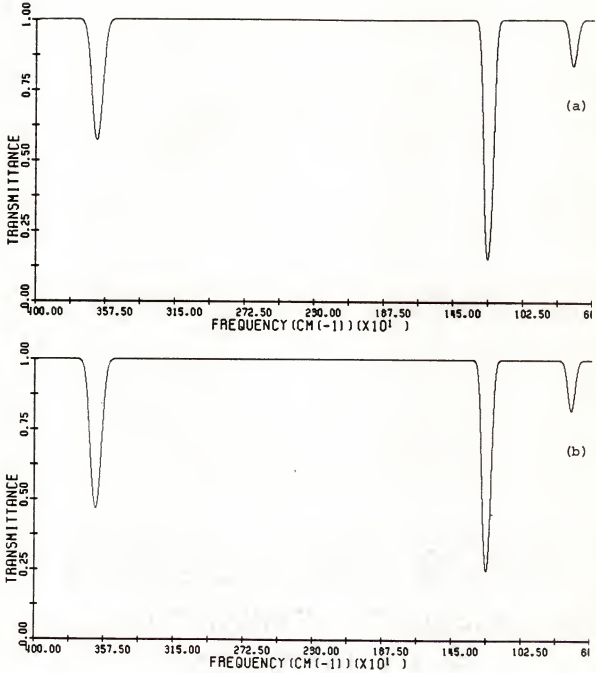
1.00
0.75
0.50
0.25
0.00
TRANSMITTANCE
(a)
400.00
357.50
315.00
272.50
230.00
187.50
145.00
102.50
FREQUENCY (CM(-1)) (X10¹ )
1.00
0.75
0.50
0.25
0.00
TRANSMITTANCE
(b)
400.00
357.50
315.00
272.50
230.00
187.50
145.00
102.50
FREQUENCY (CM(-1)) (X10¹ )

In conclusion, we believe we have demonstrated how powerful these techniques for predicting spectra can be in the interpretation of the spectra of free radical species trapped in inert matrices or for any unstable species in gas phase. Valuable predictions can be made either by using APTs transferred from chemically similar molecules or by using APTs from quantum mechanical calculations made by ab initio SCF methods. We have also pointed out some qualitative and quantitative applications of this theory. Most of our absolute intensities, either quantum mechanically calculated or predicted by proper transfer of APTs, are within factor of two agreement with the experimental values and therefore often within the experimental uncertainties. For free radical species trapped in a matrix or for unstable intermediate species, it is more than optimistic to expect experimental accuracy to be better than a factor of two due to the difficulties in handling and measuring the integrated absorbances.

We have also pointed out that not all APTs are transferable. We have analyzed the changes in these APTs in terms of the quantum mechanical CCFO model of the APT. We found that these changes are reflected in the charge, charge-flux and overlap contributions to the APT and these changes often reflect on changes in the chemical environment in the new molecule and in the molecule to which the APT is being transferred. We have also pointed out the importance of an additional criterion for choosing a quality basis set for dipole moment derivative calculations.

Finally, the success of our calculations indicates certainly that this new technique can be one of the most important and useful techniques for the qualitative and quantitative studies of free radicals or unstable intermediate species trapped in inert matrices. It has important analytical applications in the study of the photochemistry of those species, as well as in studies of the concentrations of these unstable species in planetary atmospheres.

REFERENCES


1. J. F. Biarge, J. Herranz and J. Morcillo, An. R. Soc. Esp. Fis. Quim. A57, 81 (1961).

2. W. B. Person and J. H. Newton, J. Chem. Phys. 61, 1040 (1974).

3. W. B. Person and D. Steele, in "Molecular Spectroscopy," D. A. Long, Ed., Specialist Periodical Report of the Chemical Society (the Chemical Society, London, 1974), Vol. 2, Chap. 5.

4. W. B. Person, in "Proceedings of the NASA Workshop on Vibrational Rotational Spectroscopy for Planetary Atmospheres," K. Fox, Ed. (to be published, 1980).

5. W. B. Person, J. D. Rogers and R. G. A. Maia, American Chemical Society National Meeting, Las Vegas, Nevada (August, 1980).

6. W. B. Person, in "Matrix Isolation Spectroscopy," A. J. Barnes, R. Gaufries, A. Müller, and W. J. Orville-Thomas, Eds. (Elsevier, Amsterdam, to be published, 1981).

7. J. H. Newton and W. B. Person, J. Chem. Phys. 68, 2799 (1978); J. H. Newton and W. B. Person, Appl. Spectrosc. 32, 290 (1978).

8. B. A. Thrush, Phil. Trans. R. Soc. Lond. A296, 149 (1980).

9. D. H. Ehhalt, Phil. Trans. R. Soc. Lond. A296, 175 (1980).

10. L. T. Molina and M. J. Molina, J. Phys. Chem. 82, 2410 (1978).

11. R. L. Jaffe and S. R. Langhoff, J. Chem. Phys. 68, 1638 (1978).

12. B. Reimann and F. Kaufman, J. Chem. Phys. 69, 2925 (1978).

13. M. J. Molina, T. Ishiwata and L. T. Molina, J. Phys. Chem. 84, 821 (1980).

14. These experiments have been presented as a report to the Manufacturing Chemists Association (MCA) in 1977 and 1978, and are cited as references 33 and 34 of reference [11].

15. W. C. Fergusson, L. Slotin and D. W. G. Style, Trans. Faraday Soc. 32, 956 (1936).

16. S. Jaffe and W. B. DeMoore, NASA Ref. Publ., No. 1010, Washington, D. C., 1977.

17. H. D. Knauth, H. Alberti and H. Clausen, J. Phys. Chem. 83, 1604 (1979).

18. D. J. Seery and D. Britton, J. Phys. Chem. 68, 2263 (1964).

19. E. B. Wilson, J. Chem. Phys. 7, 1047 (1939).

20. E. B. Wilson, J. Chem. Phys. 9, 76 (1941).

21. E. B. Wilson, Jr., J. C. Decius and P. C. Cross, "Molecular Vibrations" (McGraw-Hill, New York, 1955).

22. D. Steele, "Theory of Vibrational Spectroscopy" (W. B. Saunders Co., Philadelphia, 1971).

23. I. M. Mills, in "Infrared Spectroscopy and Molecular Structure," M. Davies, Ed. (Elsevier, Amsterdam, 1963), Chap. 5.

24. S. Califano,"Vibrational States" (John Wiley, New York, 1976).

25. G. Zerbi, in "Vibrational Spectroscopy-Modern Trends," A. J. Barnes and W. J. Orville-Thomas, Eds. (Elsevier, Amsterdam, 1977), Chap. 17.

26. J. H. Schachtschneider, "Vibrational Analysis of Polyatomic Molecules. VI," Shell Development Company Technical Report (Shell Development Company, California, 1964), No. 57-65, pp. 12-43.

27. J. Overend, "Program Manual of the Molecular Spectroscopy Library" (University of Minnesota, Minneapolis, 1966), Vol. II.

28. W. T. King, Ph.D. Thesis, University of Minnesota (1956).

29. J. H. Newton, R. A. Levine and W. B. Person, J. Chem. Phys. 67, 3282 (1977).

30. W. B. Person and J. Overend, J. Chem. Phys. 66, 1442 (1977).

31. B. J. Krohn, W. B. Person and J. Overend, J. Chem. Phys. 65, 969 (1976).

32. B. J. Krohn, W. B. Person and J. Overend, J. Chem. Phys. 67, 5091 (1977).

33. J. H. Newton and W. B. Person, J. Phys. Chem. 82, 226 (1978).

34. J. H. Newton and W. B. Person, J. Chem. Phys. 64, 3036 (1976).

35. J. D. Rogers, Ph.D. Dissertation, University of Florida (1980).

36. J. Overend, in "Infrared Spectroscopy and Molecular Structure," M. Davies, Ed. (Elsevier, Amsterdam, 1963), Chap. 10.

37. W. J. Hehre, W. A. Latham, R. Ditchfield, M. D. Newton and J. A. Pople, "GAUSSIAN 70," program 236, Quantum Chemistry Program Exchange, Indiana University, 1971.

38. W. J. Hehre, R. F. Stewart and J. A. Pople, J. Chem. Phys. 51, 2657 (1969).

39. R. Ditchfield, W. J. Hehre and J. A. Pople, J. Chem. Phys. 52, 5001 (1970).

40. R. Ditchfield, W. J. Hehre and J. A. Pople, J. Chem. Phys. 54, 724 (1971).

41. W. J. Hehre and W. A. Lathan, J. Chem. Phys. 56, 5255 (1972).

42. W. J. Hehre and J. A. Pople, J. Chem. Phys. 56, 4233 (1972).

43. W. J. Hehre, R. Ditchfield and J. A. Pople, J. Chem. Phys. 56, 2257 (1972).

44. D. Steele, Mol. Phys. 38, 145 (1979).

45. P. Pulay, in "Modern Theoretical Chemistry," H. F. Schaefer III, Ed. (Plenum Press, New York, 1977), Chap. 4.

46. R. H. Schwendeman, J. Chem. Phys. 44, 2115 (1966).

47. G. E. Sanchez, Ph.D. Dissertation, University of Florida (1971).

48. J. H. Newton, Ph.D. Dissertation, University of Florida (1974).

49. H. Kim, E. F. Pearson and E. H. Appelman, J. Chem. Phys. 56, 1 (1972).

50. J. F. Ogilvie, Can. J. Spectrosc. 19, 171 (1974).

51. E. H. Appelman and H. Kim, J. Chem. Phys. 57, 3272 (1972).

52. W. T. King, in "Vibrational Intensities," W. B. Person and G. Zerbi, Eds. (Elsevier, Amsterdam, to be published, 1981), Chap. 6.

53. B. A. Zilles, Ph.D. Dissertation, University of Florida (1980).

54. R. S. Mulliken, J. Chem. Phys. 23, 1833, 1841 (1955).

55. R. S. Mulliken, J. Chem. Phys. 36, 3428, (1962).

56. J. I. Steinfeld, "Molecules and Radiation" (the MIT Press, Massachusetts, 1978).

57. "Manual on Practices in Molecular Spectroscopy," American Society for Testing and Materials, Philadelphia, 1979.

58. J. W. Smith and L. Andrews, J. Chem. Phys. 60, 81 (1974).

59. J. A. Goleb, H. H. Claassen, M. H. Studier and E. H. Appelman, Spectrochim. Acta 28A, 65 (1972).

60. J. H. Newton, unpublished work, University of Florida, 1976.

61. Gould 4800/5000 Series, IBM System/360/370, Plot Package Programming Manual, Gould Inc., Instrument Systems Division, 1974.

62. M. T. Bowers, G. I. Kerley and W. H. Flygare, J. Chem. Phys. 45, 3399 (1966).

63. P. N. Noble and G. C. Pimentel, Spectrochim. Acta 24A, 797 (1968).

64. W. B. Person and J. H. Newton, J. Mol. Struct. 46, 105 (1978).

65. S. N. Foner and R. L. Hudson, J. Chem. Phys. 21, 1608 (1953).

66. D. E. Milligan and M. E. Jacox, J. Chem. Phys. 38, 2627 (1963).

67. M. E. Jacox and D. E. Milligan, J. Mol. Spectrosc. 42, 495 (1972).

68. T. T. Pankert and H. S. Johnston, J. Chem. Phys. 56, 2824 (1972).

69. J. F. Ogilvie, Nature 243, 210 (1973).

70. H. E. Hunziker and H. R. Wendt, J. Chem. Phys. 60, 4622 (1974).

71. Y. Beers and C. J. Howard, J. Chem. Phys. 64, 1541 (1976).

72. P. A. Freedman and W. J. Jones, J. Chem. Soc., Faraday Trans. II, 72, 207 (1976).

73. S. Saito, J. Mol. Spectrosc. 65, 229 (1977).

74. R. P. Tuckett, P. A. Freedman and W. J. Jones, Mol. Phys. 37, 379, 403 (1979).

75. D. H. Liskow, H. F. Schaefer III and C. F. Bender, J. Am. Chem. Soc. 93, 6734 (1971).

76. A. Komornicki and R. L. Jaffe, J. Chem. Phys. 71, 2150 (1979).

77. A. Komornicki, GRADSCF, An Efficient Gradient-SCF Program System, available through the NRCC, Lawrence Berkeley Laboratories, Berkeley, CA, 1979.

78. F. Su, J. G. Calvert, C. R. Lindley, W. M. Uselman and J. H. Shaw, J. Phys. Chem. 83, 912 (1979).

79. D. C. Lindsey, D. G. Lister and D. J. Millen, Chem. Comm. 950 (1969).

80. A. M. Mirri, F. Scappini and G. Cazzoli, J. Mol. Spectrosc. 38, 218 (1971).

81. R. A. Ashby, J. Mol. Spectrosc. 23, 439 (1967).

82. I. Schwager and A. Arkell, J. Am. Chem. Soc. 89, 6006 (1967).

83. B. Liu, K. M. Sando, C. S. North, H. B. Friedrich and D. M. Chipman, J. Chem. Phys. 69, 1425 (1978).

84. P. Pulay, Mol. Phys. 18, 473 (1970).

85. J. A. Smith, P. Jorgensen and Y. Ohrn, J. Chem. Phys. 62, 1285 (1975).

86. B. J. Krohn and C. W. Kern, J. Chem. Phys. 69, 5310 (1978).

87. S. A. Clough, Y. Beers, G. P. Klein and L. S. Rothman, J. Chem. Phys. 59, 2254 (1973).

88. R. A. Toth, J. Quant. Spectrosc. Radiat.Transfer 13, 1127 (1973).

89. J. M. Flaud and C. Camy-Peyret, J. Mol. Spectrosc. 55, 278 (1975).

90. E. Clementi, J. Chem. Phys. 36, 33 (1962).

91. W. B. Person, K. G. Brown, D. Steele and D. Peters, J. Phys. Chem. (to be published, 1981).

92. H. Sambe, J. Chem. Phys. 58, 4779 (1973).

93. T. Amano, S. Saito, E. Hirota, Y. Morino, D. R. Johnson and F. X. Powell, J. Mol. Spectrosc. 30, 275 (1969).

94. P. E. Wells, in "Progress in Physical Organic Chemistry," A. Streitweiser Jr. and R. W. Taft, Eds. (Interscience, New York, 1968), Vol. 6, p. 11.

BIOGRAPHICAL SKETCH

Roberto Guedes Alves Maia was born on May 13, 1949, in Recife, Pernambuco, Brazil. He received, in 1971, the Bachelor's degree in chemistry from Catholic University of Pernambuco in Recife and the Master's degree in science in 1973 from the Pontifex Catholic University of Rio de Janeiro in Rio de Janeiro, Brazil. He then joined the Chemistry Department of the University of Brazilia in Brazilia as an assistant professor. He entered the Graduate School at the University of Florida in January of 1976 and received his Ph.D. in physical chemistry in December, 1980. He married Rosa Maria Barros Coelho on December 27, 1972 in Recife, Pernambuco and they have three children: Roberta, Rosana and Renata.

I certify that I have read this study and that in my opinion it conforms to acceptable standards of scholarly presentation and is fully adequate, in scope and quality, as a dissertation for the degree of Doctor of Philosophy.

Willis B. Person, Chairman
Professor of Chemistry

I certify that I have read this study and that in my opinion it conforms to acceptable standards of scholarly presentation and is fully adequate, in scope and quality, as a dissertation for the degree of Doctor of Philosophy.

Merle A. Battiste
Professor of Chemistry

I certify that I have read this study and that in my opinion it conforms to acceptable standards of scholarly presentation and is fully adequate, in scope and quality, as a dissertation for the degree of Doctor of Philosophy.

Robert J. Hanrahan
Professor of Chemistry

I certify that I have read this study and that in my opinion it conforms to acceptable standards of scholarly presentation and is fully adequate, in scope and quality, as a dissertation for the degree of Doctor of Philosophy.

Martin T. Vala
Professor of Chemistry

I certify that I have read this study and that in my opinion it conforms to acceptable standards of scholarly presentation and is fully adequate, in scope and quality, as a dissertation for the degree of Doctor of Philosophy.

John R. Sabin
Professor of Physics

This dissertation was submitted to the Graduate Faculty of the Department of Chemistry in the College of Liberal Arts and Sciences and to the Graduate Council, and was accepted as partial fulfillment of the requirements for the degree of Doctor of Philosophy.

December, 1980

Dean, Graduate School